People's Democratic Republic of Algeria
Ministry of Higher Education and Scientific Research

National Polytechnic School
Department of Electronic
Laboratory of Communication Devices
and Photovoltaic Conversion

PhD Thesis in Electronic

Presented by:

Karim KACED

Entitled:

Study of MPPT techniques for photovoltaic systems under partial shading conditions

---

Members of jury:

M. HADDADI	Professor, ENP	President
C. LARBES	Professor, ENP	Supervisor
A. MALEK	Researches Director, CDER	Examiner
L. BARAZANE	Professor, USTHB	Examiner
M. S. AIT-CHEIKH	Professor, ENP	Examiner

ENP 2018

People's Democratic Republic of Algeria
Ministry of Higher Education and Scientific Research

National Polytechnic School
Department of Electronic
Laboratory of Communication Devices
and Photovoltaic Conversion

PhD Thesis in Electronic

Presented by:

Karim KACED

Entitled:

Study of MPPT techniques for photovoltaic systems under partial shading conditions

---

Members of jury:

M. HADDADI	Professor, ENP	President
C. LARBES	Professor, ENP	Supervisor
A. MALEK	Researches Director, CDER	Examiner
L. BARAZANE	Professor, USTHB	Examiner
M. S. AIT-CHEIKH	Professor, ENP	Examiner

ENP 2018

République Algérienne Démocratique et Populaire
Ministère de l'Enseignement Supérieur et de la Recherche Scientifique

Ecole Nationale Polytechnique
Département d'Electronique
Laboratoire des Dispositifs de Communication
et de Conversion Photovoltaïque

Thèse de Doctorat En Electronique

Option: **Electricité Solaire**

Présentée par :

Karim KACED

Intitulée

Etude des techniques MPPT pour systèmes photovoltaïques dans des conditions partiellement ombragées

---

Membres du jury :

M. HADDADI	Professeur à l'ENP	Président
C. LARBES	Professeur à l'ENP	Directeur de thèse
A. MALEK	Directeur de Recherche au CDER	Examinateur
L. BARAZANE	Professeur à l'USTHB	Examinateur
M. S. AIT-CHEIKH	Professeur à l'ENP	Examinateur

ENP 2018

Laboratoire de Dispositifs de communication et de Conversion Photovoltaïque (LDCCP),
10 Avenue Hassen BADI, El-Harrach 16200
Alger Algérie

ACKNOWLEDGEMENT

This thesis has been conducted at the Laboratory of Communication Devices and Photovoltaic Conversion in the Department of Electronic of Ecole Nationale Polytechnique (ENP) of Algiers.

First of all, I would like to take this opportunity to express my deepest gratitude and thanks to my project supervisor, Professor **Cherif Larbes** for his constant guidance, assistance and support as well as all the knowledge he shared during the course of this research.

I also wish to thank President of jury Mr **Mourad Haddadi**, Professor at ENP, and the members of the jury: Ms **Linda Barazane**, Professor at USTHB, Mr **Ali Malek**, Director of Research at the CDER and Mr **Mohamed Saleh Ait-Cheikh**, Professor at ENP for accepting to be members of the reading committee and for their constructive analysis of the present work.

Further, I sincerely thank Professor **Naeem Ramzan** for kindly inviting me to stay as a PhD student visitor at the School of Engineering and Computing, University of the West of Scotland (UWS), in United Kingdom. The friendly and focused atmosphere at the UWS has been a very memorable experience.

Last but not least, I would like to express my appreciation and gratitude to my family members, who have encouraged, motivated and supported me during my studies.

Abstract

ملخص:

من أجل زيادة مردود المولدات الكهروضوئية، فإن تتبع نقطة الاستطاعة العظمى لكل لوح كهروضوئي أمر ضروري. من المعروف أن استطاعة اللوح الكهروضوئى تتأثر بالإشعاع الشمسي ودرجة الحرارة. بالإضافة إلى هذه العوامل، لظاهرة الظل الجزئي تأثير مباشر على الاستطاعة المنتجة من المنشآت الشمسية، و تؤدي إلى خلل في نظام تتبع نقطة الاستطاعة العظمى. تحت ظروف التظليل الجزئي، يتميز منحنى الخاصية طاقةتوتر للألواح الشمسية بظهور عدة نقاط للاستطاعة العظمى. تحت هذه الظروف، لا تقدم الطرق التقليدية لتتبع نقطة الاستطاعة العظمى نتائج جيدة ومن هنا ظهرت فكرة دراسة طرق أخرى لتتبع نقطة الاستطاعة العظمى. في هذا السياق، تقدم هذه الأطروحة مساهمة في الدراسة و التثبيت على شرائح قابلة للتشكيل، لأنظمة تحكم تتبع نقطة الاستطاعة العظمى اعتمادا على ثلاثة خوارزميات: خوارزمية الخفافيش، إستمثال عناصر السرب وخوارزمية التطور التفاضلي. استخدمت هذه الخوارزميات الثلاثة لتصميم أنظمة ذكية لتتبع نقطة الاستطاعة العظمى، و التي من شأنها أن تتعامل بكفاءة عالية مع المنحنيات المميزة، متعددة الوسائط، للأنظمة الكهروضوئية في ظروف مظللة جزئيا. بالإضافة إلى ذلك، تم تثبيت هذه الأنظمة على شريحة مصفوفة البوابات المنطقية القابلة للبرمجة. تم التحقق من أداء هذه الطرق المقترحة بالمحاكاة و التجارب العملية، والنتائج المحققة تؤكد فعالية هذه الخوارزميات للإدارة المثلى للطاقة المنتجة من الألواح الشمسية في ظروف مظللة جزئيا.

الكلمات المفتاحية: تتبع نقطة الاستطاعة العظمى، المنشآت الكهروضوئية، الظل الجزئي، خوارزمية الخفافيش، إستمثال عناصر السرب، خوارزمية التطور التفاضلي، مصفوفة البوابات المنطقية القابلة للبرمجة.

Résumé :

Pour augmenter le rendement des générateurs photovoltaïques (PV), la poursuite du point de puissance maximale (MPP) de chaque module PV est nécessaire. La puissance de sortie du module solaire dépend du rayonnement solaire et de la température ambiante. Aussi, le phénomène d'ombrage partiel a une incidence directe sur la puissance de sortie des installations solaires et conduit à un mauvais fonctionnement de la poursuite du MPP i.e. du MPPT. Dans les conditions d'ombrage partiel, la caractéristique *P-V* du panneau solaire présente plusieurs maximums. Les méthodes MPPT classiques ne donnent pas dans ce cas de bons résultats d'où l'idée d'étudier d'autres approches d'optimisation et de poursuite du MPP. Dans ce contexte, cette thèse présente une contribution à l'étude et à l'implémentation sur circuit reconfigurable des contrôleurs MPPT basés sur trois métaheuristiques d'optimisation : l'algorithme de chauve-souris (BA), l'optimisation par essaim particulaire (PSO) et l'évolution différentiel (DE). Ces trois algorithmes sont utilisés pour concevoir des contrôleurs MPPT intelligents qui peuvent gérer, avec une grande efficacité, les courbes caractéristiques multimodales des systèmes photovoltaïque dans des conditions partiellement ombragées. De plus, ces contrôleurs sont implémentés sur circuit reconfigurable FPGA. Les performances des méthodes proposées sont vérifiées par simulation et par expérimentation et les résultats confirment l'efficacité de ces algorithmes pour une gestion optimale de l'énergie disponible à la sortie des panneaux photovoltaïques dans des conditions partiellement ombragées.

Mots clés : MPPT, système photovoltaïque, ombrage partiel, algorithme de chauve-souris (BA), optimisation de l'essaim particulaires (PSO), Algorithme d'évolution différentielle (DE), FPGA.

Abstract:

To increase the efficiency of photovoltaic (PV) generators, tracking of the maximum power point (MPP) of each PV module is necessary. The output power of photovoltaic module depends on solar irradiance and ambient temperature. Also, the phenomenon of partial shading has a direct impact on the output power of photovoltaic installations and leads to a malfunction of the MPP tracking (MPPT). Under partial shading conditions, the *P-V* characteristic of the photovoltaic panel presents several maxima. In this case, the conventional MPPT methods do not give good results, hence the idea of studying other approaches for optimizing and tracking the MPP. In this context, this thesis presents a contribution to the study and implementation into reconfigurable circuit of MPPT controllers based on three metaheuristics of optimization: bat algorithm (BA), particle swarm optimization (PSO) and differential evolution (DE) algorithm. These three algorithms are used to design intelligent MPPT controllers that can efficiently handle the multimodal characteristic curves of photovoltaic systems under partially shaded conditions. Furthermore, these controllers are implemented into a reconfigurable FPGA circuit. The performances of the proposed methods are verified by simulation and by experiments and the results confirm the high accuracy of these algorithms for an optimal management of the energy available at the output of the photovoltaic panels subjected to partial shaded conditions.

Keywords: MPPT, photovoltaic system, partial shading conditions, bat algorithm (BA), particle swarm optimisation (PSO), differential evolution (DE) algorithm, FPGA.

CONTENTS

LIST OF FIGURES

LIST OF TABLES

GENERAL INTRODUCTION

RENEWABLE energy resources have enormous potential and offer many advantages over conventional energy resources. Renewable energy comes from several resources like solar, wind, geothermal, bio-mass and water. They can produce electricity in large quantities over a long term without too emit greenhouse gases. The renewable sources of energy derived from the sun can be used both directly and indirectly. The direct use of solar energy by means of devices is related to two distinct technologies: the first produces calories, it's solar thermal energy, and the second produces electricity through the photovoltaic effect. Photovoltaic (PV) technology is one of the most promising renewable energy technologies. Photovoltaic systems are configured as stand-alone, grid-connected and hybrid systems [1].

Various configurations are used for the PV modules interconnection to meet the voltage-current requirement [2]. The overall characteristics of photovoltaic generators are varying and depend on several factors, especially the meteorological conditions such as solar radiation, ambient temperature and wind speed, the aging of photovoltaic cells and partial shading or inhomogeneity of the illumination. When PV modules receive a uniform sunlight, the resulting *P-V* characteristic is uni-modal and characterized by a single point of maximum power. When part or the entire module receives a non-uniform illumination, some cells (dimly lit) become reversed bias and turn into receiving elements. This phenomenon is called "hot spot" and can result in the destruction of these cells. To remedy this problem, the photovoltaic modules

are equipped with bypass diodes which function is to protect the cells that become passive [3]. The integration of bypass diodes in solar module has as consequence the changing of the *P-V* characteristic which becomes multimodal when the partial shading occurs [4]. The *P-V* characteristic is then characterized by the appearance of several maxima: several local maximum power points (LMPPs) and one global maximum power point (GMPP). The number of maxima depends on the type of shading (uniform or partial), distribution of the illumination on the photovoltaic generator and the number of bypass diodes incorporated in each photovoltaic module.

The objective of this work is to contribute to the optimization of photovoltaic systems under partial shaded conditions. Despite efforts to improve the technology of photovoltaic cells, the electrical efficiency is still low [5]. Also, the partial shading (PS) issue has attracted considerable interest due to its significance in influencing the energy yield of a photovoltaic system [6,7]. It is statistically presented in literatures that the power loss due to the PS can vary from 10 to 70% of the system yield, depending on the severity and type of shading pattern [8]. Although the PS phenomena itself is a well-defined problem, its mitigation approaches varies markedly-with various degrees of complexities, performance and cost trade-off. Since, in most of the cases, it is neither possible to predict nor to prevent the PS from occurring, researchers normally concentrate on how to maximize energy yield from the PV system when the phenomena takes place. These approaches include system architectures, converter topologies, PV array configurations and maximum power point tracking (MPPT) techniques [9]. Despite the improvements that can be achieved by the first three approaches, additional material increases the complexity of the system which becomes more expensive. So a good compromise cost-efficiency can be achieved by development of MPPT techniques which can handle the partial shading.

Conventional MPPT methods are effective under uniform conditions but their performance deteriorates when partial shading occurs. Indeed, these methods (like Perturbe and Observe P&O and Incremental Conductance INC) lack the intelligence that will allow them to distinguish between LMPP and GMPP and can be trapped into a LMPP when the *P-V* characteristic is multimodal. To solve the case of partial shading,

several global MPPT techniques are developed [10, 11]. These methods vary in complexity, in the types and the number of sensors used and the equipment used for the implementation. The proposed approach is to treat the tracking of maximum power point as an optimization problem and then applying the metaheuristics inspired by nature to find the global maximum. In fact, methaheuristic algorithms are gained more attention and are proposed by many researchers to deal with the multimodal *P-V* characteristic under partial shading conditions. Due to their ability to handle multimodal objective functions, these algorithms are envisaged to be well suited for a problem of this nature. We have mainly interested at the following metaheuristics: Bat Algorithm (BA), Particle Swarm Optimization (PSO) and Differential Evolution algorithm (DE). Bat, PSO and DE algorithms are very effective due to their superior efficiency with minimal control parameters, robust performance and simple structures. For these reasons, these metaheuristic algorithms are proposed in this thesis to develop MPP tracker for PV system subjected to in-homogeneous irradiance.

The main objective of this thesis is to propose, design and implement global MPPT techniques based on metaheuristic for PV system under partial shading conditions. In order to achieve the objective of the research, firstly, a critical and strategic literature review of MPPT methods is presented. In this review, several previous works on MPPT used for PV system are discussed. Furthermore, the modeling and simulation of PV system under uniform and partial shading conditions are carried out. In order to accurately study the partial shading of PV systems, a good model of the PV module is required. Thus, a simple, fast and accurate PV system simulator based on two-diode model is developed. Then, maximum power point tracking (MPPT) controllers based on the Bat Algorithm (BA), Particle Swarm Optimization (PSO) and Differential Evolution algorithm (DE) algorithms are developed. To verify the performance of the proposed method, several simulations have been carried out in Matlab/Simulink environment for various shading patterns. The simulations results highlight the accuracy of the proposed scheme for optimal management of the energy available at the output of the photovoltaic panels. In addition, the comparison with the P&O and methods shows that the proposed method outperforms them

in term of global search ability and dynamic performance. The MPPT controllers are implemented on Xilinx Virtex-5 (XC5VLX50-1FFG676) Field Programmable Gate Array (FPGA) using direct "very high speed integrated circuit hardware description language" (VHDL) programming. The use of FPGA for designing the MPPT controller provides high performance, increases the robustness and makes the hardware implementation more flexible. The algorithms are tested in real time application on a buck-boost converter using a real photovoltaic panel. Experimental results confirm the efficiency of the proposed methods in the global peak tracking and their high accuracy to handle the partial shading. This thesis is organized into four chapters. Their contents are outlined as follows:

- Chapter 1 provides an overview of solar photovoltaic systems including the PV array and DC-DC converter modelling. Behaviour of the PV systems under varying environmental conditions and partial shading is critically analysed. In additions, this chapter provides an extensive review of MPPT techniques used to track the maximum power point (MPP) of PV array. Different MPPT methods are analyzed and compared on the basis of hardware requirement, speed, accuracy, applicability, cost and the sensors used. The merits and drawbacks of each method are highlighted. The benefits of applying the global search MPPT methods to conventional MPPT methods are stressed.

- In chapter 2, the key features of Bat algorithm (BA), Particle Swarm Optimization (PSO) and Differential Evolution (DE) algorithm are presented. Furthermore, the formulation of MPPT as an optimization problem is presented and the application of each proposed technique for MPPT is discussed.

- Chapter 3 presents the system simulations in Matlab/Simulik environnement. The tracking performances of the soft computing global search MPPT techniques; BA, DE and PSO are evaluated and compared in terms of the tracking speed and accuracy under partial shading conditions. As a benchmark, their performance to handle the partial shading conditions is compared with the conventional P&O technique.

- Chapter 4 describes the laboratory experimental set-up to implement the proposed MPPT algorithms. Detailed description is provided on the implementation of the proposed MPPT controllers into FPGA.

Finally, a conclusion is made in order to highlight the major contributions of this research. Besides, some probable directions towards the future works are also provided.

CHAPTER 1

REVIEW OF PHOTOVOLTAIC SYSTEM AND MPPT TECHNIQUES UNDER PARTIAL SHADING CONDITIONS

Contents

1.1 Introduction

The increase in the cost of conventional energy and the limitation of their resources make solar energy more and more a solution among promising energy options with benefits like abundance, the absence of any pollution and the availability in greater or lesser quantities in all points of the terrestrial globe. Currently, there is renewed interest in solar energy facilities, especially in areas with favourable weather conditions. The development of the photovoltaic market requires a perfect knowledge of the electrical production of these systems at different sites, especially to estimate its economic profitability. This precise estimate can only be done by taking into account the shading effects that have dramatic consequences on the electrical power delivered.

The chapter begins by an overview of photovoltaic generation systems. Then, the PV array characteristics under partial shading are critically examined. It is followed by the brief presentation of partial shading mitigating techniques. Finally, a review of maximum power point tracking techniques that have been prominently used in for shaded PV system is presented.

1.2 Overview of photovoltaic system

Photovoltaic is the field of technology and research related to the application of solar cells as solar energy. A solar cell or photovoltaic (PV) cell is a device that converts solar energy into electricity by the photovoltaic effect. The photovoltaic effect can be defined as being the appearance of a potential difference (voltage) between two layers of a semiconductor slice in which the conductivities are opposite, or between a semiconductor and a metal, under the effect of a light stream [12].

The photovoltaic effect was experimentally demonstrated first by French physicist Edmond Becquerel In 1839. However, it was not until the 1950s that researchers at Bell Laboratories in the United States managed to manufacture the first solar cell, the primary element of a photovoltaic system. Then, solar cells gained prominence with their incorporation into the 1958 Vanguard I satellite.

Solar cells are made of various materials and with different structures in order to reduce the cost and achieve maximum efficiency. There are various types of solar cell material, single crystal, polycrystalline and amorphous silicon, compound thin-film material and other semi-conductor absorbing layers, which give highly efficient cells for specialized applications [12]. Among silicon-based solar cells, crystalline silicon cells are most popular, though they are expensive whereas the amorphous silicon thin-film solar cells are less expensive. Monocrystalline solar panels have the highest efficiency rates since they are made out of the highest-grade silicon. The efficiency rates of monocrystalline solar panels are typically 15-20%. A variety of compound semi-conductors can also be used to manufacture thin-film solar cells like cadmium telluride (CdTe) and copper indium gallium diselenide (CIGS) [13].

A solar cell constitutes the basic unit of a PV generator. In fact, a photovoltaic module is a packaged interconnected assembly of photovoltaic cells. The electrical output of the module depends on the size and number of cells, their electrical interconnection and the environmental conditions to which the module is exposed. To achieve the desired voltage and current, modules are usually wired in series and in parallel into what is called a PV array. The flexibility of the modular PV system allows designers to create solar power systems that can meet a wide variety of electrical needs, no matter how large or small.

PV systems can be classified into three types: stand-alone, grid-connected and hybrid systems [14]. Stand-alone photovoltaic systems are designed to operate independent of the electric utility grid, and are generally designed and sized to supply certain DC and/or AC electrical loads. The two types of stand-alone photovoltaic power systems are direct-coupled system without batteries and stand alone system with batteries. The simplest type of stand-alone photovoltaic system is a direct-coupled system, where the DC output of a photovoltaic module or array is directly connected to a DC load. Since there is no electrical energy storage (batteries) in direct-coupled systems, the load only operates during sunlight hours, making these designs suitable for common applications such as ventilation fans and water pumps. However, in stand-alone photovoltaic power systems, the electrical energy produced by the photovoltaic panels

cannot always be used directly. As the demand from the load does not always equal the solar panel capacity, battery banks are generally used for energy storage. The second category is the grid-connected systems. Grid-connected or utility-interactive photovoltaic systems are designed to operate in parallel with and interconnected with the electric utility grid. The primary component in grid-connected photovoltaic systems is the inverter. The inverter converts the DC power produced by the photovoltaic array into AC power consistent with the voltage and power quality requirements of the utility grid, and automatically stops supplying power to the grid when the utility grid is not energised. In addition, these PV systems are used to reduce the consumption from the electricity grid and, in some instances to feed the surplus energy back into the grid. This system can produce significant quantities of high-grade energy near the consumption point, avoiding transmission and distribution losses. The third category is the hybrid systems that combine solar power from a photovoltaic system with another power generating energy source such as diesels, gas or wind generators.

1.3 Modelling of the photovoltaic system

1.3.1 PV module model

The general equivalent electrical circuit of the two-diode model, shown in Fig. 1.1 is used to simulate the behaviour of the solar cell. This model contains a current source I_{PV}, which describes the photocurrent, two diodes D1 and D2, a series resistance R_S and a parallel resistance R_P. An accurate model of PV array based on this model is presented in [15]. Eq. (1.1) describes the output current of the PV array:

$$\begin{aligned} I =& I_{PV}\, N_{PP} - I_{01}\, N_{PP} \left[\exp\left(\frac{V + I\, R_S\, N_S \left(\frac{N_{SS}}{N_{PP}}\right)}{a_1\, V_T\, N_S\, N_{SS}} \right) - 1 \right] \\ & - I_{02}\, N_{PP} \left[\exp\left(\frac{V + I\, R_S\, N_S \left(\frac{N_{SS}}{N_{PP}}\right)}{a_2\, V_T\, N_S\, N_{SS}} \right) - 1 \right] - \left(\frac{V + I\, R_S\, N_S \left(\frac{N_{SS}}{N_{PP}}\right)}{R_P\, N_S \left(\frac{N_{SS}}{N_{PP}}\right)} \right) \end{aligned} \tag{1.1}$$

where I and V refer to the output current and the output voltage of the PV array, respectively. N_S is the number of solar cells connected in series incorporated in each PV module, whereas N_{SS} and N_{PP} denote the number of PV modules connected in series and parallel, respectively. V_T (equal to kT/q) is the thermal voltage of the diodes, k is the Boltzmann constant ($1.3806503 \times 10^{-19}$ J/K), q is the electron charge ($1.60217646 \times 10^{-19}$ C) and T is the temperature in Kelvin. a_1 and a_2 are the ideality factors of the diodes D1 and D2, respectively.

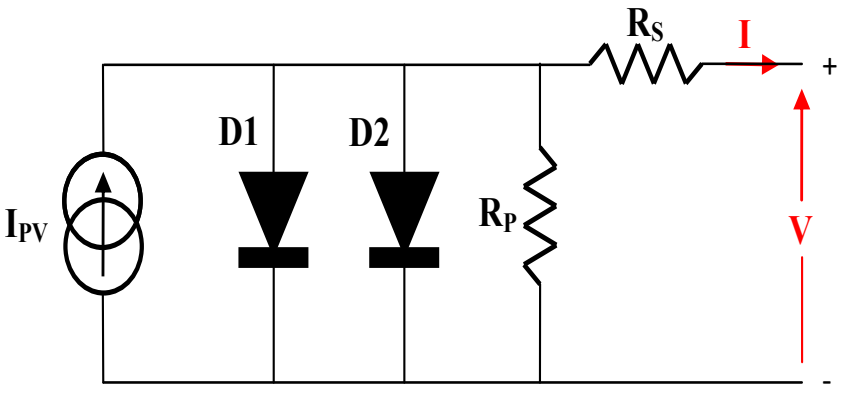

Figure 1.1: Equivalent circuit of a solar cell.

The photocurrent I_{PV} is directly influenced by the solar irradiance G and the temperature T. It is given by

$$I_{PV} = \frac{G}{G_{STC}}\left(I_{sc\_STC} + K_I\left(T - T_{STC}\right)\right) \tag{1.2}$$

The diodes saturation currents I_{01} and I_{02} are given by

$$I_{o1} = I_{o2} = \frac{I_{sc\_STC} + K_I\left(T - T_{STC}\right)}{exp\left(\frac{V_{oc\_STC} + K_V\left(T - T_{STC}\right)}{N_S V_T}\right) - 1} \tag{1.3}$$

where I_{sc_STC} and V_{oc_STC} are the short circuit current and the open circuit voltage of the PV module in the standard test condition (STC), i.e. $T = T_{STC} = 298.15$ °K and $G = G_{STC} = 1000$ W/m^2.

1.3.2 Uniform irradiance condition

The PV module used in this paper is SM55. The parameters of this module under STC are given in Table 1.1. Fig. 1.2 and Fig. 1.3 show the corresponding static I-V

and P-V curves for different values of irradiance G and temperature T. The module receives a uniform solar insulation, thus, the P-V curves exhibit a unique maximum power point (MPP).

Table 1.1: SM55 module specifications.

Parameters	Value
Maximum power (P_{mpp})	55 W
Short circuit current (I_{sc})	3.45 A
Open circuit voltage(V_{oc})	21.7 V
Maximum power current (I_{mpp})	3.15 A
Maximum power voltage (V_{mpp})	17.4 V
Temperature coefficient of I_{sc} (K_I)	1.2×10^{-3} A/°C
Temperature coefficient of V_{oc} (K_V)	-77×10^{-3} V/°C
Number of series cells in the module (N_s)	36
Number of bypass diodes	2

The effect of the irradiance on the current-voltage (I-V) and power-voltage (P-V) characteristics is depicted in Fig. 1.2. As was previously mentioned, the photo-generated current is directly proportional to the irradiance level, so an increment in the irradiation leads to a higher photo-generated current. Moreover, the short circuit current is directly proportional to the photo-generated current; therefore it is directly proportional to the irradiance. For this reason the current-voltage characteristic varies with the irradiation. In contrast, the effect in the open circuit voltage is relatively small, as the dependence of the light generated current is logarithmic.

The temperature, on the other hand, affects mostly the voltage and the open circuit voltage is linearly dependent on the temperature. Fig. 1.3 shows how the voltage-current and the voltage-power characteristics change with temperature. The effect of the temperature on V_{oc} is negative, i.e. when the temperature rises, the open circuit voltage decreases. The current increases with the temperature but very little and it does not compensate the decrease in the voltage caused by a given temperature rise. That is why the PV power also decreases. PV panel manufacturers provide in

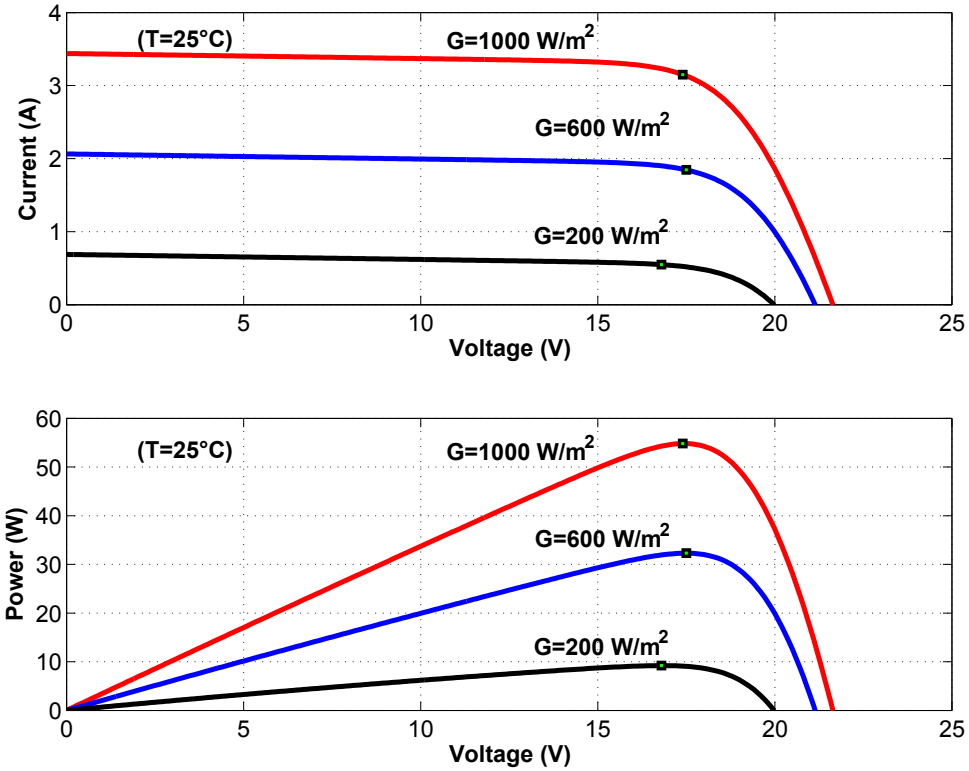

Figure 1.2: The characteristic of PV system under uniform variation in irradiance.

their data sheets the temperature coefficients (K_V and K_I), which are the parameters that specify how the open circuit voltage, the short circuit current and the maximum power vary when the temperature changes.

1.3.3 Partial shading conditions

Under uniform irradiance conditions, the PV module exhibits a single MPP. By contrast, when some part of the PV module receives different irradiance levels than others, then it is subject to partial shading. This condition may occur because of many factors like clouds, buildings, trees, dust, etc [9]. When partial shading occurs, the shaded PV cells may get reverse biased and behave as a loads receiving current from the fully illuminated cells which causes hot spot phenomenon that results in the destruction of these cells. To protect the PV cells against this problem, by-pass diodes are used. The photovoltaic module used is consisting of 36 cells connected in series, and protected by two bypass diodes. Each diode is connected in antiparallel with a group

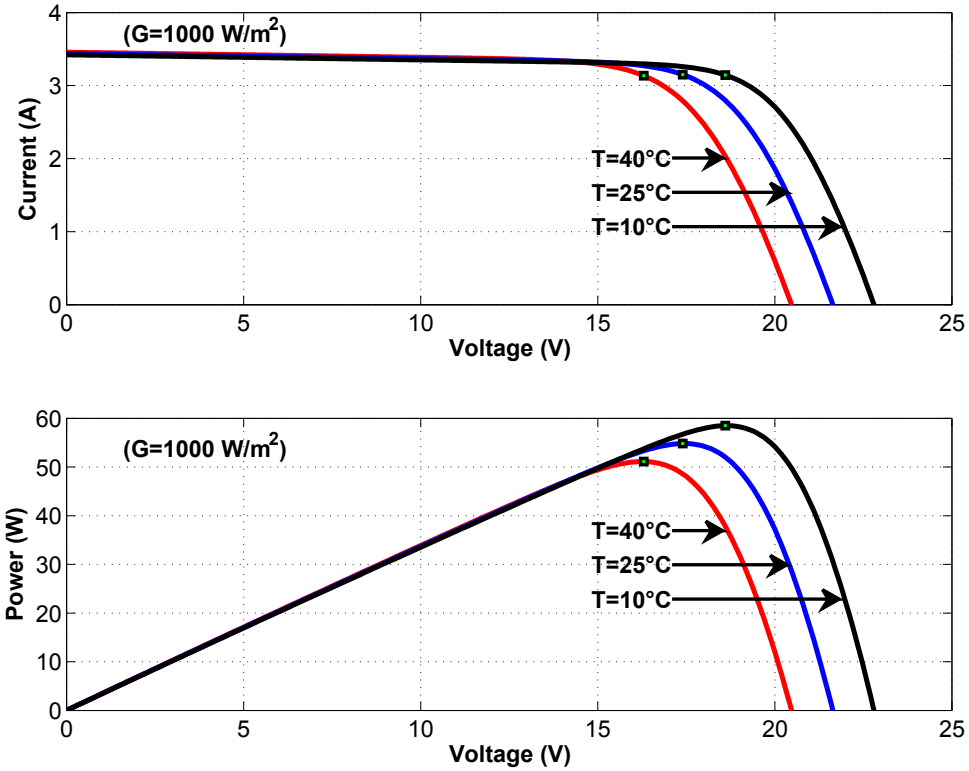

Figure 1.3: The characteristic of PV system under variation in temperature.

of 18 solar cells. The presence of these protection diodes changes the shape of the *P-V* characteristic and makes it more complicated when PV panel is subjected to partial shading. In partially shaded conditions, the resulting *P-V* characteristic presents several points of maximum power, several local maxima and one global maximum. Fig. 1.4(a) shows a photovoltaic panel consisting of two serially connected modules SM55. The resulting panel can be considered as four (4) sub-modules and each sub-module is protected by one bypass diode.

In a first case, we assume that the first module receives a uniform irradiance of $G_1 = 1000$ W/m^2 while the second receives an insulation of $G_2 = 500$ W/m^2 . The resulting *P-V* characteristic is shown in Fig. 1.4(b). We can notice the appearance of two maximum power point $P_1 = 53.14$ W and $P_2 = 58.04$ W at $V_1 = 17$ V and $V_2 = 37$ V, respectively. Fig. 1.4(b) shows the *P-V* curve in the case where each sub-module receives a different irradiance, for example $G_{11} = 1000$ W/m^2 , $G_{12} = 800$ W/m^2 , $G_{21} = 600$ W/m^2 et $G_{22} = 400$ W/m^2 (the notation G_{ij} refers to the insulation G for

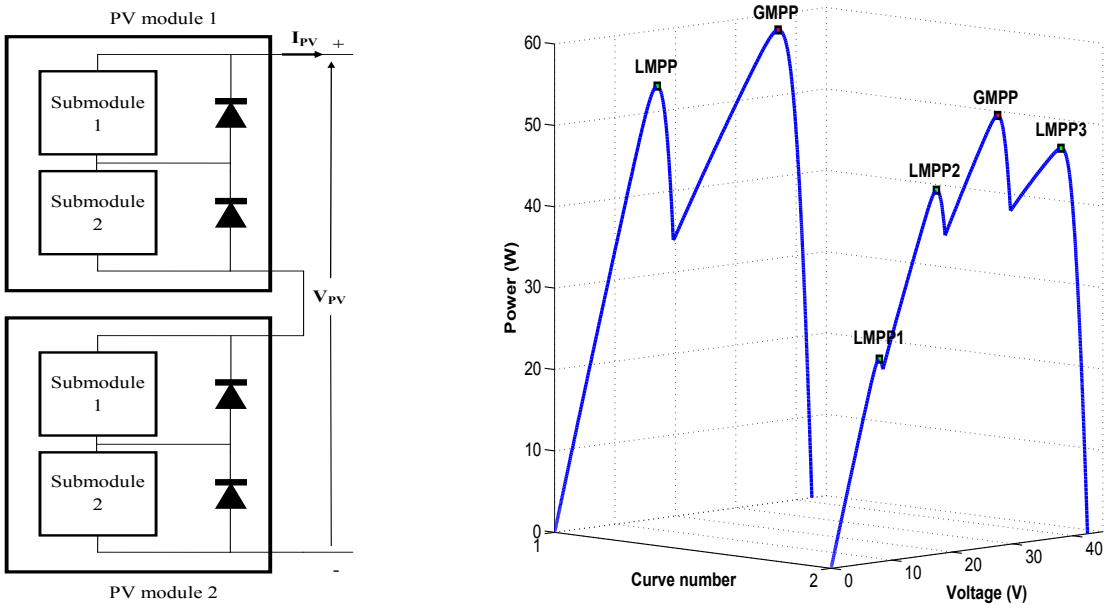

(a) (b)

Figure 1.4: (a) Model of PV panel consisting of two photovoltaic modules connected in series and (b) *P-V* curves of PV panel under two partial shading patterns.

the sub-module j of the module i). In this case, the *P-V* characteristic is characterized by the appearance of four maximum power point whose the global is $P = 52.89$ W at $V = 27.59$ V. Thus, the *P-V* characteristic can take various forms according to the shading pattern and the tracking of the global maximum power point (GMPP) becomes a more challenging task.

1.4 DC-DC converter modelling

The three basic switching power supply topologies in common use are the buck, boost and buck-boost. These topologies are non-isolated, i.e., the input and output voltages share a common ground. There are, however, isolated derivations of these non-isolated topologies. The power supply topology refers to how the switches, output inductor, and output capacitor are connected.

A DC-DC converter can operate in continuous or discontinuous inductor current mode. Continuous inductor current mode is characterized by current flowing con-

tinuously in the inductor during the entire switching cycle in steady-state operation. Discontinuous inductor current mode is characterized by the inductor current being zero for a portion of the switching cycle. It starts at zero, reaches a peak value, and returns to zero during each switching cycle. It is very desirable for a converter to stay in one mode only over its expected operating conditions because the power stage frequency response changes significantly between the two different modes of operation.

The simplified schematics of the basic topologies, buck, boost and buck-boost converter are shown in Figs. 1.5 to 1.7. In addition to input and output capacitors, the power stage consists of a power metal-oxide semiconductor field-effect transistor (MOSFET), a diode, and an inductor.

The DC-DC converter assumes two states per switching cycle. The ON State is when Q is close and the OFF State is when Q is open. The gate of the switch is driven by a Pulse Modulation Signal (PWM) signal. The duration of the ON state is $d\,T_s$, where d is the duty cycle of PWM signal and T_s is the switching period.

1.4.1 Buck converter

Fig. 1.5 shows a simplified electric schematic of a basic buck converter. When the switch is on, the power supply is connected to the inductor and the diode is reverse polarized. A current flows in the inductor L, which results in accumulating energy in the inductor. When the transistor turns off, the energy stored in the inductor is output through the diode D. DC-DC buck converter operates as a step down system that will step down the high input voltage to the low output voltage which the magnitude of output voltage is always lower than the input voltage. The objective of this circuit is to produce a purely DC output by adding the LC low pass filter to the basic circuit of this converter. This DC-DC buck converter can be connected to low voltage DC load or battery bank from a high PV array voltage.

The dynamics of the converter in one switching period is represented by the following system :

$$\begin{cases} C_1 \dfrac{\mathrm{d}v_{in}(t)}{\mathrm{d}t} = i_{in}(t) - d\, i_L(t) \\ C_2 \dfrac{\mathrm{d}v_{out}(t)}{\mathrm{d}t} = i_L(t) - i_{out}(t) \\ L \dfrac{\mathrm{d}i_L(t)}{\mathrm{d}t} = d\, v_{in}(t) - v_{out}(t) - R_L\, i_L(t) \end{cases} \tag{1.4}$$

where $i_{in}(t)$, $i_{out}(t)$ and $i_L(t)$ are the input, the output and the inductor current, respectively. $v_{in}(t)$, $v_{out}(t)$ and $v_L(t)$ are the input, the output and the inductor voltgae, respectively.

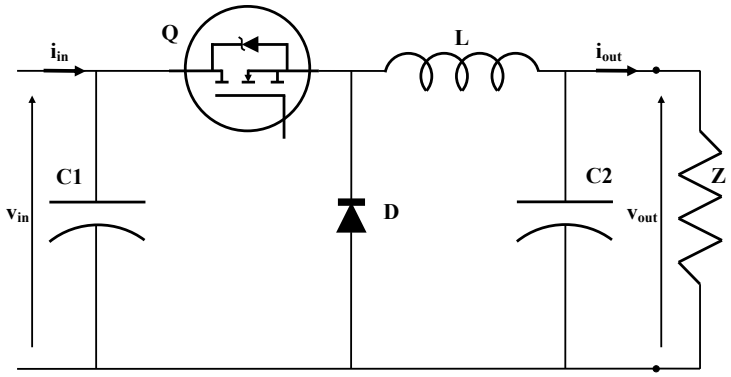

Figure 1.5: Electrical circuit of a buck converter.

1.4.2 Boost converter

Another basic switched-mode converter is the boost converter shown in Fig. 1.6. This converter converts an input voltage to a higher output voltage. It is also named the step-up converter. The transistor works as a switch which is turned on and off by a pulse-width modulated control voltage. During the on-time of the transistor, the voltage across L is equal to Vin and the inductor current increases linearly. When the transistor is turned off, the inductor current flows through the diode and charges the output capacitor. The function of the boost converter can also be described in terms of energy balance: During the on-phase of the transistor, energy is loaded into the inductor. This energy is then transferred to the output capacitor during the blocking phase of the transistor. The output voltage is always larger than the input voltage. Even if the transistor is not switched on and off the output capacitor charges via the diode until $V_{out} = V_{in}$. When the transistor is switched the output voltage will increase to higher levels than the input voltage.

The dynamics of the converter in one switching period is represented by the following system :

$$\begin{cases} C_1 \dfrac{\mathrm{d}v_{in}(t)}{\mathrm{d}t} = i_{in}(t) - i_L(t) \\ C_2 \dfrac{\mathrm{d}v_{out}(t)}{\mathrm{d}t} = (1-d)\, i_L(t) - i_{out}(t) \\ L \dfrac{\mathrm{d}i_L(t)}{\mathrm{d}t} = v_{in}(t) - (1-d)\, v_{out}(t) - R_L\, i_L(t) \end{cases} \tag{1.5}$$

where $i_{in}(t)$, $i_{out}(t)$ and $i_L(t)$ are the input, the output and the inductor current, respectively. $v_{in}(t)$, $v_{out}(t)$ and $v_L(t)$ are the input, the output and the inductor voltgae, respectively.

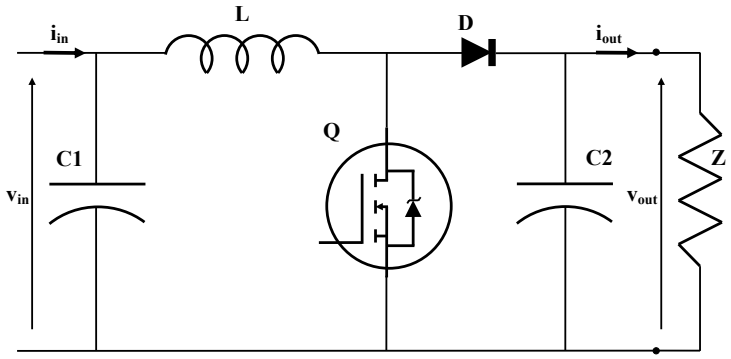

Figure 1.6: Electrical circuit of a boost converter.

1.4.3 Buck-boost converter

Fig. 1.7 shows a simplified electric schematic of a basic inverting buck-boost converter. During the closing time $d\,T_s$ of the transistor, the source voltage V_{in} is applied across the inductor L, which results in accumulating energy in the inductor. During the opening period $(1-d)T_s$, the diode D is forward-biased and the voltage of the inductance is applied to the load Z. The current flows anticlockwise through the diode D. Thus, the output voltage will be negative.

The dynamics of the converter in one switching period is represented by the following system :

$$\begin{cases} C_1 \dfrac{\mathrm{d}v_{in}(t)}{\mathrm{d}t} = i_{in}(t) - d\, i_L(t) \\ C_2 \dfrac{\mathrm{d}v_{out}(t)}{\mathrm{d}t} = -(1-d)\, i_L(t) - i_{out}(t) \\ L \dfrac{\mathrm{d}i_L(t)}{\mathrm{d}t} = d\, v_{in}(t) + (1-d)\, v_{out}(t) - R_L\, i_L(t) \end{cases} \tag{1.6}$$

where $i_{in}(t)$, $i_{out}(t)$ and $i_L(t)$ are the input, the output and the inductor current, respectively. $v_{in}(t)$, $v_{out}(t)$ and $v_L(t)$ are the input, the output and the inductor voltgae, respectively.

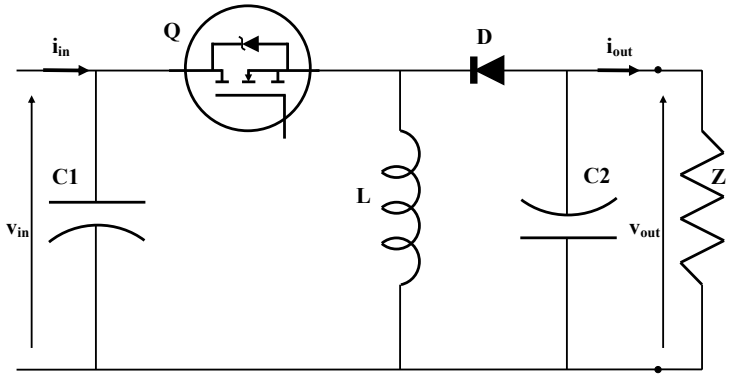

Figure 1.7: Electrical circuit of a buck-boost converter.

1.5 Partial shading mitigating techniques

PV modules are very sensitive to shading. Partial shadowing has been identified as a main cause for reducing the energy yield of grid-connected photovoltaic systems [12]. Shading of a single cell within a PV module, which itself is part of a string containing a number of modules connected in series, leads to a reverse- bias operation of the cell, which may result in hot-spots and potential break-down of the shaded cell. In order to avoid this threat, bypass diodes are inserted into the modules, which take over the string current in case of a partially shaded module [3].

Partial shading even one cell (or even a small portion of a cell) of a SM-55 module (which contains 36 cells) will reduce its power output. Because all cells are connected in a series string, the weakest cell will bring the others down to its reduced power level.

The best way to avoid a drop in output power is to avoid shading whenever possible. However, since it is impossible to prevent occasional shading, the use of bypass diodes around series-connected modules is recommended. Many module manufacturers will provide modules with the bypass diodes integrated into the module junc-

tion box. Using bypass diodes may postpone failure, but it does not prevent the loss of energy production from the shading. It is important to check for potential shading before installing the PV array. After installation, the area must be maintained to prevent weeds or tree branches from shading the array.

To reduce losses caused by partial shading and increase the efficiency of photovoltaic panels, several approaches are presented in the literature. These approaches include the use of maximum power point tracking (MPPT) techniques which can track the GMMP, PV array configurations, PV system architectures and converter topologies [9].

1.5.1 Maximum power point tracking techniques for shaded photovoltaic arrays

Maximum power point tracker is a power conversion system with an appropriate control algorithm to extract the maximum power from the PV source irrespective of the changes in the operating conditions. The objective of the MPPT algorithm is to govern the voltage or current or duty cycle in a way that the PV system will always deliver the maximum power. Up to date there are numerous MPPT techniques have been reported in the literature. Despite the fact that these methods are designed for the same objectives, they differ markedly in terms of complexity, convergence speed, steady state oscillations, cost, range of effectiveness and flexibility. Furthermore, each technique may work best in certain conditions while not in others. For instance, some MPPT techniques yield better performance under uniform irradiances but under partial shading conditions, the results are found to be unsatisfactory. A review of different MPPT techniques that address the partial shading condition is presented in Section 1.6.

1.5.2 Array configuration

The partial shading effects can be alleviated by employing different array configurations for interconnecting PV modules [16–18]. PV array configuration pertains to the

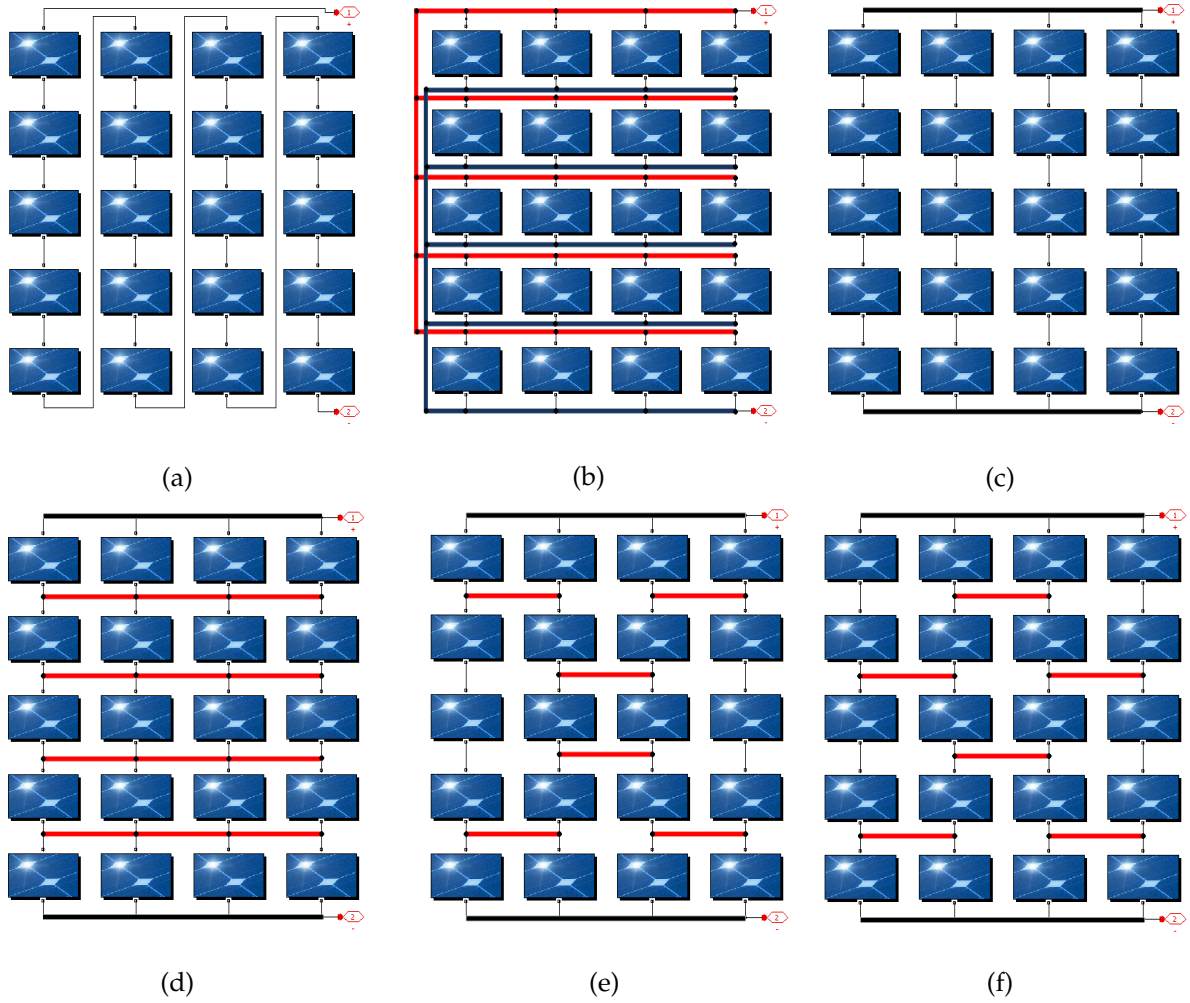

Figure 1.8: Different array configurations: (a) S, (b) P, (c) SP, (d) TCT, (e) HC and (f) BL.

interconnections of individual PV modules which are Series (S), Parallel (P), Series-Parallel (SP), Total-Cross-Tied (TCT), Bridge-Linked (BL), and Honey-Comb (HC) [2].

The Series (S) and Parallel (P) configurations are the basic configurations for the interconnection of PV modules. The series connexion of PV modules makes possible to increase the voltage of the PV array. Parallel wiring (P) increases the current output of a PV array while keeping the voltage the same. Series-Parallel (SP) connection, shown in Fig. 1.8(c), is the most commonly used. In series-parallel (SP) connection modules are connected in series to form strings in order to achieve the required voltage and then, theses strings are connected in parallel. On other in total cross tied connection (TCT) the modules, shown in Fig. 1.8(d) are first connected in parallel and then these parallel connections are connected in series. The HC and BL configura-

tions are shown in Fig. 1.8(e) and Fig. 1.8(f), respectively. They reduce the number of connections between the adjacent strings modules by approximately half, compared to the TCT configuration, which significantly reduces cable losses and wiring time of the installation. In [2], a comparative study have shown that TCT configuration is superior and provides the best performances under most studied cases of PSC, uneven or random distribution of partial shading.

Reconfigurable PV arrays are another viable solution to compensate the power loss due to the partial shading condition [19]. In [19], Adaptive reconfiguration of solar PV arrays under shadow conditions has been presented. A matrix of switches is used to connect a fixed TCT PV array with a solar adaptive bank that can be reconfigured. Simple control algorithms that determine how the switches can be controlled to optimize output power are presented and implemented in real time. Once shading is detected, the switching matrix reconfigures the PV modules. The shaded modules in the fixed part are compensated by the modules in the adaptive bank. Thus, the PV system produces a constant power even when shaded. An experimental adaptively reconfigurable solar PV array has been built and tested to verify the proposed configurations.

1.5.3 Photovoltaic system architectures

The PV system architecture describes how the power electronics converters are connected to configurations of PV modules. An architecture that permits the module-level MPPT can often harvest more energy than a string-level or array-level inverter [20, 21]. Grid connected PV inverter architectures normally have four conceivable settings: (a) central, (b) string, (c) multi-strings and (d) modular inverters. The central inverter topology, the most used one for its low cost and high productivity, is recommended in PV systems with a power greater than 10 kW [22]. Major disadvantages of this topology are the utilization of a high DC link voltage and one common MPPT. Therefore, this architecture is more vulnerable to shading and mismatching loss [20,21]. The string inverters topology, in contrast to the central inverter topology, comprises a separate MPPT at each string, leading to a maximum energy yield. Simi-

larly, this topology has some drawbacks with the PV modules associated in series. In the modular inverter topology [23], each module is fitted with its own MPPT and own inverter. The main weakness of the modular inverter configuration is its complex and costly control system. Multi-string inverter topology is a suitable setup [24], situated somewhere between the modular inverter and the string inverter topologies. In this arrangement, each PV string can be controlled easily and separately.

1.5.4 Circuit topologies

The circuit topology of the power electronics converters can be modified to further enhance the output power of PV systems under the partial shading condition and provide module-level MPPT [22, 25]. Examples are using multilevel converters [26], injecting a bias voltage into the shaded strings or modules [27], controlling the operating voltage of PV modules via a generation control circuit [28], additional circuitry to separate the current between the shaded and unshaded modules [29], or employing module-integrated converters (DC-DC converter is integrated to each module) [30] or multiple input converters [21].

1.6 Review of maximum power point tracking techniques for use in partially shaded conditions

Several MPPT techniques are presented in the literature to handle the multimodal *P-V* characteristic in partial shading conditions. These methods vary in complexity, in the types and the number of sensors used and the equipment used for the implementation. [31] proposed a two stage MPPT algorithm for tracking the GMPP. The authors introduce an analytic condition to distinguish partially shaded conditions from normal conditions. This condition is based on the comparison of the sensed photovoltaic current around $(0.8 \times N_{SS} \times V_{oc})$ and a reference value calculated at uniform insolation conditions with $G = 1000\ \mathrm{W/m^2}$, where N_{SS} is the number of series photovoltaic module and V_{oc} is the open circuit voltage. When the region of GMPP is located, the

algorithm calls a hill climbing subroutine to reach the GMPP. However, in the first stage, $(N_{SS}+1)$ points should be tested each time the partial shading conditions are detected before calling the hill climbing algorithm to locate the GMPP. This method will become time-costly if the number of series module is large [8]. In addition, temperature sensors must be used to determine the open circuit voltage.

Another two-stage search method is proposed by [32] for locating the GMPP. The first stage involved using a fixed spacing method to divide the *P-V* characteristic curve into various segments and to obtain the block in which GMPP is located. During the second stage, a variable step-size perturb and observe (P&O) method is used to locate the precise location of the GMPP. The authors recommended using $(N_{SS}+1)$ segments at the first stage to enhance the tracking performance, where N_{SS} denotes the number of PV modules serially connected.

It is shown in [33] that the function describing the PV power as a function of the PV voltage is a Lipschitz function. Therefore, [33] adopted the dividing rectangles (DIRECT) algorithm to search for the GMPP. Although the presented experimental results showed the efficiency of this method in tracking the GMPP under partial shading conditions, an appropriate choice of the first sampling interval is primordial for the GMPP tracking performance [34].

[35–37] employed two-stage search methods to track the GMPP, which first scanned the *PV* characteristic curve and then recorded the GMPP. In the second stage, these methods applied either the P&O method [35] or fuzzy logic control [36,37] to maintain the operating point at the GMPP.

[38] proposed a three stage tracking technique to find the GMPP under partial shaded condition. In the first stage, the control space of PV array voltage is subdivided into predetermined n number of partitions based on the measured open circuit array voltage, where n is the number of PV modules connected in series. Then, the slopes on the *P-V* characteristic in the portioned regions are computed. In the second stage, the sector or interval wherein the GMPP is located is determined based on the estimation of local maximum PV power in the portioned regions. In the third stage, the conventional P&O technique is used in the optimal partitioned region to finally

reach the GMPP and this technique continues to track the MPP until a change in the irradiation pattern is observed. The proposed technique was validated using PSIM simulations for both uniform and non-uniform irradiation. Furthermore, the proposed scheme was verified by experiments, where the MPPT controller was configured with a buck converter controlled by a versatile 8 bit microcontroller, ATmega16A. The experimental results confirmed that the proposed method works effectively and yields excellent steady state tracking efficiency.

Evolutionary algorithms and metaheuristics have attracted special attention by the academic community in recent years. Indeed, several articles have appeared in scientific journals, highlighting the effectiveness of these algorithms in the tracking of maximum power point in partially shaded conditions. Thanks to its simple structure, the particle swarm optimisation (PSO) algorithm is developed and improved by many researchers.

Authors in [39] used conventional PSO algorithm to control several PV arrays with one pair of voltage and current sensors. Rather than using individual MPPT blocks to control each of the PV arrays, the authors proposed a single PSO MPPT scheme to control multiple PV arrays. The scheme has the advantages of providing lower cost, higher efficiency and simplicity with respect to its implementation. The proposed scheme tracking capability is tested with experiment for both normal and partial shading patterns. In addition, the PSO MPPT dynamic response of the PV system under the partial shading condition is analysed and compared with other MPPT methods (conventional fixed voltage MPPT , Hill-climbing algorithm, Fibonacci search MPPT). A digital signal processor (DSP-TMS320C32) is used to realise the proposed scheme. The average tracking time of the PSO algorithm is 2 s, and it was observed that this response time was almost independent of the shape of the partial shading pattern.

[40] proposed a dual-algorithm search method based on dormant particle swarm optimization (DPSO) and incremental conductance (INC) algorithm to track the MPP. When the occurrence of partial shading conditions is confirmed, DPSO is activated and applied to search the area of global peak, and then the algorithm will be switched

to conventional INC algorithm to track the maximum output power of photovoltaic arrays. A comparative study including the analyses of convergence time and the power losses is performed in order to choose the initial number of particles in the first population (initial size of population) and to determine the optimal searching sequence of particles. In order to enhance the tracking speed and improve efficiency, the particles in DPSO have two states: dormant state and active state. During iteration, the particles are turned into dormant state (not participate in the next iteration) one after one until there is no active particle. Simulation and experimental results show that this scheme reduces the fluctuation of PV voltage and presents good performance no matter how complex shaded conditions the PV arrays are under. In addition, it performs better than both conventional PSO which take longer time to converge to the GMPP and conventional INC technique which falls to handle partially shaded conditions.

[41] proposed a modified PSO algorithm based MPPT to enhance the tracking capability of the conventional PSO method and improve it's dynamic performance. The proposed methods is verified under very challenging conditions, namely large step change in (uniform) solar irradiance, step changes in load, and partial shading conditions. The results reveals that this method presents the advantages of fast tracking speed and reduction of the steady-state oscillation (to practically zero) once the maximum power point (MPP) is reached, thus improving the MPPT efficiency. The proposed method is implemented on a TMS320F240 digital signal processor and verified experimentally using a buck-boost converter fed by a solar array simulator. Furthermore, the simulation experimental results highlight the superiority of the proposed method over the conventional HC in terms of tracking speed and steady-state oscillations.

In [42], the authors used the PSO technique for the tracking of GMPP using direct duty cycle control method. PI control loops are eliminated and the duty cycle of the PWM signal is adjusted directly by the MPPT algorithm. The proposed method is tested experimentally using a PV array simulator and compared to the conventional HC method. The experiments results done on ten different irradiance pattern includ-

ing uniform and partial shading conditions have shown that the proposed method performs excellently under all shading conditions and yields an average efficiency of 99.5%. In addition, the algorithm presented high efficiency when tested using a 10 h weather (irradiance and temperature) profile of Malaysia.

In [43], the authors have improved their algorithm (PSO) by removing random factors from the conventional PSO velocity equation. The proposed algorithm becomes deterministic and its structure becomes simpler. However, a restriction is imposed on the maximum of particle velocity to not fall into a LMPP. The value of limiting velocity factor is determined based on a critical study of P-V characteristics during partial shading. In this paper, the complete algorithm is divided on two modes: global mode and local mode. The DPSO algorithm was used only when partial shading conditions is occurred. The local mode is activated in two cases; when uniform insulation is detected or when the convergence criterion of DPSO in global mode is reached. In this case, variable step-size HC method is employed minimize the energy loss due to oscillations in the vicinity of MPP. The DPSO method is implemented by the TMS320F240 DSP on the Dspace DS1104 environment. The simulation and experimental results have shown that the proposed technique offers remarkable accuracy and tracking speed compared to conventional HC under several scenarios of irradiance including uniform insulation, partial shading conditions, slow variation of partial shading conditions and extreme partial shading. The proposed method yields an average efficiency of 99.5% when tested using the measured data of a tropical cloudy day.

[44] presented a FPGA implementation of PSO based MPPT for PV systems under partial shading conditions. First, Matlab/Simulik simulations are presented to demonstrate the accuracy of PSO for global peak tracking and its superiority over the P&O technique. After that, the PSO method has been designed using very high speed integrated circuit hardware description language (VHDL) and implemented on Xilinx Virtex5 (XC5VLX50-1FFG676) FPGA in order to achieve a high degree of flexibility and robustness for the MPPT algorithm. The developed architecture is tested in real time application on a buck-boost converter and the experimental results confirm the

efficiency of the PSO scheme and its high accuracy to handle the partial shading.

[45] proposed an improved MPPT strategy for PV systems based on PSO algorithm. To increase the tracking speed, a variable sampling time strategy (VSTS) based on the investigation of the dynamic behaviour of DC-DC converter current is deployed. To insure that particles (the duty cycle) don't exceed the interval [0,1], the velocity is controlled by using the inverse tangent function which permit to retain the speed of particles within a safe margin. In order to access the superiority of the proposed approach over the fixed sampling time strategy (FSTS), Matlab/Simulink simulations and experimentation, in which a TMS320F335 DSP is used to implement both tracking strategies on a real boost converter connected to a an Agilent E4360 Modular Solar Array Simulator, are performed under uniform irradiance, fast transient changes in insulation, and partial shading conditions.

[34] combined P&O and PSO to form a hybrid method to reduce the search space of the PSO. Initially, the P&O method is employed to identify the nearest local maximum. Then, the PSO method is used to search for the GMPP. The advantage of this method is the improvement of the time that is required for convergence since the search space for the PSO is reduced in early stage. The proposed controller was implemented in a 32-bit digital signal processor (DSP-TMS320F28035) and has been validated with experiments for three static *P-V* characteristic curves. In addition, the dynamic tracking capability was investigated for two scenarios of changing sequences of the shaded patterns. The experiments results has shown that the proposed hybrid method can track the GMPP dynamically, requires less tracking time and exhibits better dynamic response than the conventional PSO method.

[46] proposed a hybrid method to track the GMPP of PV system subjected non-homogeneous irradiance conditions. This method involves sequential integration of particle swarm optimization technique and perturb and observe algorithm; the former is used in the initial stage of tracking whereas the latter is performed at the final stage. The global search ability of the proposed method has been verified by simulations and experimentally tested on two different PV configurations (6S and 3S2P) under different partial shading patterns. The presented results have shown that this

method is superior to the conventional PSO technique and P&O algorithm in terms of convergence speed toward the GMPP. In addition, the application of this combined method resulted in reduction of output power oscillation and improvement of transient response compared to when PSO technique is used.

[47] adopted the PSO algorithm to realise MPPT for centralized-type photovoltaic generation system (PGS). The standard version of PSO is modified to meet the practical consideration of PGS operating under partial shading conditions and to take the hardware limitation into account. Among the practical design considerations, the authors suggested using a number of particles for the PSO algorithm equals to the number of photovoltaic modules connected in series. In addition, the inertia weight and cognitive and social coefficients in the velocity equation were linearly updated to enhance the tracking ability. To reduce the voltage stress, authors suggested to sort the obtained particle positions according to the last outputted position in advance, and output the nearest particle first. The proposed technique is validated on a 500 W prototype by simulation and experiments. The authors tested their method by simulation for 1000 different shading patterns. The simulations results have shown that this technique can successfully track the GMPP in all tested cases with average convergence iterations less than 27 and yields an average tracking efficiency higher than 99.9%.

An other adaptive PSO technique is proposed in [48]. An exponential-form parameter control method was used to shorten tracking time and improve MPPT efficiency when multi-peak *P-V* characteristic curves appeared in the PV arrays. This improved version is implemented on PIC181F8720 microprocessor and tested with experiment for six selected partial shading patterns. In term of tracking speed, the average iteration numbers required for MPPT tracking using the proposed PSO was 21.1. The results indicated that the proposed PSO method exhibited superior tracking accuracy and performance with comparison to the traditional PSO method.

Authors in [49] integrated the PSO technique in a new control structure for two multilevel three-phase inverter topologies for photovoltaic (PV) systems connected to the grid. This control scheme includes the use of the space vector pulse wide modu-

lation (SVPWM) technique to control the Diode Clamped Inverter (DCI) and cascade inverter topologies and the integration of the PSO technique to operate the PV system at the maximum power point (MPP). PSO method is used to overcome the problem of MPP tracking under partial shading conditions. This MPPT technique is implemented into FPGA and validated under different shading patterns for two PV architectures; string and modular, in order to select the optimal PV system architecture and circuit topologie offering the highest performance and to evaluate the behaviour of each PV inverter setting due to non-uniform irradiation. In these conditions, it is observed that the modular connection is dominant but, the results also highlight the benefit of inserting an adaptation stage with PSO-based MPPT between the PV array and the load in order to optimize the produced power at any time.

Authors in [50] proposed differential evolution (DE) based MPPT technique to deal with the nonlinear time-varying *P-V* characteristic curve of PV array. The performance of the algorithm was evaluated by simulations under different environmental conditions including rapid, large step changes in solar irradiation and partial shading conditions. A comparative study with the conventional hill climbing (HC) method has shown that the DE algorithm presents better accuracy and convergence speed. In addition, this algorithm significantly reduced the power oscillation once the correct MPP is reached and yield an average efficiency of 99.6% during partial shading conditions tests.

An improved differential evolution (DE) based MPPT is proposed in [51] to provide the globalized search space to track the GMPP. Since the conventional DE has no direction during the converging process, the authors made modification on the mutation strategy in order to ensure that particles always converges towards the best solution among all the particles in the generation. Simulations are performed on PSIM environment to access the effectiveness of the DE approach and its superiority over the P&O algorithm in multiple-peak tracking. The proposed algorithm is implemented on dsPIC30F6010A and it's performance under partial shading conditions are verified with experiments by an Agilent solar array simulator (E4360A) and a high step-up DC-DC converter.

A modified differential evolution (MDE) based maximum power point tracker (MPPT) is proposed in [52]. To overcome the drawback of conventional DE applied for MPPT, a deterministic mutation scheme is employed. Then, the proposed MDE does not involve any randomness and its structure become simple. In addition, only one parameter, the mutation factor is needed to be tuned. The proposed method is tested experimentally with 10 shaded curves and the results have revealed that this technique tracks the GMPP accurately within 12 perturbations of the duty cycle. The experiments result have shown that this method outperforms the PSO technique which is reported to be trapped in local maxima in some considered partial shading patterns. Furthermore, the MDE is validated for the typical weather condition of Malaysia for the duration of 8 h (9.00 am to 5.00 pm), where an average MPPT efficiency of 99.5% was achieved.

[53] introduced an improved differential evolution algorithm for tracking the GMPP. The proposed algorithm is simulated in the PSIM electronic simulation software to ensure its capability to handle the partial shading and its faster respond against load variation. The improved DE algorithm is implemented on the PIC18F4520 microcontroller and the feasibility of the approach is validated through experimentation using solar array simulator from Chroma (Model: 62150H-1000S) and single-ended primary-inductance converter (SEPIC). The experimental results show the that the proposed improved DE technique performs faster than the conventional DE algorithm and it is able to track the GMPP rapidly (within 2 s) with MPPT accuracy of above 99%. Moreover, the proposed algorithm can respond to load variation rapidly (within 0.1 s) which ultimately reduce undesirable fluctuations at the output of PV array.

[54] proposed a hybrid MPPT method called DEPSO, a combination of PSO and DE. The PSO algorithm is used in odd iterations and the DE algorithm is performed in even iterations. The proposed technique was verified through simulation and experiments for three partial shading patterns. In addition, the dynamic tracking capability is validated experimentally. For the hardware verification, the Atmega328P microcontroller (Atmel Corporation) is used to implement the DPSO technique and the Agilent modular PV simulator (E4360-A series) is used to create the output characteristic of

the PV system.

In [55], the tracking capability Cuckoo Search (CS) based MPPT method was highlighted. CS is a population based algorithm and its concept is similar to PSO. The main difference between CS and PSO is the manner to update the step sizes. In fact, the step sizes in CS are performed by Lévy Flight. The proposed method is evaluated and also benchmarked with two well established methods, namely P&O and PSO. The assessment includes gradual irradiance and temperature changes, sudden step change in irradiance, rapid step changes in both irradiance and temperature and the ability to handle partial shading conditions. The simulation results have shown that this method outperforms the P&O algorithm and the PSO technique in terms of convergence speed and transient fluctuations.

In [56], a deterministic Cuckoo search MPPT method for photovoltaic generation system (PGS) is proposed to improve the MPP tracking performance. The main concept is to remove the random number in the reference voltage calculation equation of the conventional Cuckoo search method. In fact, the Lévy distribution is replaced with a constant value, which makes the MPP tracking behaviour deterministic and simpler. The proposed MPPT technique is implemented on a low cost digital signal controller dsPIC33FJ16GS502 from Microchip Corp and verified by simulations and experiments on a 300 W prototyping system. When tested by simulation for 252 different PSC patterns in an investigated 5-series 1-parallel (5S1P) PGS, the probability of successfully tracking the GMPP achieved by the algorithm is 98.8%. The proposed technique is tested experimentally under uniform irradiance and three partial shading patterns, where tracking accuracies higher than 99.8% were achieved. In addition, the simulation and experiments results have shown that this techniques performs better than some GMPPT methods including, the conventional cuckoo search technique, PSO and GWO in terms of tracking speed and steady-state tracking performance.

[57] adopted a novel ant colony optimization (ACO) based MPPT to track the GMPP under partial shading conditions. In this work, the PV array is divided into several PV string and each PV string is equipped with a DC-DC converter. The authors used a centralized control scheme to control all the PV strings with one pair of

current and voltage sensors. Then, the MPPT controller generates the control value for each PV string converter. The feasibility of this proposed method is verified by Matlab simulation for various shading patterns. In addition, a comparison with other MPPT techniques, constant voltage tracking (CVT), perturb and observe (P&O) and particle swarm optimization (PSO), is carried out. The proposed method is found to be robust and system independent. In addition, it can handle the partial shading conditions with high accuracy.

[58] proposed a new MPPT controller based on the ant colony optimization (ACO) algorithm. In this work, a New Pheromone Updating (NPU) strategy is adopted in order to save the computation time and improves the tracking capability. The ACO_NPU MPPT controller was analyzed and compared to different MPPT techniques, namely the conventional perturb and observe (P&O) MPPT controller, Artificial Neural Network (ANN) , Fuzzy Logic Controller (FLC) , Fuzzy Logic Optimized Genetic Algorithm, the Adaptative Neuro Fuzzy Inference System (ANFIS) , PSO and the conventional ACO based MPPT. The simulation results have shown that the proposed ACO_NPU MPPT controller gives the best performances under variables atmospheric conditions. In addition, it can easily track the GMPP under partial shading conditions.

A MPPT method for PV systems under partially shaded conditions using firefly algorithm (FA) is reported in [59]. The FA is a population-based optimization introduced by Yang [60]. This optimization algorithm is inspired by the flashing patterns and behavior of fireflies. The FA based MPPT is validated under partial shading conditions by simulations and experiments for 6 S and 4S2P configurations of PV arrays. The proposed scheme is realized using a PIC16F876 microcontroller and its tracking performance is compared with conventional P&O and PSO methods. The results have shown that FA-based MPPT always converge to GMPP irrespective of the location of GMPP and the tracking efficiency in all test cases is higher than 99.5%. In addition, it is shown that this method reduces the voltage and current fluctuations in transient time before reaching GMPP in comparison with P&O and PSO methods.

[61] proposed a modified firefly algorithm (MFA) to track the GMPP. In order

to reduce the number of computation operations and tracking time, the proposed approach improves the existing firefly algorithm, and uses the average of all the brighter fireflies as the representative point so that the firefly will only move towards this point without wandering towards all the brighter flies. The MFA based MPPT technique is implemented in a 32-bit digital signal processor (DSP-TMS320F28035) and has been validated by experiment using a boost converter with an interleaved topology. Both static and dynamic tracking capabilities under partial shading conditions are considered and the MFA is compared against the original FA. Experimental results show that the proposed MFA shorten the tracking time in comparison with the FA and presents better dynamic tracking capability.

In [62], a MPPT algorithm based on a bat algorithm (BA) is proposed to deal with the multi-modal characteristic of photovoltaic panel under partial shading conditions. The bat algorithm is a swarm intelligence based method which was inspired by the echolocation behaviour of bats. Simulations are carried out in Matlab/Simulink environment under extreme shading patterns to confirm the global search ability and the good dynamic performance. The simulations results have shown that the proposed method tracks the GMPP with a high accuracy and yields a static efficiency above 99.9% for the most cases studied. In addition, the proposed scheme outperforms the P&O and the PSO methods in terms of accuracy and oscillations in PV power at the transient time. The BA based MPPT is implemented on Xilinx Virtex-5 (XC5VLX50-1FFG676) Field Programmable Gate Array (FPGA) and tested experimentally for four partial shading patterns.

Flower pollination algorithm (FPA) based MPPT is proposed in [63]. The FPA is a population-based metaheuristic which was inspired by the flow pollination process of flowering plants [60]. To assess the FPA's suitability for MPPT application, simulations are carried out in Matlab for various shading patterns. Furthermore, the proposed method was implemented on Arduino uno controller and verified experimentally using a PV simulator (CHROMA 62050H). Compared to P&O and PSO methods, FPA based MPPT exhibited better tracking performances.

Kumar et al. [64] proposed a global MPPT based on human psychology optimi-

sation (HPO) algorithm. This technique is based on mental and psychological sates of an ambition person [64]. In this work, the HPO technique is used in the case of battery charging to extract with accuracy the power from PV panel and efficiently supplying it to the battery. The performances of the HPO algorithm based MPPT are compared with two other techniques, hybrid P&O with PSO (POPSO) and hybrid Lagrange interpolation with PSO (LIPSO). The presented simulation results done on ten partial shading patterns show that the tracking speed of this algorithm is superior in comparison to the benchmarked techniques, and the average tracking time is 0.668 s. The effectiveness of this algorithm is tested with experiments by using a solar PV array simulator (AMETEK ETS600 x 17DPVF) and the HPO technique is implemented on DSP (dSpace MicroLab Box 1202).

In [65], a modified cat swarm optimisation (MCSO) is proposed to realise MPPT for PV system. The cat swarm optimisation (CSO) algorithm is a swarm intelligence based algorithm developed by Chu and Tsai [66]. To find the optimal solution of a problem, all cats in the swarm are continuously moved by combining two different searching modes; seeking mode (SM) and tracing mode (TM). At each iteration, the cats in CSO are randomly divided into two groups; the first is moved by SM while the second one is moved by TM. The switching between the two modes is randomly operated and it is controlled by a mixture ratio. This parameter decides how many cats will be moved into seeking mode process. The SM models the behaviour of a cat during a period of resting and it results in a slow move after observing its neighbourhood circumstances. The TM mimics the hunting behaviour of a cat and it is characterised by a quick move to a new position. Authors in [65] proposed a modified version of CSO to solve GMPPT problem in PV system and enhance the tracking ability of the conventional CSO. The performance of the algorithm is evaluated under three static shading patterns and also under the dynamic change of shading patterns. The simulation results show that the MCSO outperforms some existing MPPT methods, including PSO, MPSO, DE, GA and HC in term of tracking speed and accuracy. The proposed MCSO presents also some advantages like system independency and elimination of power oscillation around the MPP. The practical implementation of the

MCSO is also verified using a digital signal processor DSP-TMS320F28335 and a boost DC-DC converter. Table 1.2 summarizes the MPPT methods during partial shading based on the metaheuristic approach as discussed above.

Table 1.2: Summary of MPPT methods using metaheuristic approach

Reference	MPPT technique	Control variable	Converter type	Controller implementation
[39]	PSO	Voltage	Boost	DSP-TMS320C32
[40]	Dormant PSO with INC	Duty cycle	Boost	-
[41]	Modified PSO	Duty cycle	Buck-boost	DSP-TMS320F240
[42]	PSO	Duty cycle	Buck-boost	DSP
[43]	Deterministic PSO	Duty cycle	Buck-boost	DSP-TMS320F240
[44]	PSO	Duty cycle	Buck-boost	FPGA-XC5VLX50-1FFG676
[45]	Improved PSO	Duty cycle	Boost	DSP-TMS320F335
[34]	P&O with PSO	Voltage	Boost	DSP-TMS320F28035
[46]	PSO with P&O	Duty cycle	Boost	PIC16F876A microcontroller
[47]	Adaptive PSO	Duty cycle	Boost	dsPIC33FJ16GS502
[48]	Adaptive PSO	Duty cycle	Boost	PIC181F8720 microprocessor
[49]	PSO	Duty cycle	Boost	FPGA-XC5VLX50-1FFG676
[50]	DE	-	Buck-boost	Only simulations
[51]	Improved DE	Duty cycle	High step-up	dsPIC30F6010A
[52]	Modified DE	Duty cycle	Buck-boost	-
[53]	Improved DE	Duty cycle	SEPIC	PIC18F4520 microcontroller
[54]	DEPSO	Voltage	SEPIC	Atmega328P microcontroller
[55]	CS	Voltage	Buck-boost	Only simulations
[56]	Deterministic CS	Voltage	Boost	dsPIC33FJ16GS502
[57]	ACO	Current	-	Only simulations
[58]	ACO_NPU	Voltage	Boost	Only simulations
[59]	FA	Duty cycle	Boost	PIC16F876A microcontroller
[61]	Modified FA	Voltage	Boost	DSP-TMS320F28035
[62]	BA	Duty cycle	Buck-boost	FPGA-XC5VLX50-1FFG676
[63]	FPA	Duty cycle	Boost	Arduino uno controller
[64]	HPO	Duty cycle	Boost	DSP
[65]	Modified CSO	Duty cycle	Boost	DSP-TMS320F28335

1.7 Conclusion

In this chapter, the principle of photovoltaic system has been described. The behaviour of the PV system under different environmental conditions is discussed. The analysis is divided into two major segments, uniform irradiance and partial shading. In addition, various converters that have been used for MPPT are described and analyzed. Furthermore, a strategic review of MPPT techniques for PV systems under partial shading conditions is presented. Special attention is given towards the meta-heuristic based techniques due to their promising features. Among these algorithms, Bat, PSO and DE algorithms are envisaged to be very effective in dealing with MPPT problem particularly during partial shading occurrence.

CHAPTER 2

PROPOSED GLOBAL MPPT TECHNIQUES FOR PV SYSTEM SUBJECTED TO PARTIAL SHADING CONDITIONS

Contents

2.1 Introduction

Bio-inspired algorithms have attracted special attention by the academic community in recent years. As reported in chapter 1, several articles have appeared in scientific journals, highlighting the effectiveness of these algorithms in the tracking of maximum power point in partially shaded conditions and their superiority over conventional MPPT techniques. This chapter describes the application of the bio-inspired meta-heuristics; Bat algorithm (BA), Particle Swarm Optimization (PSO) and Differential Evolution (DE) algorithm to track the global MPP during partial shadow. The chapter begins by brief overview of metaheuristics algorithms. Then, the key feature of each algorithm is described. Furthermore, the formulation of MPPT as an optimization problem is presented and the application of each proposed technique for MPPT is discussed.

2.2 General overview on metaheuristic algorithms

Optimization is paramount in many applications, such as engineering, business activities, and industrial designs. Obviously, the aim of optimization is the searching for the optimal solution like minimizing the energy consumption and costs, to maximizing the profit, performance, and efficiency [67].

Many real-life optimization problems are difficult to solve by exact or deterministic optimization methods, due to properties, such as high dimensionality, multimodality and non-differentiability [68]. Hence, approximate or stochastic algorithms are an alternative approach for these problems. Stochastic algorithms can be decomposed into heuristics and metaheuristics. Heuristic refers to experience-based techniques for problem-solving and learning. This algorithms produce, by trial and error, acceptable solutions to a complex problem in a reasonable amount of computational time. Heuristics are problem-dependent and designed only for the solution of a particular problem. Further development of heuristic algorithms is the so-called metaheuristic algorithms. Here meta means "beyond" or "higher level", and these algorithms generally perform better than simple heuristics by using certain tradeoffs of randomization

and local search. Metaheuristics can be trajectory-based or population-based. Trajectory based metaheuristics are based on a single solution at any time whereas in population-based metaheuristics, a number of solutions are updated iteratively until the termination condition is satisfied.

Two major components of any metaheuristic algorithms are intensification and diversification, or exploitation and exploration. Diversification means to generate diverse solutions so as to explore the search space on a global scale. Intensification means to focus on the search in a local region by exploiting the information that a current good solution is found in this region. This is in combination with the selection of the best solutions. The selection of the best ensures that the solutions will converge to the optimality, whereas the diversification via randomization avoids the solutions being trapped at local optima and, at the same time, increases the diversity of the solutions. The good combination of these two major components will usually ensure that the global optimality is achievable with high accuracy [67].

Metaheuristics may be nature-inspired paradigms, stochastic, or probabilistic algorithms. Nature-inspired optimization algorithms have sparked great interest in recent years. Among them, bio-inspired especially those Swarm intelligence (SI)-based algorithms, have become very popular. In fact, these nature-inspired metaheuristic algorithms are now among the most widely used algorithms for optimization and computational intelligence [69].

Since the problem of MPP tracking in PV system can be modelled as a dynamic, multi-modal optimisation problem, bio-inspired metaheuristics are envisaged to be very effective to deal with *P-V* characteristic curve under partial shading conditions. Among them, Bat, PSO and DE algorithms are very effective due to their superior efficiency with minimal control parameters, robust performance and simple structures. Then, these metaheuristic algorithms are proposed in this thesis to develop MPP tracker for PV system subjected to in-homogeneous irradiance.

The rest of this chapter discusses the key features of the Bat, PSO and DE algorithms and describes the application of the proposed techniques for MPPT.

2.3 Bat algorithm (BA)

2.3.1 Overview of Bat search algorithm

Bat algorithm is a population based optimization algorithm inspired by the echolocation features of microbats in locating their foods. It is developed by Yang in 2010 [70].

Small bats (microbats) feed primarily on insects which detect using echolocation. The direction and intensity of the return signal enable them to locate potential prey in direction, and also in distance. At first, the bat over flies the search space, while emitting a set of ultrasonic pulses of certain amplitude (intensity) and a rate (density). Between the pulse trains, it receives the feedback signals (its own signal and eventually the signals from other bats in the swarm) by echolocation and interprets them. If the signals received in return have a low intensity and a strong rate, then it is very likely that prey is detected and the bat should head toward it. As the bat approaches the prey, it gradually intensifies the amount of pulses (the ultrasound rate) and, at the same time, progressively decreases the intensity of these pulses.

2.3.1.1 Movement of virtual bats

Bat algorithm is developed then by idealizing some of the echolocation characteristics of microbats [70]. Bat algorithm maintains a swarm of N microbats, where each microbats flies randomly with a velocity v_i at position x_i, with a varying loudness A_i and pulse emission rate $r_i \in [0,1]$ depending on the proximity of their target.

During the optimization task, every bat is randomly assigned a frequency which is drawn uniformly from $[f_{min}, f_{max}]$. Then, the velocity v_i and the position x_i of each bat at time step t are defined and updated with

$$f_i = f_{min} + (f_{max} - f_{min})\,\beta \tag{2.1}$$

$$v_i^{t+1} = v_i^t + \left(x_i^t - x_*\right) f_i \tag{2.2}$$

$$x_i^{t+1} = x_i^t + v_i^{t+1} \tag{2.3}$$

where $\beta \in [0,1]$ is a vector randomly drawn from a uniform distribution. x_* is the cur-

rent global best location (solution) which is achieved after comparing all the solutions among all the N bats at each iteration t.

If a random number is greater than the pulse emission r_i^t, then the exploitation stage is selected and the position x_i^{t+1} is replaced by the solution generated by the local search. As a result, a new solution is drawn locally by using a random walk around the current best solution [71]

$$x_{new} = x_* + \epsilon A^t \tag{2.4}$$

where ϵ is a random number which can be drawn from a uniform distribution in $[-1, 1]$ or a Gaussian distribution, while $A^t =< A_i^t >$ is the average loudness of all the bats at this time step [72].

2.3.1.2 Variations of loudness and pulse emission

If a random number is smaller than the loudness A_i^t and the new solution improves the fitness value, this means that the bat is moving towards the prey (the optimal solution). Then, the new solution is accepted and its loudness and emission rates are updated to control the exploration and exploitation. It is suggested that loudness decreases from positive value A_i^0 to $A_{min} = 0$ whereas the pulse rate of pulse emission increases from 0 to R_i

$$A_i^{t+1} = \alpha\, A_i^t \tag{2.5}$$

$$r_i^{t+1} = R_i\,[1 - \exp\,(-\gamma\, t)] \tag{2.6}$$

where α is a constant in the range of $[0, 1]$ and γ is a positive constant. In this work, A_i^0 and R_i are set to 1.

2.3.2 Application of BA for MPPT

The bat algorithm is applied to the tracking of GMPP by the direct duty cycle control method. Thus, the optimization variable is defined as the duty cycle of the PWM signal. The complete flowchart of the proposed bat algorithm based MPPT is illustrated in Fig. 2.1.

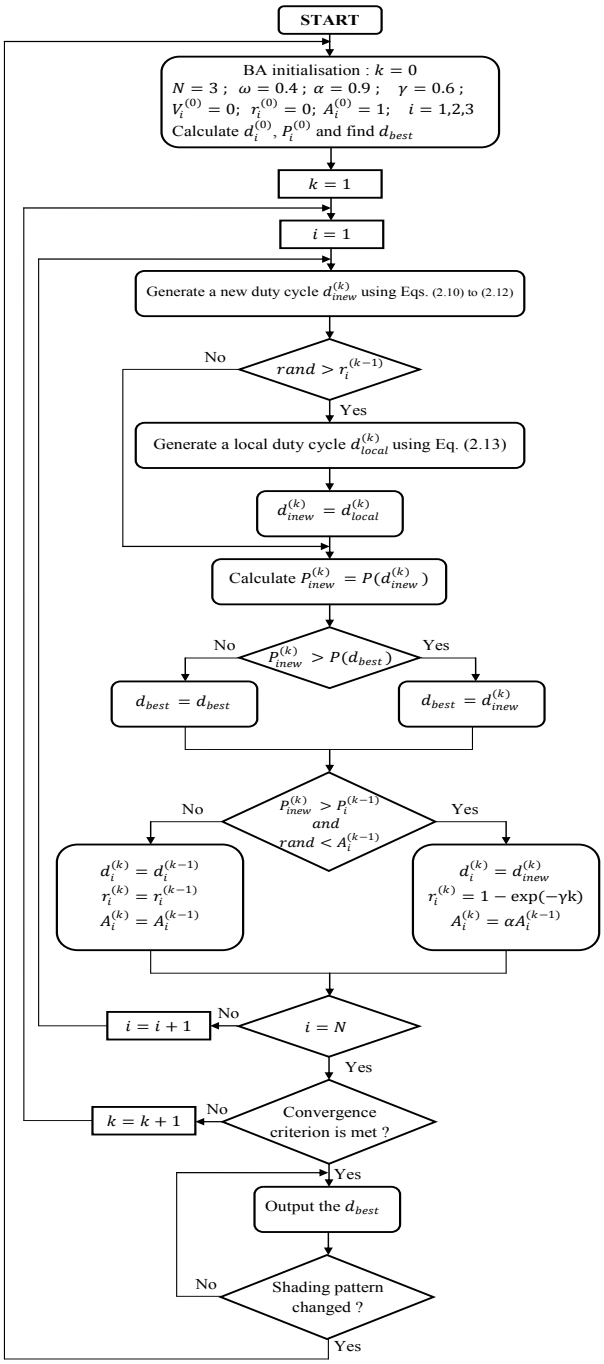

Figure 2.1: Complete flowchart of the proposed BA-MPPT method.

Initialisation

Initially, a vector of N duty cycles (first vector of solutions) is generated from a uniform distribution on $[0, 1]$ or it is predefined. The number of bats (N) is an important factor in the optimization process. A large number N guarantees the determination

of GMPP but the convergence time can be long while a small number N will save in convergence time but it can result in low GMPP tracking accuracy if the parameters of the MPPT algorithm are not well optimised. To ensure a compromise "convergence speed-efficiency", the number of duty cycle, N is chosen to be three (3).

For the choice of the first vector of duty cycles (first vector of solutions), the method of the reflective impedance is used [33]. The first three duty cycles are calculated thus:

$$d_1 = \frac{\sqrt{\eta Z_{min}}}{\sqrt{R_{PV\_max}} + \sqrt{\eta Z_{min}}} \tag{2.7}$$

$$d_2 = \frac{\sqrt{\eta Z_{ave}}}{\sqrt{R_{PV\_STC}} + \sqrt{\eta Z_{ave}}} \tag{2.8}$$

$$d_3 = \frac{\sqrt{\eta Z_{max}}}{\sqrt{R_{PV\_min}} + \sqrt{\eta Z_{max}}} \tag{2.9}$$

where η is the converter efficiency, Z_{min}, Z_{max} and $Z_{ave} = (Z_{min} + Z_{max})/2$ are the minimum, maximum and averege values of the connected load respectively. R_{PV_min} and R_{PV_max} are the minimum and maximum values of the reflective impedances of the PV array, respectively, while R_{PV_STC} is the reflective impedances of the PV panel at STC condition. In our simulations, the values of the parameters are : $\eta = 0.96$, $Z_{min} = 40\ \Omega$, $Z_{max} = 70\ \Omega$, $R_{PV\_min} = 6\ \Omega$, $R_{PV\_STC} = 22\ \Omega$ and $R_{PV\_max} = 43\ \Omega$.

It should be mentioned that the interval $[d_1, d_3]$ serves only for a first approximation of the search space. This approach leads to prevent having major disturbances and fluctuations in the voltage of the photovoltaic panel. The BA based MPPT can then search for the MPP outside of this range. The minimum duty cycle and maximum duty cycle are defined as 0.02 and 0.98, respectively.

The current and voltage of the photovoltaic array are sensed and the corresponding power is calculated for each duty cycle. The best duty cycle, d_{best} which gives the best value of fitness (PV power) is then stored.

Generating of new solutions

A new vector of solutions is globally generated following the equations

$$f_i = f_{min} + (f_{max} - f_{min})\,\beta \tag{2.10}$$

$$v_i^k = w\,v_i^{k-1} + \left(d_{best} - d_i^{k-1}\right) f_i \tag{2.11}$$

$$d_{i\,new}^k = d_i^{k-1} + v_i^k \tag{2.12}$$

Modifications are made on the equation of velocity v_i (Eq. (2.11)) to take into account the practical limits. The parameter ω called "inertia weight factor" [73] is used to limit the speeds of microbats while the term $(d_{best} - d_i^{k-1})$ serves as a search direction and ensures that solutions still move towards the best duty cycle d_{best}.

To ensure an automatic and dynamic failover between the exploration stage and the exploitation stage, a local solution is generated locally for each bat when the rate of its emission pulse r_i is lower than the rate of reception pulse randomly generated from a uniform distribution. This local solution is generated by "Random Walk" around the best solution (d_{best}) according to the relationship Eq. (2.13), and replaces that of the global search.

$$d_{i\,new}^k = d_{best} + \phi\,\varepsilon\,A^{k-1} \tag{2.13}$$

where $\varepsilon \in [-1, 1]$ is a uniform random number, $A^{k-1} = \langle A_i^{k-1} \rangle$ is the average loudness of all the bats at this step while ϕ is a fixed positive constant used to limit the random walk. This constant is set to be 0.05.

Updating of solutions

The new duty cycles are accepted or rejected not only according to the obtained values of PV power, but also depending on the amplitude of the received ultrasonic signals. This amplitude (received) is generated randomly for each duty cycle and compared with the value of the transmitted signal (A_i). Thus, for each new duty cycle, if it improves the objective function $(P(d_{inew}^k) > P(d_i^{k-1}))$ and the amplitude of its received signal is less than a random number, then it is accepted and will be a new solution for the next generation. The rate of pulsation of emission of this duty ratio is increased

while the amplitude of the ultrasound signal is decreased according to the above relationships (2.5) and(2.6).

Convergence criterion

The algorithm continues to calculate the new duty cycles until constraint on convergence is satisfied. In this thesis, the condition shown in the Eq. (2.14) is used as a convergence criterion. If the absolute difference between each two different duty cycles is less than a threshold Δd, then the algorithm stops the optimization process and brings out d_{best}

$$\left|d_i^k - d_j^k\right| \leq \Delta d;\ i, j = 1, 2, 3;\ i \neq j \tag{2.14}$$

Re-initialization

Due to varying weather and loading conditions, the global MPP is usually changing. The MPPT algorithm should have the ability to detect the variation of shading pattern and to search for the new global MPP. In this paper, the search process is initialised if the following condition is satisfied

$$\frac{|P_{PV\,new} - P_{PV\,last}|}{P_{PV\,last}} > \Delta P \tag{2.15}$$

where P_{PVnew} and P_{PVlast} are the values of photovoltaic panel power in two successive sample periods and ΔP is the power tolerance.

2.4 Particle swarm optimization (PSO)

2.4.1 General overview of PSO algorithm

Particle swarm optimization is a population based meta-heuristic invented by Russel Eberhart (electrical engineer) and James Kennedy (socio-psychologist) in 1995 [74, 75]. This algorithm uses a population of candidate solutions to develop an optimal solution to the problem under consideration. It was originally inspired in general by the artificial life and specifically by the social behaviour of swarming animals,

such as fish schooling and bird flocking. Indeed, we can observe in these animals relatively complex dynamics of displacement, whereas individually each individual has a limited "intelligence", and has only a local knowledge of its situation in the swarm. The local information and the memory of each individual are used to decide on his movement.

The swarm of particles corresponds to a population of agents, called particles. Each particle is considered as a solution of the problem and it is assigned a position (the solution vector) and a velocity. Moreover, each particle has a memory which enables it to remember its best performance (in position and value) and the best performance achieved by the neighbouring particles: each particle has a group of informants, historically called its neighbourhood. A swarm of particles, which are potential solutions to the problem of optimization, "flies" over the search space in search of the global optimum. The velocity of a particle is then influenced by the three components: a component of inertia, a cognitive component and a social component. The first one describes the trend of the particle to follow its current direction of displacement. The second one represents the trend of the particle to move towards the best position by which it has already passed. The social component characterize the trend of the particle to rely on the experience of its congeners and, thus, to move towards the best site already reached by the swarm. The strategy for moving a particle is illustrated in Fig. 2.2.

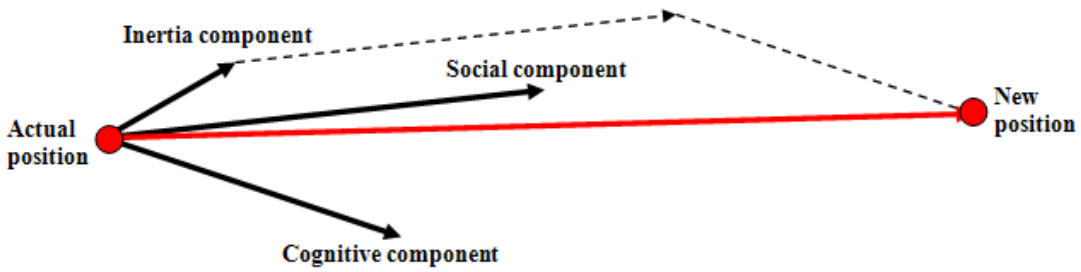

Figure 2.2: Movement of a particle.

2.4.1.1 Formalization

In a research space of dimension D, we define a swarm of particles of size N (size of the population). The particle i of the swarm is modeled by its positron vector $x_i = (x_{i1}, x_{i2}, ..., x_{iD})$ and by its velocity $v_i = (v_{i1}, v_{i2}, ..., v_{iD})$. The quality of its position is determined by the value of the objective function of that point. This particle keeps in memory the best position by which it has already passed, that we note $Pbest_i = (Pbest_{i1}, Pbest_{i2}, ..., Pbest_{iD})$. The best position reached by the swarm is noted $Gbest = (Gbest_1, Gbest_2, ..., Gbest_D)$. In our case, we are only interested in the fully connected swarm, that is, all the particles share the information; each particle knows the best position already visited by any particles in the swarm. This version of the algorithm is called, global version of PSO (Gbest), where all the particles of the swarm are considered as close to the particle i.

At the beginning of the algorithm, the particles of the swarm are initialized randomly or uniformly in the search space of the problem. Then, at each iteration, each particle moves, linearly combining the three components mentioned above. Indeed, at the iteration $t+1$, the velocity vector and the position vector are calculated from Eq. (2.16) and Eq. (2.17), respectively.

$$\begin{aligned} v_{ij}^{t+1} =& w\, v_{ij}^{t} + c_1\, r_{1_{ij}}^{t} \left(Pbest_{ij}^{t} - x_{ij}^{t} \right) \\ & + c_2\, r_{2_{ij}}^{t} \left(Gbest_{j}^{t} - x_{ij}^{t} \right), \quad j \in \{1, 2, ..., D\} \end{aligned} \tag{2.16}$$

$$x_{ij}^{t+1} = x_{ij}^{t} + v_{ij}^{t+1}, \quad j \in \{1, 2, ..., D\} \tag{2.17}$$

with w is a constant, called the coefficient of inertia; c_1 and c_2 are two constants, called acceleration coefficients; r_1 and r_2 are two random numbers drawn uniformly in $[0, 1]$, at each iteration t and for each dimension j.

Stochastic factors allow the particles to move in the problem space randomly. This property allows for extensive exploration of the search space and increases the probability of finding the best solution with high efficiency. The three components mentioned above (i.e. of inertia, cognitive and social) are represented in Eq. (2.16) by the following terms:

wv_{ij}^{t} corresponds to the inertia component of the displacement, where the param-

eter w controls the influence of the direction on the future displacement;

$c_1 r^t_{1_{ij}}(Pbest^t_{ij} - x^t_{ij})$ corresponds to the cognitive component of displacement, where parameter c1 controls the cognitive behaviour of the particle;

$c_2 r^t_{2_{ij}}(Gbest^t_j - x^t_{ij})$ corresponds to the social component of displacement, where parameter c_2 controls the social aptitude of the particle.

The PSO algorithm is summarized in the following steps:

Initialise each particle in the population by randomly selecting values for its position vector x_i and velocity v_i.
Repeat
Calculate the fitness value of each particle i;
Update the local best positions for each particle i;
Update the global best position of the swarm;
Calculate the velocity and update the location of each particle according to Eq. (2.16) and Eq. (2.17);
Until stopping criterion is met.

2.4.1.2 PSO control parameters

The inertia weight w was firstly introduced by Yuhui Shi and Russell Eberhart [76]. This parameter plays the role of balancing the global search and local search during the search process. It can be a positive constant or even a positive linear or nonlinear function of time (or iterations). The confidence constants, c_1 and c_2, also called acceleration coefficients, represent the weighting of the stochastic acceleration limits that pull each particle towards the best global and local position. Thus, adjusting these constants changes the pressure between parameters in the system. These two parameters can be positive constants, or linearly or nonlinearly varying with time (iterations).

2.4.1.3 Convergence criteria

The stopping criterion indicates that the solution is sufficiently close to the optimum. Selecting a good termination criterion has an important role to ensure a correct con-

vergence of the algorithm. Several criteria for halting the process of optimisation are possible. The algorithm can be stopped when the objective of optimisation is met. Indeed, in some optimization tasks, the objective function's minimum value is already known. For example, error functions for which the tolerable error is given or test functions whose minima are known. If the best vector's objective function value is within a specified tolerance of the global minimum, the optimization halts. In addition, the algorithm can be stopped after a sufficient number of generations for the search space to be properly explored. This criterion can prove to be expensive in computing time if the number of particles to be treated in each population is important. The algorithm can also be stopped when the population is not moving fast enough.

2.4.1.4 Neighbourhood topology

The PSO algorithm is inspired by the collective behaviour of swarms. This algorithm highlights the ability of an agent to stay at an optimal distance from others in the same group and to follow a global movement affected by the local movements of its neighbours. Thus, the authors modelled the behaviour of particles by equations (2.16) and (2.17). In practice, using Eq. (2.16), an interconnexion network must be defined in order to establish connections between the particles and allow them to exchange information with each other. This communication network between the particles is called neighbourhood topology. This topology helps to define a group of informants for each particle; this is called the neighbourhood of a particle. The neighbourhood of a particle can therefore be defined as the subset of particles of the swarm with which it has a direct communication, ie each particle can interrogate the particles in its neighbourhood (its informants), which, in turn, send it their informations. The choice of a topology (the communication network between the particles) therefore has a significant influence on the performance of PSO algorithm.

Equation (2.16) shows that the relationships between particles directly influence their velocities and hence their displacements. In the PSO literature, there are several versions that use the notion of neighbourhood of a particle with different ways. The most known topologies (those that are mainly used) are the global version "Gbest" and

the classic local version in the form of a ring ("Lbest" classic). In the global version, each particle is connected to all the other particles of the swarm (ie the neighbourhood of a particle is the set of particles of the swarm) while in the local version, each particle is connected only to a part of the other particles of the swarm (each particle has only two neighbouring particles in the classical local version). In the classical "Lbest" model, the swarm converges more slowly than in "Gbest", but it is more likely to locate the global optimum. In general, the use of the "Lbest" model makes it possible to limit the risks of premature convergence. This has a positive effect on the performance of the algorithm, especially for multimodal problems. Numerous variants for the interconnection of particles have been proposed in order to establish a balance between local search and global search and to improve the convergence of the PSO algorithm. These variants include new topologies for the particle swarm.

Kennedy and Mendes proposed several topologies in [77,78]. A graphic representation of these few models is shown in Fig. 2.3. The "star" topology has the shape of a wheel, where the particle of the center of the swarm, named focal (central), is responsible for the flow of information. In this topology, all the particles are isolated from each other and they are bound only to the focal particle. The information must be communicated through this particle, which will then use this information to adapt its trajectory. If the result of the adjustments shows an improvement in the performance of the central particle, then this improvement will be communicated to the rest of the population. So the focal particle serves as a filter, which slows the speed of transmission of information on the best solution found. The "four-cluster" topology uses four groups of particles connected together by several gateways. From a sociological point of view, this topology resembles four isolated communities. In each community, some particles can communicate with a particle from another community. In "Von Neumann", the topology takes the form of a grid (square grid), where each particle is connected to its four neighbouring particles (left, right, above and below). The "pyramid" topology represents a three-dimensional wire-frame pyramid. It has the lowest average distance of all the graphs and the highest first and second degree neighbours.

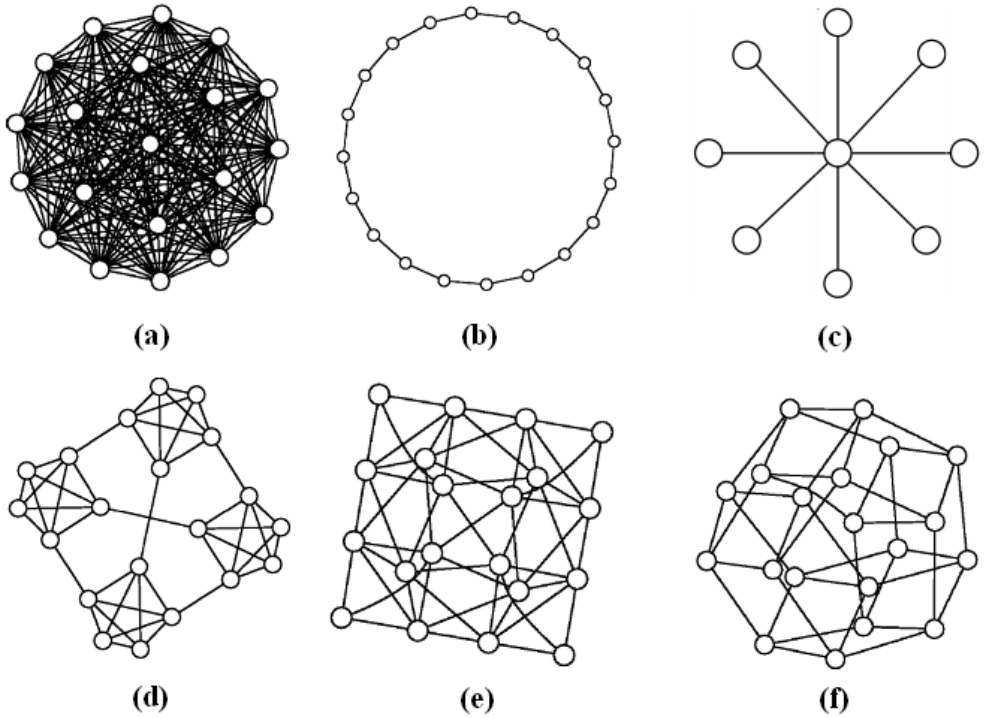

Figure 2.3: Different topologies used in PSO algorithm : (a) Gbest or All, (b) Lbest or Ring, (c) Star (d) Four clusters, (e) Pyramid, (f) Square or Von Neumann.

2.4.2 Application of PSO for MPPT

The PSO method is applied to realize the MPPT algorithm for PV system operating under partial shading conditions, wherein the *P-V* curve exhibits multiple MPPs. Flowchart of the proposed PSO based MPPT technique is shown in Fig. 2.4. The operating principles of proposed technique can be described as follows:

Step 1: PSO initialization

In order to start the optimization, the duty cycle of the PWM signal is chosen to be the optimization variable. Thus, it is adjusted directly by the MPPT controller. Initially, a solution vector of duty cycles with N_p particles is defined. Number of particles in the population should be chosen carefully. A larger number of particles results in more accurate MPP tracking even under complicated shading patterns but tracking speed reduces. As the number of particles increases, computation time also increases.

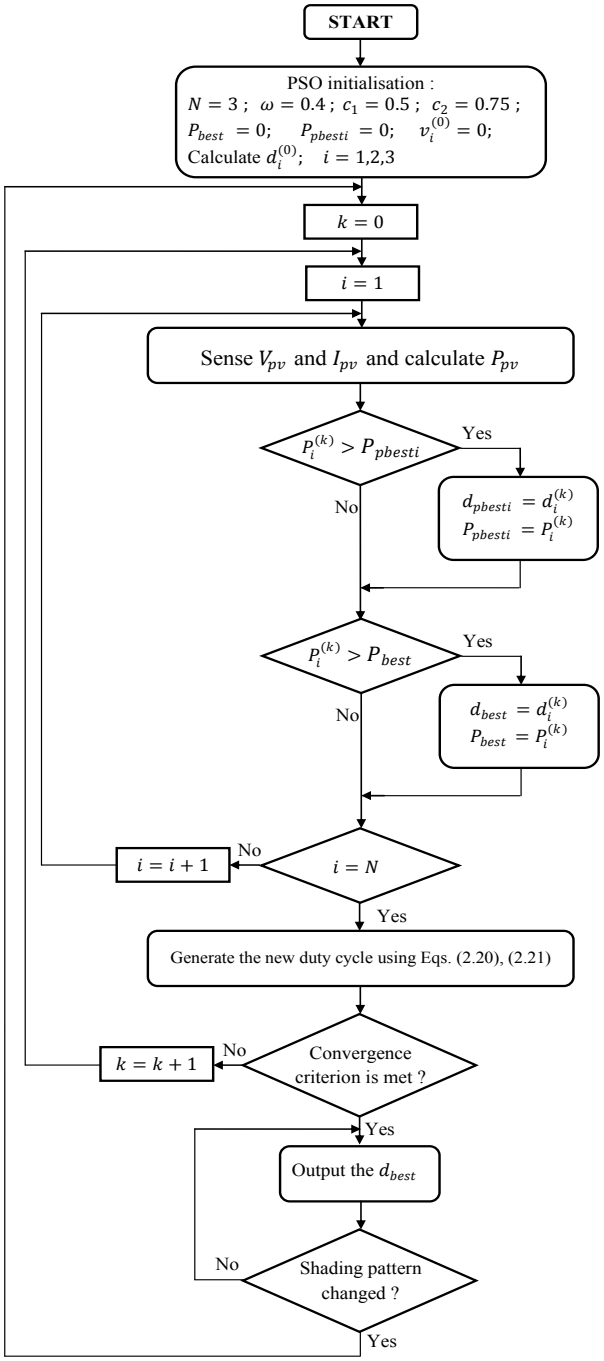

Figure 2.4: Complete flowchart of the proposed PSO method.

Therefore, population size should be chosen in such a way that it ensure good tracking speed and accuracy. To find a tradeoff, three particles are considered in this research.

$$d = (d_i) = (d_1,\ d_2,\ d_3) \tag{2.18}$$

PSO particles are usually randomly initialized in the search space. For the proposed MPPT algorithm, the particles are initialized at fixed points, using the method of the reflective impedance [33]. Then, the first vector of particles is defined in the same way as for the proposed bat algorithm based MPPT.

The purpose of the optimisation process is the maximisation of power extracted from the PV panel, which is defined to be the objective function (P). The fitness value evaluation function is defined as:

$$P(d_i^k) > P(d_{pbesti}) \tag{2.19}$$

where d_{pbesti} is the personal best position of particle i.

Step 2: Update individual and global best duty cycle

For each duty cycle d_i, the corresponding PV output power $P(d_i^k)$ is calculated by multiplying the measured voltage (V_{PVi}) and current (I_{PVi}). Then, the algorithm proceeds to check whether this duty cycle value will result in a better individual fitness value (compared to old P_{besti}). In such case, the personal best position (d_{pbesti}), as well as its corresponding best individual fitness value P_{pbesti}, are updated; otherwise, P_{pbesti} retains its present value. The global best duty cycle, d_{best}, is determined by comparing fitness values of the actual population with the global best PV power achieved, P_{best}.

Step 3: Update Velocity and Position of Each Particle

After the evaluation process, velocity and position of each particle in the swarm are updated. The new duty cycles are then calculated for the each iteration by the equations:

$$v_i^{k+1} = w\, v_i^k + c_1\, r_1 \left(d_{pbesti} - d_i^k\right) + c_2\, r_2 \left(d_{best} - d_i^k\right) \tag{2.20}$$

$$d_i^{k+1} = d_i^k + v_i^{k+1} \tag{2.21}$$

Step 4: Convergence Determination

The algorithm continues the optimisation process until constraint on convergence is satisfied. This algorithm use the same convergence criterion condition used in bat

algorithm based MPPT, shown in the Eq. (2.14). Once convergence criterion is met, the DC-DC converter operates at the optimum duty cycle corresponding to GMPP.

Step 5: Re-initialization

In a PV system, the optimum power point is not constant and global maximum available power usually changes due to varying weather and loading conditions. In such cases, the duty cycles must be reinitialized to search for the new GMPP. If re-initialization process is no carried out properly, updating of personal best duty cycles and global best duty cycle cannot be performed automatically for the change in operating point. As a result, the MPPT algorithm may stuck at some operating point, rather than searching for the new GMPP. Like in the bat algorithm, constraint given in Eq. (2.15) is utilized in the proposed PSO based MPPT to detect the irradiance and shading pattern changes and to reinitialise the search process.

2.5 Differential evolution (DE) algorithm

2.5.1 General overview of DE algorithm

Differential evolution is a stochastic optimization meta-heuristic inspired by genetic algorithms and evolutionary strategies combined with a geometric research technique. Genetic algorithms change the structure of individuals using mutation and crossover, while evolutionary strategies achieve self-adaptation through geometric manipulation of individuals. These ideas were implemented through a simple but powerful operation of mutation of vectors, proposed in 1995 by K. Price and R. Storn [79, 80]. Even though, originally, the differential evolution method was designed for continuous and unrestrained optimization problems, its current extensions can handle mixed-variable problems and handle non-linear constraints [81].

In the DE method, the initial population is generated by uniform random draw on all the possible values of each variable. The lower and upper bounds of the variables are specified by the user according to the nature of the problem. After initialization, the algorithm performs a series of transformations on the individuals, in a process

called evolution. The population contains N individuals. Each individual $x_{i,G}$ is a vector, called target vector, of dimension D, where G denotes the generation:

$$x_{i,G} = (x_{i1,G},\, x_{i2,G},\, ...,\, x_{iD,G})\,; \quad i = 1,\, 2,\, ...,\, N \tag{2.22}$$

The standard DE algorithm uses three techniques: mutation, crossover and selection. At each generation, the algorithm successively applies these three operations to each target vector to produce a trial vector:

$$u_{i,G} = (u_{i1,G},\, u_{i2,G},\, ...,\, u_{iD,G})\,; \quad i = 1,\, 2,\, ...,\, N \tag{2.23}$$

An operation of selection is then performed to choose the individuals to keep for the new generation $(G + 1)$.

2.5.1.1 Mutation

The mutation operation prevents premature local convergence and ensures global convergence in the final stage as all individuals in general evolve to one optimal point. Several mutation schemes are presented in DE literature, recognized by the notation, DE/x/y/z. In this notation, DE stands to "differential evolution", x denotes the vector to be mutated (called base vector), y is the number of difference vectors used, and z specifies the crossover scheme being used (binomial or exponential). The standard mutation operator of DE, denoted DE/Rand/1, needs three randomly selected distinct vectors from the current population for each vector $x_{i,G}$ to generate a so-called donor vector.

The differential mutation operation generates a mutated individual (donor vector) $v_{i,G}$ by :
DE/rand/1:

$$v_{i,G} = x_{r1,G} + F\,(x_{r2,G} - x_{r3,G}) \tag{2.24}$$

Other mutation strategies are used [82] to create the donor vector $v_{i,G}$:
DE/best/1:

$$v_{i,G} = x_{best,G} + F\,(x_{r1,G} - x_{r2,G}) \tag{2.25}$$

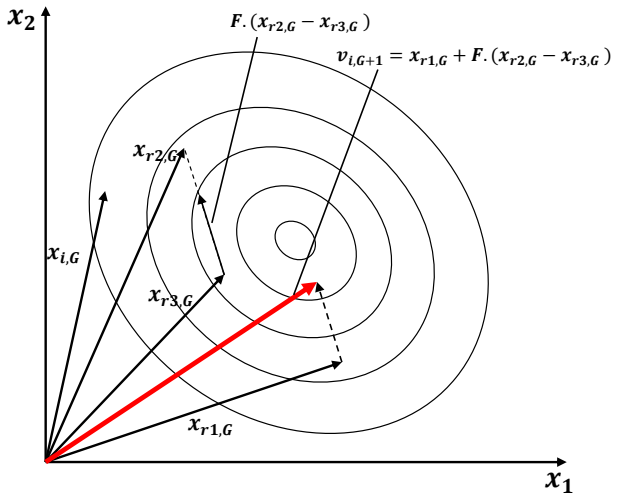

Figure 2.5: Two dimensional example of an objective function (case of minimisation) showing its contour lines and the process for generating the mutation vector in scheme DE/rand/1.

DE/target-to-best/1:

$$v_{i,G} = x_{i,G} + F\left(x_{best,G} - x_{i,G}\right) + F\left(x_{r1,G} - x_{r2,G}\right) \tag{2.26}$$

DE/best/2:

$$v_{i,G} = x_{best,G} + F\left(x_{r1,G} - x_{r2,G}\right) + F\left(x_{r3,G} - x_{r4,G}\right) \tag{2.27}$$

DE/rand/2:

$$v_{i,G} = x_{1,G} + F\left(x_{r2,G} - x_{r3,G}\right) + F\left(x_{r4,G} - x_{r5,G}\right) \tag{2.28}$$

2.5.1.2 Crossover

After the mutation, a crossover operation forms the final trial vector $u_{i,G}$, according to the target vector $x_{i,G}$ and the corresponding donor vector $v_{i,G}$. The crossover operation is introduced to increase the diversity of the perturbed parameter vectors. In DE algorithm, the crossover can be carried out in two ways: binomial (or uniform) and exponential [81]. In the case of binomial crossover, the new vector $u_{i,G}$ is given by:

$$u_{ij,G} = \begin{cases} v_{ij,G} & \text{if} \quad randb(j) \leq Cr \text{ or } j = rnbr(i) \\ x_{ij,G} & \text{otherwise} \end{cases} \quad \text{for} \quad j \in \{1, 2, ..., D\} \tag{2.29}$$

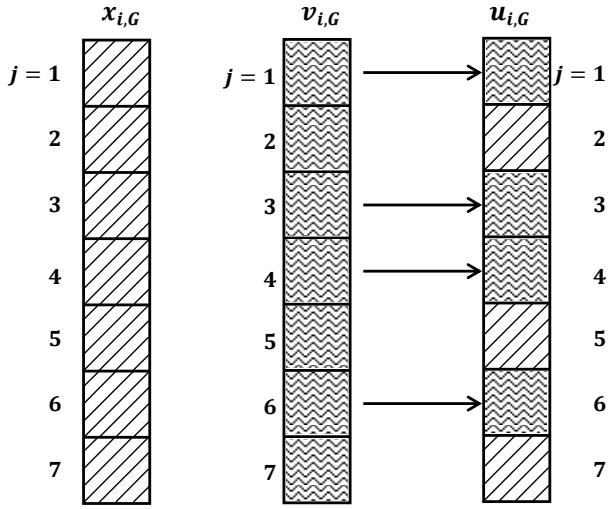

Figure 2.6: Illustration of the crossover process.

where $randb(j) \in [0,1]$ is the j^{th} evaluation of a uniform random number generator. Cr is the crossover parameter (or crossover probability) drawn in the interval $[0,1]$ and is determined by the user. $rnbr(i)$ is an index randomly chosen in $1,2,...,D$ which ensure that $u_{i,G}$ gets at least one element from $v_{i,G}$.

2.5.1.3 Selection

To decide which vector, among $u_{i,G}$ and $x_{i,G}$, must be chosen in the generation $G+1$, we have to compare the objective function values of these two vectors. Indeed, we keep the vector having the greatest value of fitness function in case of maximization. The new vector $x_{i,G+1}$ is chosen according to the following expression:

$$x_{i,G+1} = \begin{cases} u_{i,G} & \text{if} \quad f(u_{i,G}) > f(x_{i,G}) \\ x_{i,G} & \text{else} \end{cases} \tag{2.30}$$

where f is the objective (fitness) function to be maximised.

The population size over generations remains constant. Therefore, the new trial vector replaces the corresponding target vector in the next generation if it provides higher value of the objective function. Otherwise, the target vector is retained in the population. This selection criterion never decreases the fitness status because it either improves, or remains the same.

2.5.2 Application of DE algorithm for MPPT

The DE algorithm is used to realize a MPPT controller for photovoltaic system under partially shaded conditions. A new mutation strategy is proposed to improve the performance of the conventional DE algorithm and enhance the speed of the tracking process. The different operations of the DE algorithm, mainly the mutation, the crossover and the selection are executed until satisfying the convergence criterion and obtaining of the optimum individual. Regarding the structure of the control, the one based on direct duty cycle control is chosen. In this structure, the PI control loops are eliminated and the PWM signal for control of the DC-DC converter is generated directly by the MPPT controller. This control scheme has the advantage of making the control structure simpler [42]. Flowchart of the proposed DE based MPPT technique is shown in Fig. 2.7. The operating principles of proposed technique can be described as follows:

Initialisation

In order to establish a starting point for the optimization process, an initial population of individuals should be created. Individuals in the population are called target vectors and the first generation of the population in the DE algorithm is randomly generated or positioned in deterministic way in the search space.

For the application of DE for MPPT, the duty cycle of the PWM signal is chosen to be the control variable. Then, the duty cycle of DC-DC converter is used as target vector and fitness function, f is defined as the maximum of PV output power ($f = max(P)$). In order to start the tracking process, a solution vector of three duty cycles is defined as:

$$d_G = (d_{i,G}) = (d_{1,G},\ d_{2,G},\ d_{3,G}) \tag{2.31}$$

For the proposed MPPT algorithm, the individuals are initialized at fixed points, using the method of the reflective impedance [33]. Then, the first vector of duty cycles is defined in the same way as for the proposed bat algorithm based MPPT. To evaluate the duty cycles, the MPPT controller successively outputs the PWM signal according to the value of d_i.

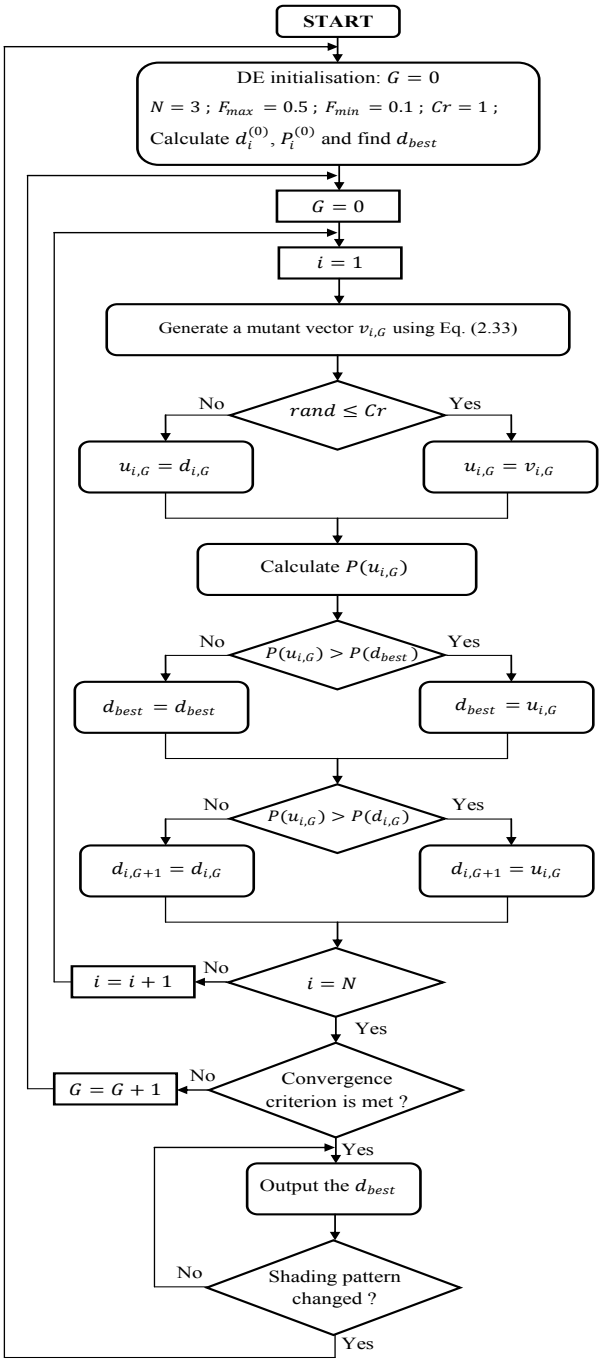

Figure 2.7: Complete flowchart of the DE proposed method.

Mutation

A mutation vector is generated for each duty cycle at each generation by the addition of a scaled, randomly selected, vector difference to the best duty cycle. The mutant

vector is calculated according to the relations Eqs. (2.32) and (2.33).

$$F_G = \begin{cases} F_{max} - (F_{max} - F_{min}) \dfrac{G}{G_{max}}; & G = 0,\ 1,\ 2,\ ...,\ G_{max} \\ F_{min}; & G > G_{max} \end{cases} \tag{2.32}$$

$$v_{i,G} = d_{best,G} + F_G \left(d_{r1,G} - d_{r2,G}\right) \tag{2.33}$$

An adaptive form is adopted to tune the mutation factor F in order to accelerate the speed of convergence. Indeed, this factor is gradually reduced from a value F_{max} to a value F_{min}. This linear decrease is justified by the fact that choosing F large at the beginning of the optimization process allows a better exploration of the search space. During the iterations, F is gradually decreased to a minimum value, F_{min}, which allows a better convergence towards the optimal duty cycle. This mutation strategy makes the DE algorithm to have a high speed of convergence towards the MPP while at the same time ensures the increase of the diversity of solutions in the population.

Since the chosen population size is 3, the vectors indices, $r1$ and $r2$, will be limited in value once the index i of the mutant vector is chosen. For example, for the calculation of mutant vector v_1, two cases are considered for the term $(d_{r1} - d_{r2})$ at each iteration: either $(d_2 - d_3)$ or $(d_3 - d_2)$. Same for vector v_2 where $(r1, r2)$ can take two values; either $(1, 3)$ or $(3, 1)$. To avoid each time the comparison between the indices i, $r1$ and $r2$ and to simplify the selection method of the two duty cycles used for the calculation of the corresponding mutant vector , an implementation of the equation (2.33) is adopted as shown on Eqs. (2.34) to (2.36):

$$v_{i,G} = d_{best,G} + F_G.S.\left(d_{r1,G} - d_{r2,G}\right) \tag{2.34}$$

with

$$S = \begin{cases} 1 & \text{if} \quad rand_i \leq Mu \\ -1 & \text{otherwise.} \end{cases} \tag{2.35}$$

and

$$(r_1, r_2) = \begin{cases} (2,3) & \text{if} \quad i = 1 \\ (1,3) & \text{if} \quad i = 2 \\ (1,2) & \text{if} \quad i = 3 \end{cases} \tag{2.36}$$

The parameter, $Mu \in [0,1]$, is a user-defined value and $rand_i \in [0,1]$ is a number randomly drawn from a uniform distribution for each index i. In this work, Mu is set to be 0.5.

Crossover

To complement the differential mutation strategy, a crossover operation is performed to form the final trial vector $u_{i,G}$, according to the target vector $d_{i,G}$ and the corresponding donor vector $v_{i,G}$. Binomial crossover is used to create the trial vector $u_{i,G}$ as:

$$u_{i,G} = \begin{cases} v_{i,G} & \text{if} \quad rand_i \leq Cr \\ d_{i,G} & \text{otherwise.} \end{cases} \tag{2.37}$$

where $rand_i \in [0,1]$ is a uniform random number. Since the vector solution (duty cycle) is one-dimensional vector, the crossover probability Cr is set to be 1 to avoid at maximum that the trail vector duplicates the target vector.

Selection

If the trial vector, $u_{i,G}$, leads to higher PV output power value than that of its target vector, $x_{i,G}$, it replaces the target vector in the next generation; otherwise, the target vector retains its place in the population for at least one more generation. The new vector $d_{i,G+1}$ is chosen according to the following expression:

$$d_{i,G+1} = \begin{cases} u_{i,G} & \text{if} \quad P(u_{i,G}) > P(d_{i,G}) \\ d_{i,G} & \text{otherwise.} \end{cases} \tag{2.38}$$

where P is the output power of the photovoltaic panel.

Convergence determination

The process of mutation, recombination and selection is repeated until a pre-specified termination criterion is satisfied. The proposed DE algorithm use the same convergence criterion condition used in bat algorithm based MPPT, shown in the Eq. (2.14). If the absolute difference between each two different duty cycles is less than a threshold Δd, then the computation process carried by the proposed DE technique will stop and the operating point is maintained by d_{best}.

Re-initialization

The characteristics of photovoltaic generators are time varying and change dynamically according to several factors, especially the metrological conditions. As a result, the optimum power point is not constant and global maximum available power will shift to another location depending on the shading pattern. In such cases, the duty cycles must be reinitialized to search for the new GMPP. Like in the bat algorithm, constraint given in Eq. (2.15) is utilized in the proposed DE based MPPT to detect the irradiance and shading pattern changes and to reinitialise the search process.

2.6 Conclusion

In this chapter, the designing procedures of BA, PSO and DE based MPPT are described in details. The comprehensive analysis of every aspects is followed by the detail flowchart. The next chapter discusses the software implementation and the GMPP tracking simulation results under partial shading conditions.

CHAPTER 3

SIMULATION OF THE PROPOSED GLOBAL SEARCH MPPT CONTROLLERS

Contents

3.1 Introduction

SINCE the energy provided by the photovoltaic (PV) system depends on the atmospheric conditions like temperature and irradiance, a stage of adaptation is inserted between the photovoltaic panel and the load to extract the maximum of the available power. This stage is a conjunction of a DC-DC converter and a maximum power point tracker (MPPT).

At the uniform irradiance conditions, i.e. when the PV panel receives homogenous irradiance, the PV panel exhibits a single MPP. By contrast, when some part of the PV panel receives different irradiance than others, then it is subjected to partial shading. When partial shading occurs, the *P-V* characteristic curve becomes multimodal. The *P-V* curve is characterised then by the appearance of several maximum power point: several local maximum power point (LMPP) and one global maximum power point (GMPP). If the true GMPP is not properly tracked, the MPPT algorithm might be trapped at one of the local peak, with the consequence of significant power losses [83].

This chapter presents the GMPP tracking results for the proposed MPPT controllers, BA, PSO and DE, respectively during partial shading. The idea is to locate the GMPP for any type of *P-V* curve regardless of environmental variations. This is made possible due to the ability of these techniques to handle non-linear objective functions effectively using relatively simple algorithm. First, a description of system model of a standalone PV system developed in this work to test the proposed global search techniques is given. The behaviour of the proposed techniques is clarified under different dynamic shading patterns. Therefore, the performance of the proposed techniques are discussed and compared in term of tracking speed, accuracy and partial shading handling capability. Furthermore, to clarify the steady state performance under partial shading, the proposed techniques are tested under extreme shading condition including 10 different shading patterns.

3.2 Description of the studied PV system

To verify the effectiveness of the proposed algorithms, a photovoltaic system is simulated on Matlab/Simulink. The different blocks constituting the model are shown in Fig. 3.1. The photovoltaic panel used consists of four SM55 photovoltaic modules connected in series. The photovoltaic module is modeled according to the model of two-diode. Using only the datasheet information of the PV module, the different PV module parameters are calculated at any irradiance and temperature point and the photovoltaic panel output voltage is determined by the Newton-Raphson iterative method [15,84].

The DC-DC converter used is a buck-boost converter. It is designed for continuous conduction current mode with the following specifications: $C_1 = 440\ \mu$F, $C_2 = 330\ \mu$F, $L = 0.7$ mH and a chopping frequency of 50 kHz.

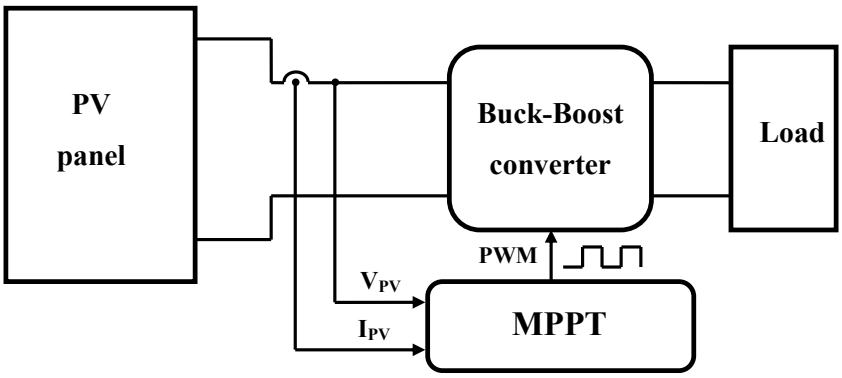

Figure 3.1: Block diagram of the proposed PV system.

3.3 *P-V* shading curves (dynamic shaded conditions)

Initially, the controllers are tested for three different configurations of partial shading. Fig. 3.2 shows the various *P-V* characteristics corresponding of the configurations as well as the sequence of test. The first *P-V* curve is characterized by the presence of five (5) maximum power points. The global maximum point is located to the right of this curve. The second configuration presents partial shading with the moving of global maximum power point to the middle of the *P-V* curve whereas this point moves to the left in the third configuration. Each shading configuration lasts 5 s.

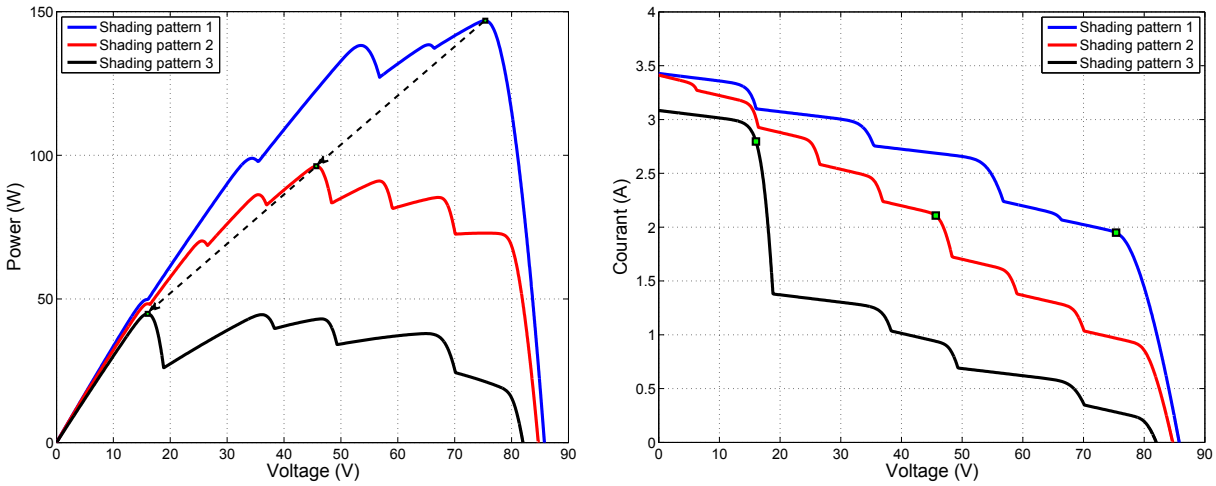

(a) (b)

Figure 3.2: (a) *P-V* and (b) *I-V* curves used in the simulation.

3.4 Tracking of GMPP using BA based MPPT

The parameters used in the implementation of the BA-MPPT algorithm are as follows: $N = 3$, $w = 0.4$, $\alpha = 0.9$, $\gamma = 0.6$, $\Delta d = 0.01$ and $\Delta P = 0.05$. After applying each duty cycle, we should wait for the transient condition to settle. Indeed, the time required for the system to reach the steady state can vary according to the difference between two successive duty cycles. This difference can be more or less important, which affects the dynamics of the DC-DC converter and its settle time. To determine the appropriate sampling time for the MPPT controller, the tracking response is analysed when the PV system is subjected to uniform irradiance of $G = 1000$ W/m^2. Starting with an initial sample time of 0.1 s, the tracked voltage is examined to determine the optimal sample time which permits to the system to reach the steady state. Fig. 3.3 presents the tracked PV voltage using the bat algorithm. From this figure, it can be noticed that the settle time of the system varies. Therefore, an appropriate choice of the sampling time for the MPPT controller is required in order to have correct samples of PV current and PV voltage. If wrong values of PV current and PV voltage are sensed (measured in transient state of the system), the considered PV power values will be wrong. Therefore, the determination of the best duty cycle may be affected, which can influence the accuracy of the tracking of maximum power point. From

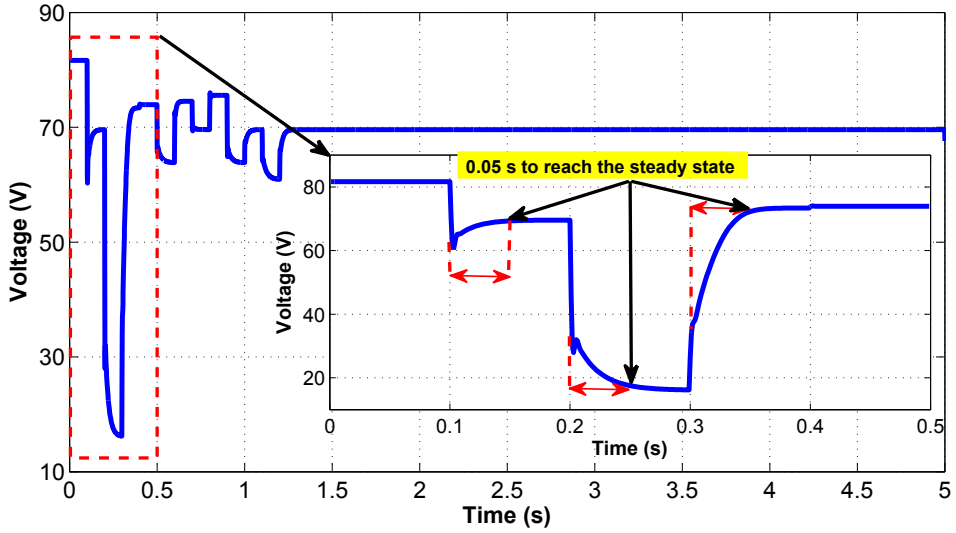

Figure 3.3: Determination of BA based MPPT sampling time.

Fig. 3.3, it can be noticed that 0.05 s is a reasonable choice.

Fig. 3.4 shows the results of the dynamic tracking. Initially, the bat algorithm transmitted the first solution vector (the first three duty cycles) and begins the optimization process. It can be seen that the proposed bat algorithm is able to distinguish between the global maximum ($P_{GMPP} = 146.85$ W) and the local maximas. At $t = 5$ s, the configuration of the shading changes. The proposed algorithm detects this change through information on the power of the photovoltaic panel that changes from $P = 146.85$ W to $P = 86.8$ W. The process of the tracking is then re-initialised and the algorithm has successfully locates the new global maximum which corresponds to $V = 45.63$ V and $I = 2.11$ A. At $t = 10$ s, the global maximum is shifted to the left of the P-V curve. The power of the photovoltaic panel has changed from $P = 96.21$ W to $P = 39.3$ W, and the condition of re-initialisation is then satisfied. The proposed algorithm has re-initialised the searching process and the new GMPP is also detected.

As mentioned in the Chapter 2, the proposed bat algorithm uses a technique of automatic switching between the exploration stage (global search) and exploitation stage (local search). To illustrate this failover, we can define the function S as follows

$$S = \begin{cases} 1 & \text{if} \quad d = d_{global} \\ 0 & \text{if} \quad d = d_{local} \end{cases} \tag{3.1}$$

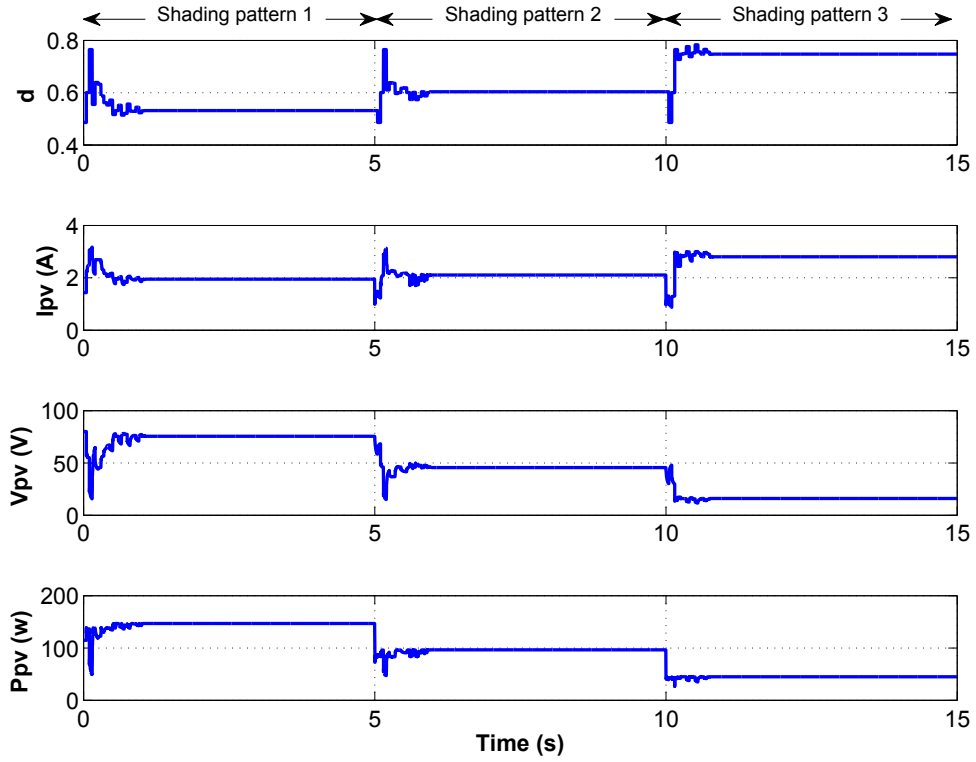

Figure 3.4: Variation of duty cycle, current, voltage and power of the PV system during GMPP tracking using BA based MPPT.

Fig. 3.5 shows the variation of the function S as a function of time. The function S is 1 when the duty cycle resulting from the global search is selected. Otherwise, when the duty cycle from the local search that is selected, the function S is 0. For example, consider the first configuration of the shading shown on the zoom of the Fig. 3.5. A MPPT cycle is achieved after evaluating all the three duty cycles. Therefore, a MPPT cycle corresponds to three perturbations. For the first vector of solutions, it is assumed that this is a global search. This assumption is justified by the fact that the first three duty cycles are selected to "explore" efficiently the search space. Therefore, S is initially 1.

In the second MPPT cycle, it can be noticed that the algorithm has applied an automatic zoom to the region where the best duty cycle is located (the duty cycle which gives the best value of photovoltaic panel power). In this cycle, it is the local search that is selected for the three duty cycles. Automatic switching between the stage of exploration and exploitation appears significantly in the third MPPT cycle. For the

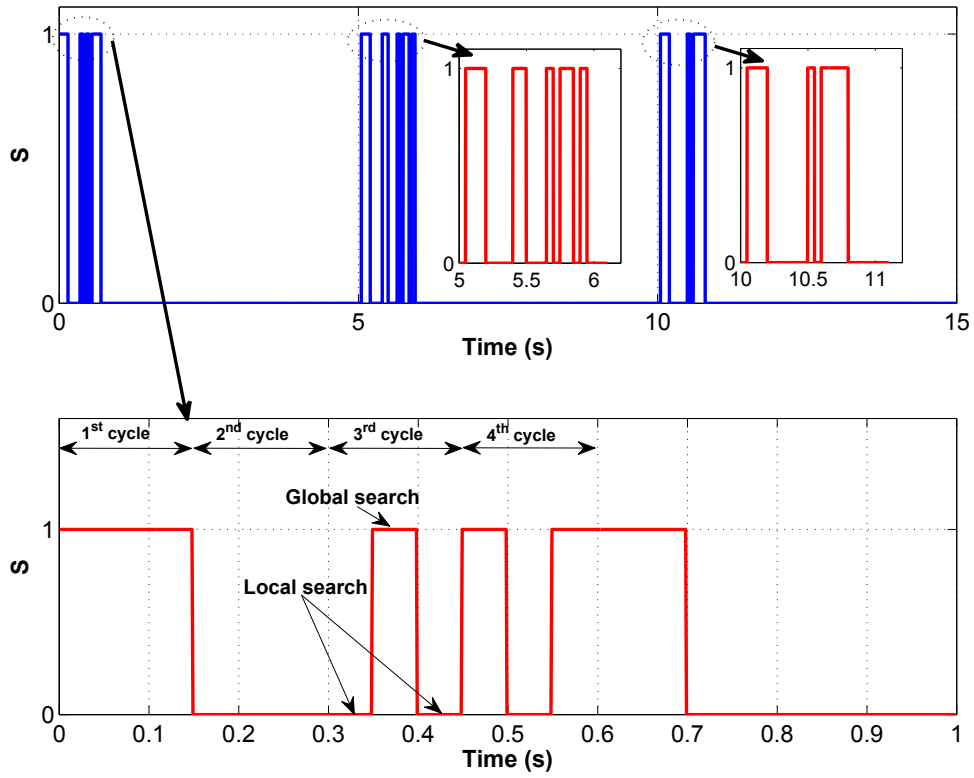

Figure 3.5: Variation of type of search (global or local) during the BA-MPPT process.

first and third duty cycle, it is the local search that is selected while for the second, it is the duty cycle generated from the global search that is chosen. Therefore, the exploration-exploitation tradeoff is very strong. This feature allows the bat algorithm to have a quick convergence rate towards the global maximum without falling into the trap of premature convergence. The advantages of the proposed algorithm appear also in the selection of the algorithm parameters. Many metaheuristics applied to MPPT use either fixed parameters (for standard versions) or adaptive parameters (in enhanced versions). In this second case, the tuning of the parameters is generally done depending on iterations. In contrast, the proposed bat algorithm uses parameter control. Indeed, the values of the algorithm parameters (A and r) are updated not only according to the iterations, but also according to the values of the objective function and loudness. This strategy provides a mechanism of automatic switching from exploration to exploitation when the global maximum is approached.

3.5 Tracking of GMPP using PSO based MPPT

The performances of the PSO algorithm are tested under the considered partial shading patterns. The parameters used for PSO algorithm are $w = 0.4$, $c_1 = 0.5$ and $c_2 = 0.75$, $\Delta d = 0.01$ and $\Delta P = 0.05$. These parameters are selected after a series of simulation on the shading configurations under test; therefore, it can be confirmed that the selected combination (w, c_1, c_2) is optimal. The first population, the convergence criterion and that of re-initialisation are the same as for the proposed bat algorithm. The sampling time for the MPPT controller is 0.05 s. This allows the DC-DC converter to reach the steady state, and as a result having correct sample of voltage and current. Fig. 3.6 shows the tracked duty cycle, current, voltage and power for PSO. Initially, the tracking process starts by sending the initial particles in the first population to the power converter. During the search for the global MPP, the exploration of P-V curves results in operating point fluctuations as can be clearly observed

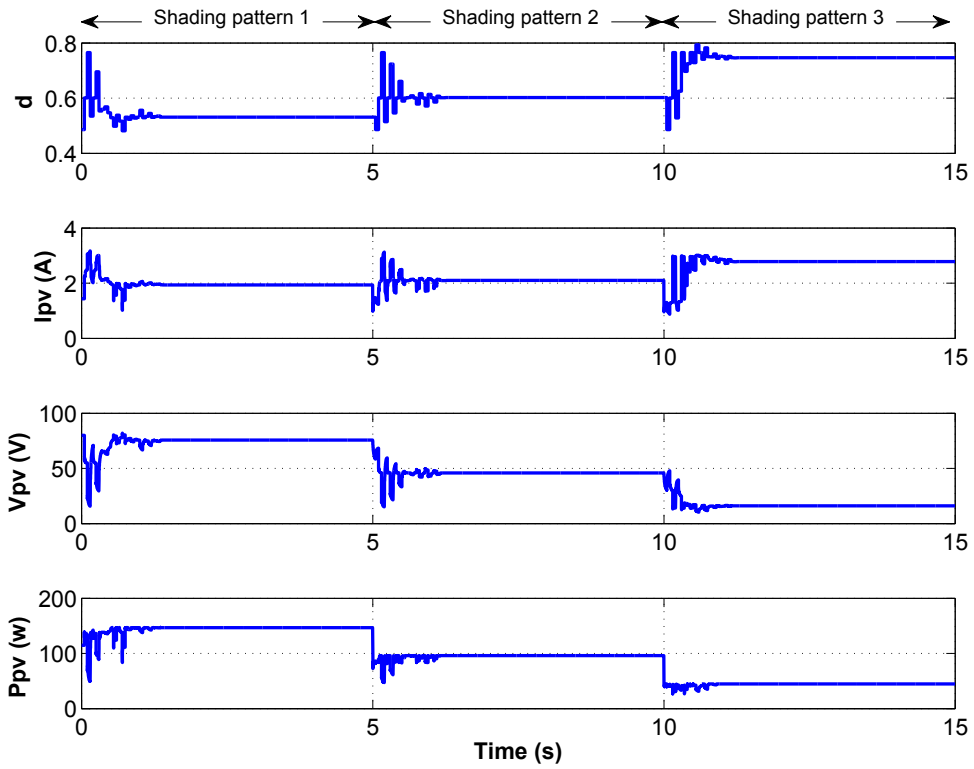

Figure 3.6: Variation of duty cycle, current, voltage and power of the PV system during GMPP tracking using PSO based MPPT.

by the rapid variation in d as shown in Fig. 3.6. The PSO algorithm successfully locates the GMPP, which corresponds to $V = 75.73$ V and $I = 1.94$ A. This operating point is maintained until further change in array power triggers the threshold value in equation (2.15). When a change in shading pattern occurs at $t = 5$ s, the operating point in term of voltage and current changes. Thus, even though the duty cycle is unchanged, a change in array power is detected by the algorithm and satisfies condition in Eq. (2.15). Consequently, the optimisation process is re-started by sending the initial population of particles to the power converter. It can be seen that the PSO technique correctly tracks the corresponding GMPP at $V = 45.86$ V and $I = 2.10$ A within 7 sampling cycles. At $t = 10$ s, another large change in irradiance is detected by the algorithm. As before, the PSO realized the sudden reduction in power using Eq. (2.15) and re-initialised the tracking process by sending three duty cycles. After 24 perturbations, the proposed algorithm successfully tracks the new global MPP. The corresponding array power, voltage and current are 44.82 W, 16.10 V and 2.78 A, respectively. It can be seen that the fluctuations in operating voltage and current consistently decreases with the increment in iteration number. Therefore, once the algorithm manages to reach at MPP, the duty cycle value remains at the converged point until subsequent irradiance change is detected.

3.6 Tracking of GMPP using DE based MPPT

To evaluate the performance of the proposed DE algorithm in dealing with partial shading conditions, the proposed DE technique is tested with three different partial shading patterns and its performance is evaluated based on the tracking speed and accuracy. The parameters used for DE based MPPT controller are as follows: $F_{max} = 0.5$, $F_{min} = 0.1$, $Cr = 1$, $\Delta d = 0.01$ and $\Delta P = 0.05$. Fig. 3.7 shows the tracking response of duty cycle, voltage, current and power. Initially, the tracking process starts by sending the initial individuals in the first population to the power converter. In third generations, the proposed algorithm successfully tracks the global MPP. The corresponding array power, voltage and current are 164.85 W, 75.49 V and 1.94 A,

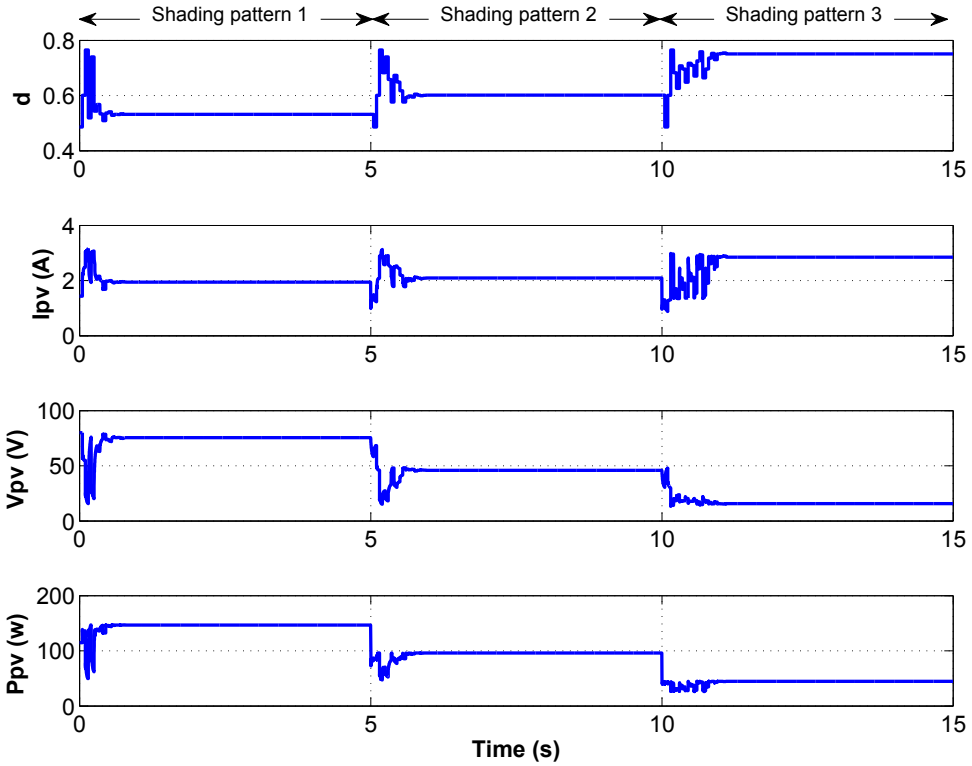

Figure 3.7: Variation of duty cycle, current, voltage and power of the PV system during GMPP tracking using DE based MPPT.

respectively . This operating point is maintained until subsequent irradiance change is detected by equation (2.15).

For better insight of the evolutionary process and the method of generating the new duty cycles at each MPPT cycle, the zoom of the tracking of the GMPP under the first configuration of the shading is illustrated in Fig. 3.8. Initially, the first duty cycle, calculated by Eqs. (2.7) to (2.9), are successively sent to the buck-boost converter. Among them, the duty cycle d_2 is the best duty cycle since it gives the best PV power value. By mutation, the proposed DE algorithm generates three mutant duty cycles around d_2 (which is d_{best}) according to the equation (2.34). These new duty cycles are then transmitted to the DC-DC converter in the second MPPT cycle to evaluate the power of the photovoltaic system and select the new generation. Since the mutation factor F is initially equal to F_{max}, the difference between these duty cycles is initially large. This difference becomes smaller and smaller during the tracking process until satisfying the convergence criterion. The large initial value of F has the advantage

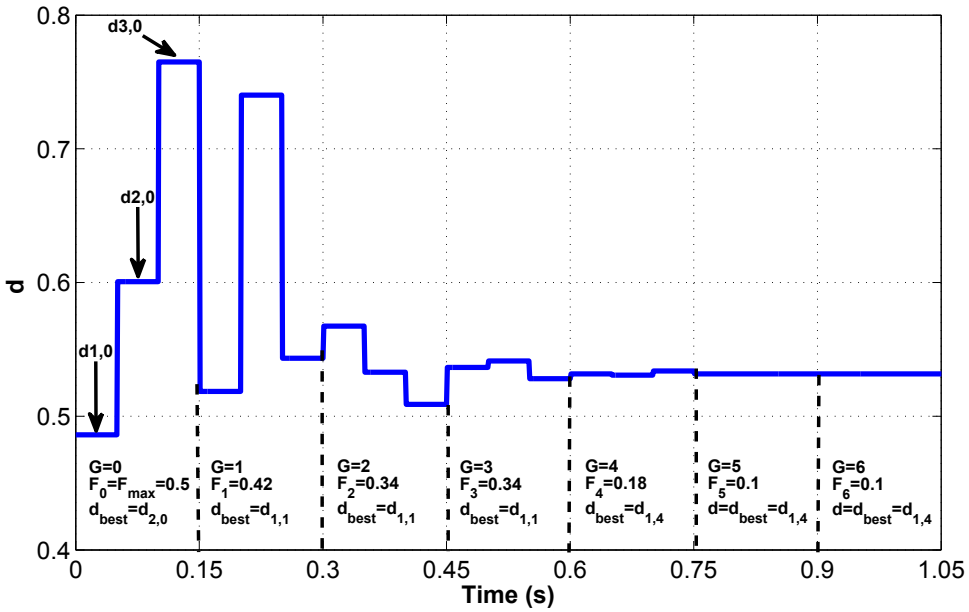

Figure 3.8: Duty cycle response during evolutionary process.

of allowing a better exploration of the search space while the progressive decrease of this factor makes possible the increasing of the tracking speed without falling in the problem of premature convergence. Once the algorithm manages to reach at MPP, the duty cycle value remains at the converged point until subsequent irradiance change is detected. Fix duty cycle at the exact MPP is highly beneficial because the steady-state oscillation around the MPP is completely diminished. As can be seen from Fig. 3.7 that when the shading pattern changed at $t = 5$ s, the proposed DE algorithm detects a significant change in the array power and responds by initializing the tracking procedure. The evolutionary process including mutation, crossover and selection is then commences and the process continues until all the duty cycles in the population converge. The duty cycle has successfully converge at $d = 0.6$ in 18 perturbations, i.e. 6 generations and the correct MPP is reached at $V_{MPP} = 45.94$ V and $I_{MPP} = 2.09$ A. The corresponding MPP value is 96.14 W which is 99.92% from ideal MPP value of 96.87 W. In third condition at $t = 10$ s, the shape of the I-V and P-V curves change with the changes in the shading pattern. Again, the reduction in array power satisfies the condition in Eq. (2.15) and hence the re-initialization process is restarted. The initial population of duty cycles are evaluated and the loop of mutation, crossover and selection are continuously repeated until the new GMPP is found. The same process

continues and finally after ten perturbations all particles converge around $d = 0.75$. Once again, the algorithm proves to be capable of locating the new MPP accurately. The new GMPP is found after 21 perturbations. The corresponding tracked voltage and current are 15.73 V and 2.84 A, respectively. The tracking accuracy is 99.78%.

3.7 Tracking of GMPP using P&O based MPPT

The performances of the meta-heuristic algorithms are compared with the conventional P&O algorithms. Fig. 3.9 shows the results obtained by the P&O algorithm. A fixed perturbation step of $\Delta d_{P\&O} = 0.01$ is imposed every 0.05 s. For the first configuration, the P&O algorithm has successfully located the GMPP, which is found to the right of the *P-V* characteristic. For the other configurations, the algorithm could not distinguish the GMPP from LMPPs and trapped in a LMPP. These results prove the inability of the P&O algorithm to handle the case of partial shading.

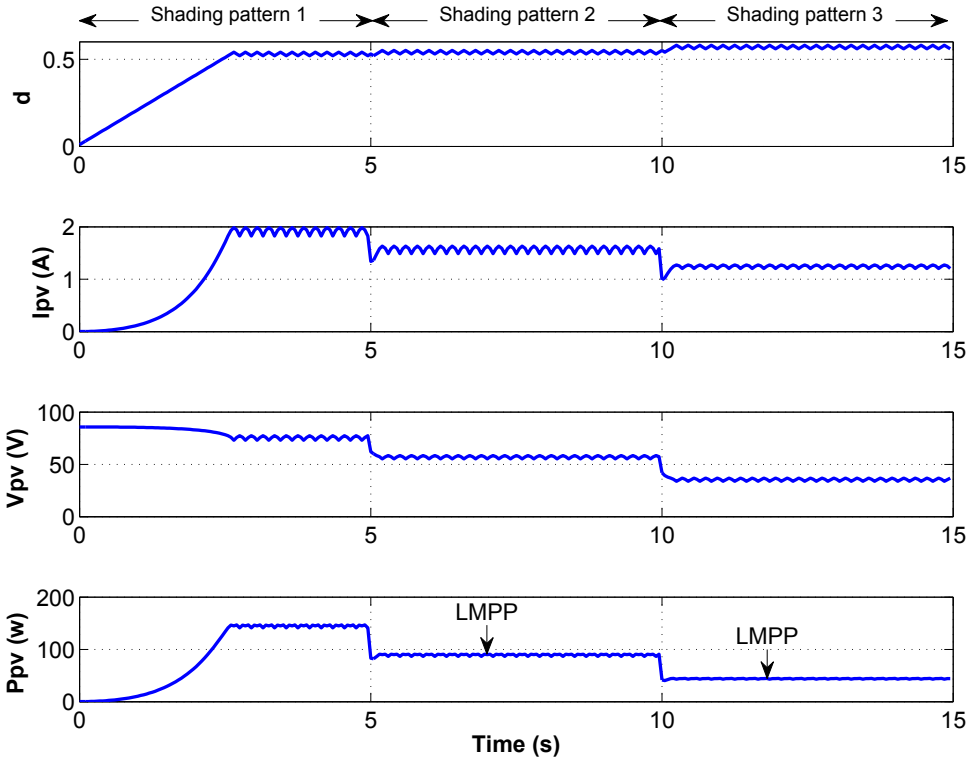

Figure 3.9: Variation of duty cycle, current, voltage and power of the PV system during GMPP tracking using P&O algorithm.

3.8 Comparative evaluation

The tracking performances of the soft computing global search MPPT techniques; BA, DE and PSO are evaluated and compared in terms of the tracking speed and accuracy. As a benchmark, their performance to handle the partial shading condition is compared with the conventional P&O technique.

3.8.1 Handling of partial shading

As can be noticed from the previous waveforms of tracking, BA, DE and PSO techniques have detected the changes in the shading configurations and the re-initialisation of the MPPT process. They also successfully located the global maxima in the three configurations of partial shading. On the other hand, the performance of P&O degrades significantly under partial shading conditions as it often stuck in a LMPP. For the first shading pattern, the global MPP is situated at the right side of the *P-V* characteristic curve. The procedure tracking of the P&O algorithm starts by transmitting the first duty cycle to the DC-DC converter. The value of the initial duty cycle is 0.02, which results in a voltage in the vicinity of open circuit voltage. The procedure of perturbing the duty cycle continues until tracking the first peak. Then, the P&O oscillates around this peak which is fortuitously the global one. For the second and the third configuration of shading, it can be seen that P&O algorithm erroneously identifies the local peak as the GMPP due to the inability of the algorithm to differentiate the local and global peak. In these two scenarios, P&O algorithm failed to track the global MPPs and trapped in LMPPs. These results prove the superiority of the metaheuristic techniques over the conventional P&O algorithm to handle the multimodal *P-V* characteristic curves under partial shading conditions.

3.8.2 Tracking speed

An attractive characteristic of good MPPT methods is their high convergence speed. However, it is a difficult task to sort tracking speed because a fair comparison is hard to be reach among MPPT techniques. In this work, the speed of tracking is estimated

by the capability of the meta-heuristic technique to meet the convergence criterion. As mentioned before, the proposed techniques stop the optimization process when the absolute difference between each two different duty cycles is less than a threshold. Then, the number of iterations (perturbations) to meet this criterion are recorded and multiplied by the sampling period of the MPPT controller. The result of this multiplication is considered to be the speed of convergence. A MPPT cycle is achieved after evaluating all the three duty cycles. Therefore, a MPPT cycle corresponds to three perturbations. Table 3.1 summarizes the tracking speed performance of the three algorithms. As can be observed, the Bat and DE algorithms are superior in term of its tracking convergence compared to the PSO technique. For the first shading pattern, the DE algorithm achieved the GMPP tracking faster. It takes only 5 MPPT cycles to settle at the GMPP. PSO algorithm is the slower one and takes 9 MPPT cycles (27 perturbations) to meet the convergence criterion whereas the BA method takes only 7 cycles. It can be noticed from Fig. 3.5 that the BA method locates the region of the GMPP in less than 5 MPPT cycles and activates only the local search after 15 perturbations. For the second shading configuration, bat and DE algorithms perform 18 perturbations to reach the steady state, less than the PSO algorithm by 4 perturbations. In the third shading pattern, the PSO algorithm lasts 8 MPPT cycles and the bat algorithm requires only 5 MPPT cycles to settle at the GMPP. In this case, DE algorithm has difficulties to meet the convergence criterion. Nevertheless, it tracking speed is superior to PSO algorithm.

Table 3.1: Tracking convergence speed during partial shading test.

Shading pattern N°	Tracking speed (s)		
	BA	PSO	DE
Shading pattern 1	1.05	1.35	0.75
Shading pattern 2	0.90	1.10	0.90
Shading pattern 3	0.75	1.20	1.05

3.8.3 Steady-state and dynamic MPPT response

As reported before, the studied soft computational techniques have the ability to track the GMPP and can handle the partial shading with high accuracy. This is supported by the results of the calculation of the static and dynamic efficiency. The static efficiency is given by

$$\eta_{static} = \frac{P_{MPPT}}{P_{max}} \tag{3.2}$$

with P_{mppt} is the power obtained in the steady state condition and P_{max} is the maximum power available on the photovoltaic panel.

The dynamic performance takes into account the transient time and the steady state condition. It is calculated as

$$\eta_{dynamic} = \frac{\int_0^T P_{PV}\,\mathrm{d}t}{\int_0^T P_{max}\,\mathrm{d}t}.100 = \frac{\int_0^{15} P_{PV}\,\mathrm{d}t}{\int_0^{15} P_{max}\,\mathrm{d}t}.100 \tag{3.3}$$

Table 3.2 shows the results of the tracking in steady state condition. In the three PS conditions, the three meta-heuristic techniques are capable of searching and reaching the right MPP with high accuracy. In term of the steady-state tracking accuracy, all these algorithms are basically at the same par. This is due to the fact that these algorithms are all global search techniques and work with close principles. The main difference is the manner to update the new duty cycles in the population. Table 3.3 reports the results of the calculation of the dynamic efficiency of BA and PSO and DE. It can be observed that the bat algorithm gives the best results in static and presents the best dynamic behaviour. Although the PSO and DE algorithms present good static efficiency, the fluctuations in the voltage are very high compared to the BA algorithm. These fluctuations appear significantly in the third case of shading pattern for the DE algorithm and with a less degree for PSO algorithm. This is due to the evolution nature of the DE algorithm and the inability of exploitation of best solution found in some cases. From Table 3.3, we can notice the superiority of BA based MPPT over the other techniques in terms of dynamic tracking behaviour. These results are justified by the fact that the bat algorithm combines the global search and local search in the optimization process. This combination avoids large fluctuations and disturbances in

the photovoltaic panel voltage and provides better control of the search space.

Table 3.2: Comparison between BA, PSO and DE based MPPT methods in steady state condition.

Shading pattern N°	Ideal power P_{max} (W)	Power obtained P_{MPPT} (W)			Static efficiency η_{static} (%)		
		BA	PSO	DE	BA	PSO	DE
Shading pattern 1	146.87	146.85	146.72	146.85	99.98	99.90	99.98
Shading pattern 2	96.22	96.21	96.19	96.14	99.98	99.97	99.92
Shading pattern 3	44.83	44.82	44.82	44.73	99.97	99.97	99.78

Table 3.3: Dynamic tracking performance comparison between BA, PSO and DE based MPPT techniques.

	BA	PSO	DE
Dynamic efficiency $\eta_{dynamic}$ (%)	98.36	97.87	97.81

3.9 Test under extreme shading configurations

The tracking performance of the proposed method is tested using ten different *P-V* curves, as shown in Fig. 3.10. These curves are generated by imposing various shading patterns on the PV array model. The first curve is the normal condition with uniform irradiation whereas the subsequent curves are partial shading curves. The *P-V* characteristics corresponding to these configurations provide an example of the influence of partial shading on the output power of the photovoltaic panel. These *P-V* curves can have different number of MPP and the location of the GMPP is variable, making its tracking difficult. Table 3.4 summarizes the tracked voltage, current, and power for the bat, PSO and DE techniques for the considered configurations of shading. As shown in Table 3.4, the proposed methods have accurately located the GMPP for all given shading conditions.. It can be seen that they yield more than 99% static efficiency for all the cases studied.

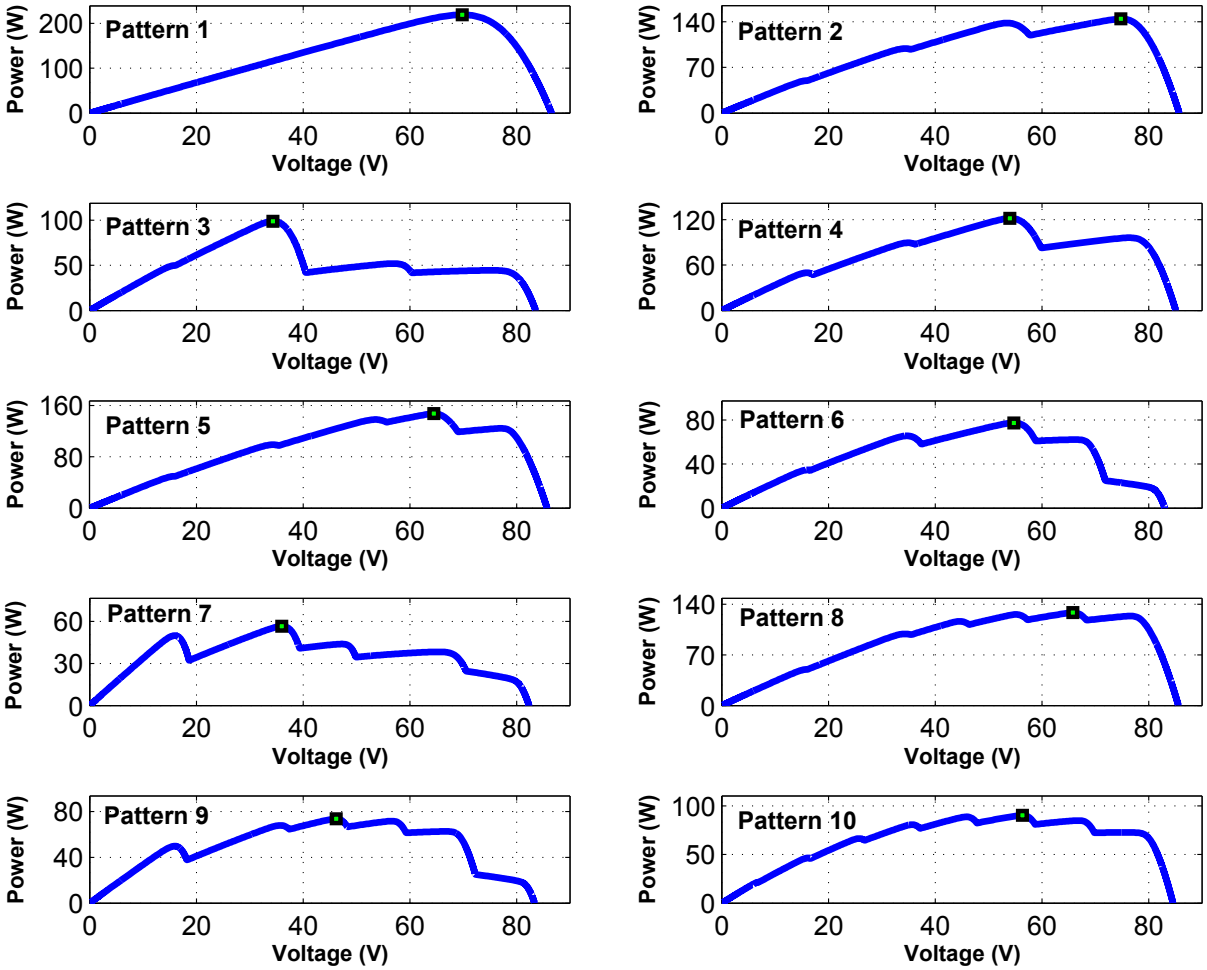

Figure 3.10: Ten (10) different sets of *P-V* curve used in the simulation.

Table 3.4: Steady state tracking results for BA, PSO and DE based MPPT techniques under various shading patterns.

	Shading pattern (1 = 1000 W/m^2)								Global peak values			BA-MPPT			PSO-MPPT			DE-MPPT			Static efficiency		
	G_{11}	G_{12}	G_{21}	G_{22}	G_{31}	G_{32}	G_{41}	G_{42}	V_{GMPP} (V)	I_{GMPP} (A)	P_{GMPP} (P)	V_{MPPT} (V)	I_{MPPT} (A)	P_{MPPT} (P)	V_{MPPT} (V)	I_{MPPT} (A)	P_{MPPT} (P)	V_{MPPT} (V)	I_{MPPT} (A)	P_{MPPT} (P)	BA (%)	PSO (%)	DE (%)
1	1	1	1	1	1	1	1	1	69.78	3.15	219.25	69.6	3.15	219.24	69.6	3.15	219.24	69.6	3.15	219.24	99.99	99.99	99.99
2	1	1	0.9	0.9	0.8	0.8	0.6	0.6	74.88	1.94	144.64	75.04	1.93	144.62	74.12	1.95	144.33	73.79	1.95	144.05	99.98	99.79	99.59
3	1	1	0.9	0.9	0.3	0.3	0.2	0.2	34.37	2.88	98.96	34.94	2.82	98.65	35.23	2.79	98.2	34.85	2.83	98.74	99.68	99.23	99.78
4	1	1	0.8	0.8	0.7	0.7	0.4	0.4	54.08	2.26	121.77	53.88	2.26	121.74	54.91	2.21	121.21	53.63	2.27	121.63	99.97	99.54	99.89
5	1	1	0.9	0.9	0.8	0.8	0.7	0.5	64.56	2.29	147.49	64.57	2.28	147.48	64.14	2.3	147.33	64.71	2.28	147.46	99.99	99.89	99.98
6	0.7	0.7	0.6	0.6	0.45	0.45	0.3	0.1	54.74	1.42	77.44	55.05	1.41	77.39	55.61	1.38	77	53.68	1.43	77.02	99.93	99.43	99.46
7	1	1	0.5	0.5	0.2	0.2	0.3	0.1	36.04	1.57	56.48	36.18	1.56	56.47	35.21	1.59	56.11	35.69	1.58	56.4	99.98	99.34	99.86
8	1	1	0.9	0.9	0.8	0.7	0.6	0.5	65.86	1.95	128.26	66	1.94	128.24	66.51	1.92	127.76	64.92	1.97	127.72	99.98	99.61	99.58
9	1	1	0.6	0.6	0.5	0.4	0.3	0.1	46.17	1.6	73.77	46.32	1.59	73.74	45.27	1.62	73.31	46.29	1.59	73.75	99.96	99.38	99.97
10	1	0.9	0.8	0.7	0.6	0.5	0.4	0.3	56.34	1.61	90.37	56.56	1.6	90.33	56.92	1.58	90.01	56.49	1.6	90.35	99.95	99.6	99.98

3.10 Conclusion

This chapter analyzed the performance of the proposed global search MPPT controllers based on Bat, PSO and DE algorithms for photovoltaic systems. The Matlab/Simulink environment is used to simulate various *I-V* and *P-V* characteristic curves under various partial shading patterns and to analyze the proposed MPPT control schemes robustness and performance. For benchmarking, comparison with conventional P&O algorithm is carried out. From simulation studies, the ability of the proposed controllers to successfully track the correct GMPP with high accuracy and speed during partial shading condition is remarkable and clearly demonstrated. Despite the simpler structure, the proposed MPPT controllers yield a static efficiency above 99% in all the cases studied.

CHAPTER 4

HARDWARE IMPLEMENTATION OF PROPOSED MPPT CONTROLLERS

Contents

4.1 Introduction

In this chapter, the hardware implementation of the MPPT controllers based on the proposed Bat, PSO and DE algorithms is presented. Except for the size of PV array, the system parameters used in the hardware implementation are the same as used in simulation. An overview on FPGA circuit and their advantages are provided first. Then, the general block diagram of experimental set-up is presented, followed by the descriptions on hardware prototype construction. For completeness, brief explanation on the power converter, feedback sensor and gate driver development are given. Finally, the overall MPPT system implementation using Xilinx Virtex-5 (XC5VLX50-1FFG676) Field Programmable Gate Array (FPGA) is presented.

4.2 FPGA circuits

Field-programmable gate arrays (FPGAs) are reprogrammable silicon chips. When a FPGA is configured, the internal circuitry is connected in a way that creates a hardware implementation of the software application. Unlike processors, FPGAs use dedicated hardware for processing logic and do not have an operating system. FPGAs are truly parallel in nature so different processing operations do not have to compete for the same resources. As a result, the performance of one part of the application is not affected when additional processing is added. Also, multiple control loops can run on a single FPGA device at different rates. FPGA-based control systems can enforce critical interlock logic and can be designed to prevent input/output (I/O) forcing by an operator. However, unlike hard-wired printed circuit board (PCB) designs which have fixed hardware resources, FPGA-based systems can literally rewire their internal circuitry to allow reconfiguration after the control system is deployed to the field. FPGA devices deliver the performance and reliability of dedicated hardware circuitry. A single FPGA can replace thousands of discrete components by incorporating millions of logic gates in a single integrated circuit (IC) chip. The internal resources of an FPGA chip consist of a matrix of configurable logic blocks (CLBs) surrounded by a periphery of I/O blocks. Signals are routed within the FPGA matrix by programmable

interconnect switches and wire routes.

A generalized example of an FPGA is shown in Fig. 4.1 where configurable logic blocks (CLBs) are arranged in a two dimensional grid and are interconnected by programmable routing resources. I/O blocks are arranged at the periphery of the grid and they are also connected to the programmable routing interconnect. The configurable logic blocks (CLBs) are the basic logic unit of an FPGA. Sometimes referred to as slices or logic cells, CLBs are made up of two basic components: flip-flops and lookup tables (LUTs). The "programmable/reconfigurable" term in FPGAs indicates their ability to implement a new function on the chip after its fabrication is complete. The re-configurability/programmability of an FPGA is based on an underlying programming technology, which can cause a change in behavior of a pre-fabricated chip after its fabrication. There are a number of programming technologies that have been used for reconfigurable architectures. Each of these technologies has different characteristics which in turn have significant effect on the programmable architecture. Some of the well known technologies include static memory, flash and anti-fuse [85].

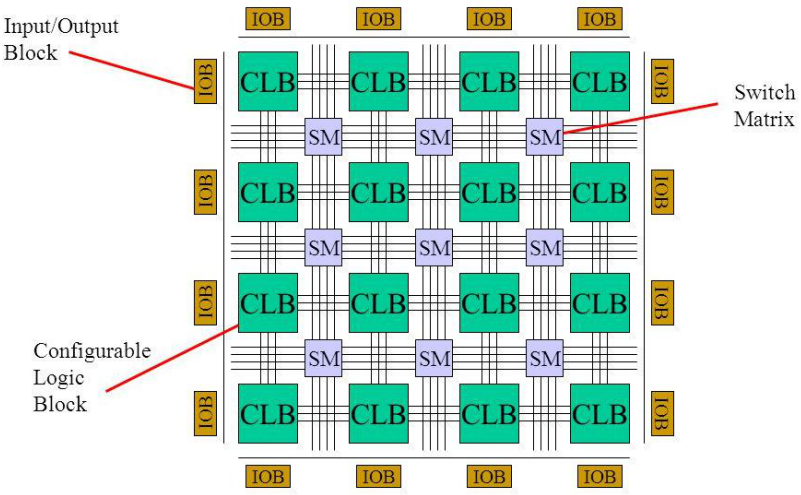

Figure 4.1: Architecture of FPGA circuits.

4.3 Benefits of FPGA technology

Since their invention by Xilinx in 1984, FPGAs have gone from being simple glue logic chips to actually replacing custom application-specific integrated circuits (ASICs) and processors for signal processing and control applications. FPGA chip adoption across all industries is driven by the fact that FPGAs combine the best parts of ASICs and processor-based systems. In fact, FPGAs provide hardware-timed speed and reliability, but are more cost effective than custom ASICs. Taking advantage of hardware parallelism, FPGAs exceed the computing power of digital signal processors (DSPs) by breaking the paradigm of sequential execution and accomplishing more operations per clock cycle. Reprogrammable silicon also has the same flexibility of software running on a processor-based system, but it is not limited by the number of processing cores available. Unlike processors, FPGAs are truly parallel, so different processing operations do not have to compete for the same resources. Each independent processing task is assigned to a dedicated section of the chip, and can therefore function autonomously without any influence from other logic blocks. As a result, speeds can be very fast, and multiple control loops can run on a single FPGA device at different rates. Furthermore, thanks to their re-configurability, FPGA's are reusable, making them flexible for faster prototyping in the face of increased time-to-market concerns, and mistakes are not so costly. After prototyping is completed, often the FPGA used to develop the prototype will be converted to a permanent ASIC.

4.4 Description of the experimental set-up

Fig. 4.2 shows the block diagram of the experimental system developed for the validation of the proposed MPPT controllers. The photograph of the experimental setup is shown in Fig. 4.3. The photovoltaic panel is assembled by the association of SM55 photovoltaic modules. The power converter used is a buck-boost converter designed to operate in continuous conduction current mode. The acquisition circuit of current and voltage of the photovoltaic panel is based on sensors LA 55-P and LV 25-P, respectively. Two ADCs, ADC0804 are used to convert the obtained analog images of

current and voltage into digital values for the MPPT controller. The proposed MPPT techniques are implemented on an FPGA circuit XC5VLX50-1FFG676 of Vertex5 family [86]. This circuit is built around an ML501 development board. The codes are written in VHDL and are synthesized with ISE 10.1 of Xilinx. The tracked PV current and PV voltage are visualised on oscilloscope and recorded for further analysis.

The use of FPGA circuit for the implementation of MPPT control algorithms offers many advantages. Indeed, FPGA offers real hardware implementation of MPPT algorithm. Taking advantage of hardware parallelism, FPGAs overtake the computing performance of digital signal processors (DSPs) and perform more operations per clock cycle. Being reconfigurable, FPGAs can offer a high degree of flexibility and robustness. Therefore, these circuits offer the possibility of implementing complex control algorithms with low latency of computing time. In addition, the speed of FPGAs allows better temporal resolution and improves the performance of MPPT control algorithms.

A brief description of the main components used in the experiments is presented in the following sub-sections.

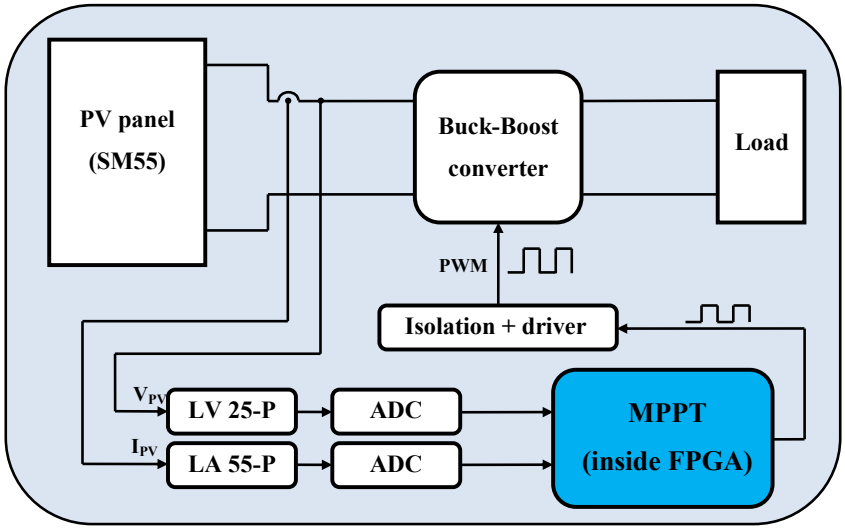

Figure 4.2: Schematic of connections in the experimental PV system with the proposed MPPT controller.

Figure 4.3: Photograph of the experimental setup.

4.4.1 DC-DC converter

The power converter used is a buck-boost converter designed to operate in continuous conduction current mode. The buck-boost topology is used due to several reasons, namely because it exhibits superior characteristics (compared to other types of converters) with respect to the performance of PV array's MPP, and it allows the follow-up of the MPP at all times, regardless of the PV panel temperature, the solar irradiance and connected load [41,87]. Fig. 4.4 shows the schematic of the buck-boost converter. The specifications of the converter are shown in Table 4.1.

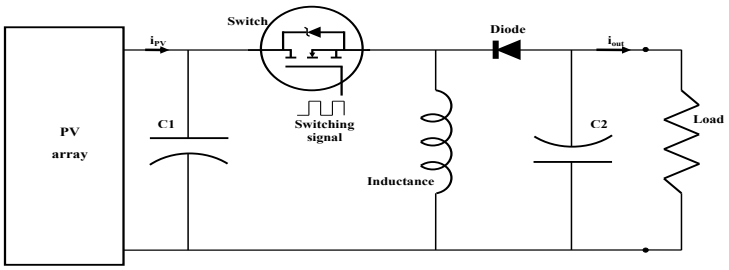

Figure 4.4: Buck-boost circuit used as a MPPT converter.

Table 4.1: Specifications of the buck-boost converter.

Parameters	**Value**
Capacitor C1	440 μF
Capacitor C2	330 μF
Inductance	0.7 mH
Switch	MOSFET IRFP450 (500 V, 14 A)
Diode	MUR1640 (400 V, 16 A)
Switching frequency	50 kHz

4.4.2 Gate drive circuit

The MOSFET is a voltage-controlled switch that needs a pulse signal at the gate for turning on/off. The PWM control signal generated by the FPGA is 0-3.3V voltage level. However, the switch used requires a control signal of at least 0-10V voltage level. For this purpose, gate drive circuit is implemented to ensure the adaptation of control signal voltage. The gate drive circuit acts also as an interface which ensures the electrical isolation between the electronic circuit and power circuit. Figure 6.4 shows the gate drive circuit. It consists of two main components: an opto-coupler and a MOSFET gate driver. The HCPL-2200 opto-coupler is employed to provide the electrical isolation between the power circuit and electronics circuits. The input of the opto-coupler circuit is connected to the PWM signal generated by the FPGA device. The output of the opto-coupler serves as an input of IR2118 gate driver. The IR2118 is a high voltage, high speed power MOSFET and IGBT driver. The output driver features a high pulse current buffer stage designed for minimum cross-conduction. The floating channel can be used to drive an N-channel power MOSFET or IGBT in the high or low side configuration which operates up to 600 volts. The gate drive circuit is powered by a 12V power supply. Since the IR2118 gate driver has an inverting input (out of phase with the output), the logic level of PWM signal is inverted at earlier stage by the FPGA devise.

4.4.3 Acquisition circuit

The proposed MPPT algorithms require the values of PV current and PV voltage. Measurement Transducers should then be used to obtain these two parameters. Since the MPPT techniques are implemented into FPGA, which is a digital device, the analog PV current and voltage values should be converted with an external analog-digital converter (ADC), and then read the digital output of the ADC by the FPGA. The measurement of current and voltage of the photovoltaic panel is performed with transducer LA 55-P and LV 25-P, respectively. These Hall-effect sensors provide galvanic isolation between the primary circuit (high power) and the secondary circuit (elec-

tronic circuit) and it presents advantages like very good linearity and excellent accuracy. An analog low-pass filter is placed at both sensors output port to provide cleaner signals measurements. Furthermore, an amplification stage based on LM358-N operational amplifier is used in order to amplifies the obtained signals and maintain them in the range of 0-5V required by the analog to digital (ADC) module. Two ADCs, ADC0804 are used to convert the obtained analog images of current and voltage into digital values for the MPPT controller. The ADCs are configured to operate at free-running or continuous conversion mode. This means that a new analog to digital conversion is performed automatically after the end of a conversion cycle. A dedicated block is then implemented into FPGA in order to interface this latter with the ADCs and to determine the instant of sampling and reading the PV current and the PV values.

The ADCs outputs could not be connected directly to the pin of the FPGA because their voltage level is 5V whereas FPGA works with lower voltage (3.3 V). Then, a logic-level shifter is required to resolve the voltage incompatibility and translate the 5 V CMOS outputs of the ADCs to 3.3 V level signals, compatible with FPGA requirement. For this purpose, four CD4050 devises are used. To ensure the transmission of data in one way (from the ADC to FPGA), two SN74HC245 octal bus Transceivers are added and interconnected to the outputs of CD4050 devises. In fact, these bus transceivers are designed for asynchronous two-way communication between data buses. The SN74HC245 devices allow data transmission from the A bus to the B bus or from the B bus to the A bus, depending on the logic level at its direction-control input.

4.4.4 FPGA implementation platform

4.4.4.1 Hardware environment

The ML501 evaluation/development platform provides easy and practical access to resources available in the on-board Virtex-5 LX50 FPGA device. Supported by industry standard interfaces and connectors, ML501 is a versatile development platform for multiple applications. The video, audio, and communication ports along with gener-

ous memory resources extend the functionality and flexibility of the ML501 beyond a typical FPGA development platform.

The central element of the evaluation board is XC5VLX50-1FFG676 FPGA chip of Xilinx Virtex-5 family. This chip contains 7200 slices, 48 DSP48E slices and Block RAM up to 1728 Kb. It should notice that a typical CLB of Virtex-5 FPGA is two slices, and each slice contains four 6-input logic-function generators or LUTs, four storage elements or flip-flops, three wide function multiplexers, and a length-4 carry chain comprising of multiplexers and XOR gates. Depending on the nature of LUTs, the slice is called a "SLICEL" or "SLICEM" in Xilinx terminology. The LUTs present in SLICEL can implement any arbitrary combinational logic, whereas the LUTs in SLICEM can be configured to operate as 32-bit shift registers (or 16-bit x 2 shift registers) or as 64-bit distributed RAM. The four storage elements in a slice can be configured as either edge-triggered D-type flip-flops or level sensitive latches. On the other hand, DSP slices in FPGAs are specifically designed for DSP data and signal analysis operations, include built-in multiply and adder circuitry. FPGAs are efficient for digital signal processing (DSP) applications because they can implement custom, fully parallel algorithms. DSP applications use many binary multipliers and accumulators that are best implemented in dedicated DSP slices. In fact, the DSP slices enhance the speed and efficiency of many applications beyond digital signal processing while retaining system design flexibility. The Virtex-5 FPGA DSP48E slice contains a 25 x 18 multiplier, an adder, and an accumulator.

Fig. 4.5 shows the ML501 development platform. In addition to the FPGA chip, this board contains several components, we can mention:

- Xilinx XC95144XL CPLD for glue logic,
- Xilinx XCF32P Platform Flash PROM configuration storage device,
- 256 MB DDR2 small outline DIMM (SODIMM),
- JTAG configuration port for use with Parallel Cable III, Parallel Cable IV, or Platform USB download cable,
- Single-ended and differential expansion I/O connectors,
- 10/100/1000 tri-speed Ethernet PHY transceiver,
- RS-232 serial port,

- 3.3V clock oscillator socket populated with a 100-MHz oscillator,
- General purpose DIP switches, LEDs, and pushbuttons.

Figure 4.5: Vertex-5 FPGA ML501 evaluation platform.

4.4.4.2 Software environment

Xilinx ISE 10.1 (Integrated Synthesis Environment) is used for the implementation of the MPPT controller into FPGA. Xilinx ISE is a design software produced by Xilinx for synthesis and analysis of HDL designs. This design environment integrates various tools to pass through the entire design flow of a FPGA/CPLD based system. The top-level design file can be created using a Hardware Description Language (HDL) or using a schematic. ISE enable the developer to synthesize their designs, perform timing analysis, simulate the design at different level of conception, and configure the target Xilinx device.

4.4.4.3 FPGA design flow

First of all, different architectures are designed and developed for each MPPT algorithm (BA, DE, PSO). After that, the ISE design flow is adopted in order to verify the effectiveness of the hardware implementation of the MPPT controllers into FPGA.

The codes of MPPT technique are synthesised and implemented into FPGA with Xilinx ISE 10.1 in order to get the PWM switching signal required to control the DC-DC converter.

The ISE design flow comprises the following steps: design entry, design synthesis, design implementation, and Xilinx device programming. Design verification, which includes both functional verification and timing verification, takes places at different points during the design flow. Fig. 4.6 describes the ISE design flow and the methodology used for the implementation MPPT algorithms.

Design entry is the first step in the ISE design flow. The top-level design file, which includes various sub-files is created using VHDL. In addition, a pin constraints file is defined in order to specify the physical location (in FPGA) of the logical signals in the VHDL entity. VHDL stands for VHSIC (Very High Speed Integrated Circuits) Hardware Description Language. This language was developed in 1981 at the behest of thefor the U.S. department of Defence (DoD) under the VHSIC program. It was the first hardware description language standardized by the IEEE, through the 1076 and 1164 standards. VHDL is a hardware description language. The code describes the behaviour or structure of an electronic circuit, from which a compliant physical circuit can be inferred by a compiler. Its main applications include synthesis of digital circuits onto CPLD/FPGA (Complex Programmable Logic Device/Field Programmable Gate Array) chips and layout/mask generation for ASIC (Application-Specific Integrated Circuit) fabrication. VHDL is technology/vendor independent, so VHDL codes are portable and reusable. VHDL allows circuit synthesis as well as circuit simulation. The former is the translation of a source code into a hardware structure that implements the intended functionality, while the latter is a testing procedure to ensure that such functionality is indeed achieved by the synthesized circuit.

After design entry and optional simulation, synthesis is performed. The synthesizer converts the VHDL code into a gate-level netlist and synthesis process describes the circuit at the Register Transfer Level (RTL), into a netlist at the gate level.

After synthesis, design implementation is performed to converts the logical design into a physical file format that can be downloaded to the selected target device. Xilinx

design flow has three implementation stages: translate, map and place and route. From Project Navigator, we can run the implementation process in one step, or we can run each of the implementation processes separately. It should be noticed that we can verify the functionality of the design at several points in the design flow.

After implementation process, we generate the programming file and we configure the target device (XC5VLX50-1FFG676 FPGA) with iMPACT. Then the bitstream is generated and uploaded to the FPGA. The FPGA reads then the PV voltage and PV current values, performs the MPPT process and generates the PWM signal to control the buck-boost converter.

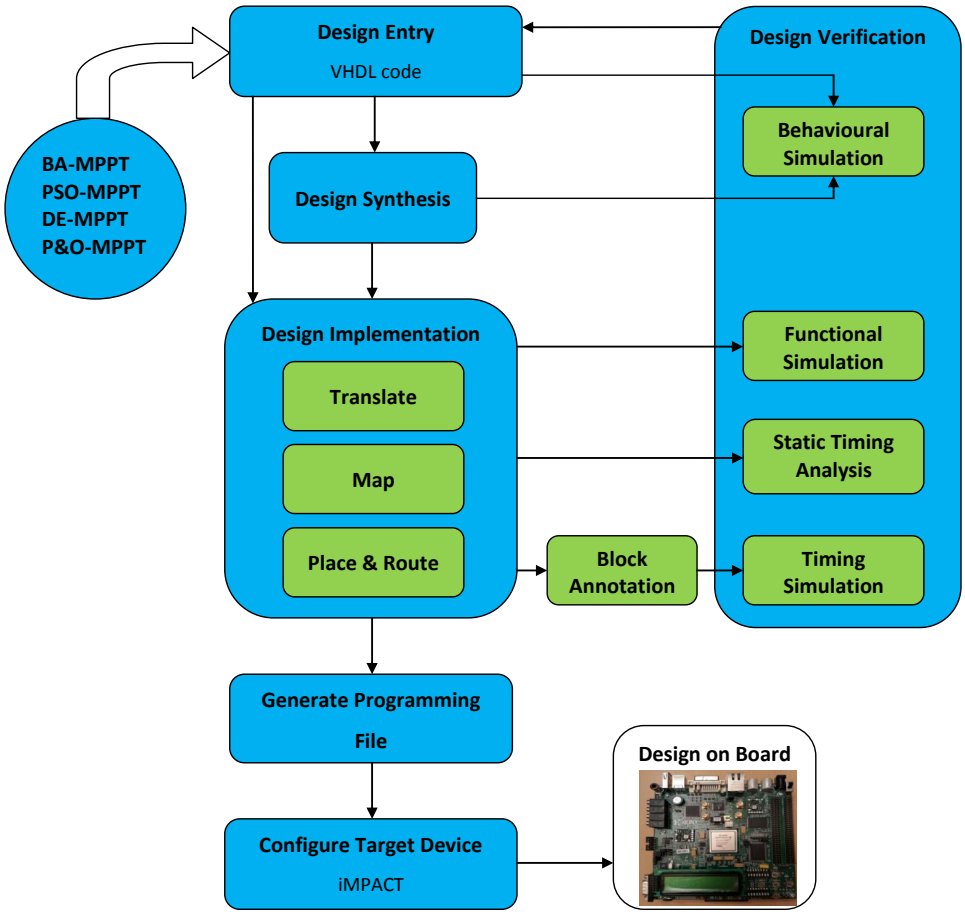

Figure 4.6: Design flow used for the FPGA implementation of MPPT techniques.

4.5 FPGA implementation of proposed MPPT techniques

4.5.1 Architecture of developed MPPT controllers

The general architecture adopted for the development of the MPPT controllers (BA, PSO and DE) is shown in Fig. 4.7. This synoptic scheme includes three blocks: "acquisition", "MPPT" and "PWM". The "acquisition" block serves as an input interface between the FPGA device and the external measurement circuit. It allows the reading of the digital data buses of PV voltage and PV current, the calculation the PV power and the calculation of the ΔP value. The "MPPT" block is the main block that allows the execution of different steps of the MPPT algorithm and the determination of the duty cycle. The "PWM" block allows the generation of the PWM signal to control the DC-DC converter. It should be noted that the two blocks, "MPPT" and "PWM" are similar for the three MPPT controllers. However, the internal architecture of the "MPPT" block varies according to the considered MPPT algorithm (BA, PSO or DE).

The proposed architectures are described in VHDL and implemented into XC5VLX50-1FFG676 FPGA. As illustration, the Register Transfer Level (RTL) schematic of the synthesized BA-MPPT controller implemented on FPGA is shown in Fig. 4.8. It includes various blocks coded separately. This modular programming allows a better optimization of hardware resource and a more flexible and reusable structure. The "acquisition" block allows the reading of digital values of the current and voltage generated by the analog-digital converters and the calculating of the value of the photovoltaic panel power. The "clk_divider" block allows the generation, from the clock of the FPGA, of various clocks needed for the functioning and synchronization of different blocks. The "MPPT" block is the key element of calculating of bat algorithm. It

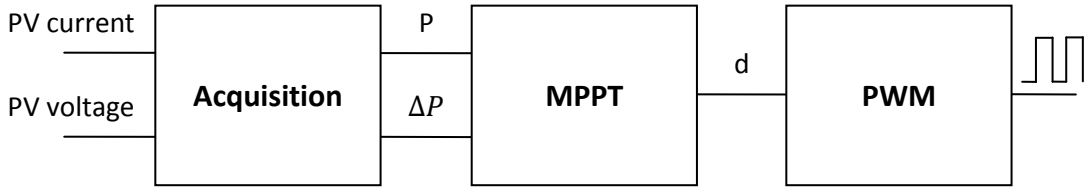

Figure 4.7: Synoptic diagram of the MPPT controllers implemented in FPGA.

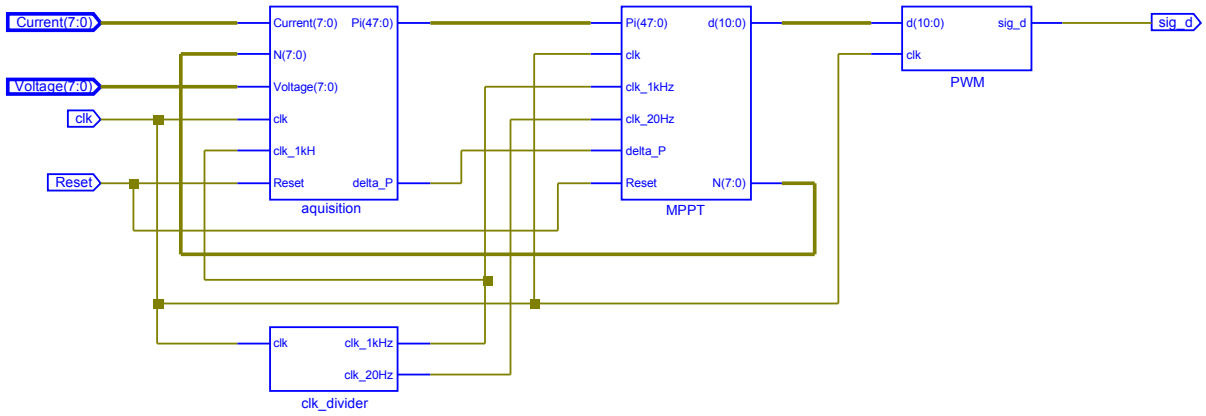

Figure 4.8: The RTL schematic of the synthesized BA based MPPT.

comprises several sub-blocks which allow the execution of the deferent instructions of the bat algorithm and the calculation of the duty cycle. The "PWM" block allows the generation of the PWM signal from the duty cycle d for the control of the DC-DC converter. As mentioned earlier, the architecture of BA, DE and PSO based MPPT are different at "MPPT" bloc. As a result, theirs RTL schematics are different also at the "MPPT" blocks.

4.5.2 Hardware resources utilisation

Once the MPPT design is synthesized and implemented , we can access to FPGA Editor in the ISE Processes window to visualise the routed design on FPGA. FPGA Editor is a graphical displaying and editing tool for physical (layout and routing) designs implemented in Xilinx FPGAs. This tool can be used to fine-tune the FPGA design and improve the performance of the Place & Route process. Table 4.2 illustrates the hardware resources utilisation and power consumption of each implemented MPPT techniques. The power consumption of the implemented MPPT techniques is obtained by Xilinx Power Analyzer (XPA) and reported also in Table 4.2. Xilinx Power Analyzer helps to perform power estimation and analysis for a given real design. Total power in an FPGA is the sum of two components:

- Static power: Static power results primarily from transistor leakage current in the device. Leakage current is either from source-to-drain or through the gate oxide, and exists even when the transistor is logically "OFF".

- Dynamic power: Dynamic power is associated with design activity and switching events in the core or I/O of the device. Dynamic power is determined by node capacitance, supply voltage, and switching frequency ($C\,V^2\,f$).

From these results, we can conclude that the implementation is performed accurately. It can be noticed that the material cost of BA based MPPT is higher than the other techniques. This result is justified by the fact that the optimisation strategy in bat algorithm is more complex.

Table 4.2: Hardware resources utilisation for each developed MPPT technique

Device Utilization Summary (xc5vlx50-1ff676)	**BA-MPPT**	**PSO-MPPT**	**DE-MPPT**	**P&O-MPPT**	**Available**
Number of Slice Registers	3179 (11%)	2293 (7%)	2324 (8%)	113 (1%)	28800
Number of Slice LUTs	3172 (11%)	2161 (7%)	2238 (7%)	148 (1%)	28800
Number of bonded IOBs	19 (4%)	19 (4%)	19 (4%)	19 (4%)	440
Number of BUFG/BUFGCTRLs	2 (6%)	2 (6%)	2 (6%)	2 (6%)	32
Number of DSP48Es	11 (22%)	11 (22%)	5 (10%)	1 (2%)	48
Total quiescent power (W)	0.345	0.345	0.345	0.344	–
Total dynamic power (W)	0.018	0.029	0.018	0.002	–
Total estimated Power consumption	0.363	0.375	0.363	0.346	–

4.6 Experimental verification

The performances of the proposed MPPT algorithms are tested experimentally for different configurations of partial shading. The photovoltaic panel is composed of photovoltaic modules connected in series. The PV panel is exposed to real irradiance conditions. Since it is difficult to predict exactly the appearance moment of partial shading, this latter is created artificially by blocking small portions of the PV panel. This is done by using sheets of different dimensions. Due to variation of solar irradiance and real time test, each MPPT technique is tested individually with four different shading patterns. As a result, the obtained real time P-V curves are not the same for the MPPT techniques.

4.6.1 Tracking results with BA based MPPT

Fig. 4.9 shows the recorded experimental results for the four tests. Each one of these figures includes the *P-V* characteristic in the presence of partial shading, the voltage, the current and power of the photovoltaic panel during the tracking process. Fig. 4.9(a) shows the experimental results obtained for the first test. The first configuration is characterized by the presence of two points of maximum power, $P_{LMPP} = 29.33$ W and $P_{GMPP} = 35.6$ W, respectively. The global maximum power point is to the left of the *P-V* curve, at $V_{GMPP} = 15$ V. It can be noticed that the bat algorithm has successfully located the GMPP and the operating point is maintained around $V = 15.49$ V and $I = 2.29$ A.

In the second and the third cases shown in Fig. 4.9(b) and Fig. 4.9(c), the *P-V* characteristic has three points of maximum power. In the second case, the global maximum power point, $P_{GMPP} = 33.81$ W is in the middle of the *P-V* curve at $V_{GMPP} = 17.25$ V. The proposed algorithm was able to distinguish the GMPP from the LMPPs and the steady state is reached after four MPPT cycles. In the third case, the global maximum point (GMPP) and the local maximum point (LMPP2) are at very close power levels, $P_{GMPP} = 31.05$ W and $P_{LMPP2} = 30.46$ W, respectively. The bat algorithm effectively tracked the GMPP and the voltage of the photovoltaic panel is maintained around $V = 17.95$ V.

The effectiveness of the proposed scheme is proved also when the PV array is subjected to extreme partial shading condition. In the fourth shading pattern shown in Fig. 4.9(d), the *P-V* characteristic curve exhibits four (4) peaks. For this configuration, the proposed MPPT controller implemented into FPGA has also successfully tracked the GMPP at $V = 38.48$ V and $I = 0.92$ A.

4.6.2 Tracking results with PSO based MPPT

To evaluate the performance of the algorithm, four tests are conducted under different shading conditions. The experimental power, voltage and current curves are shown in Fig. 4.10.

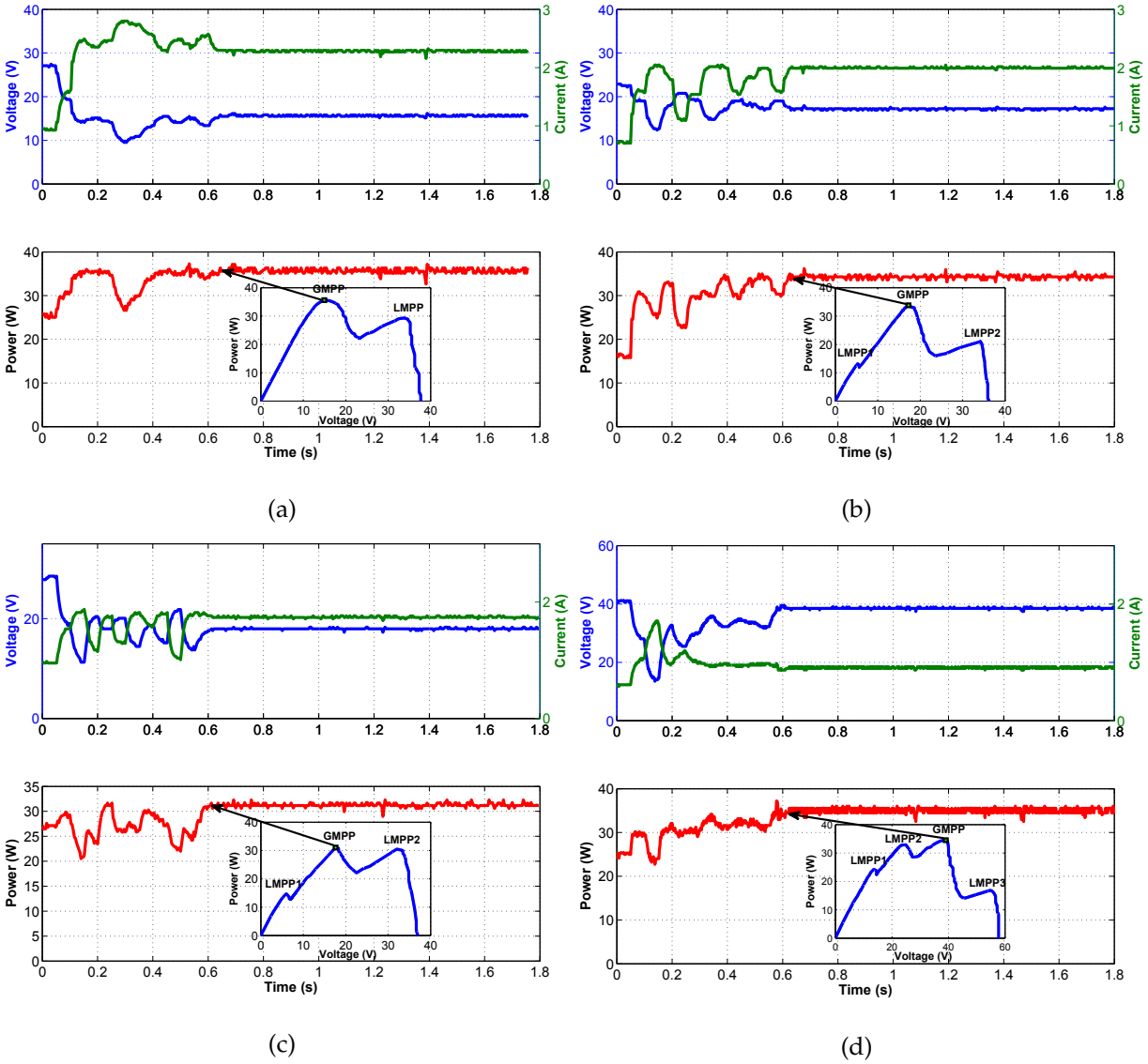

Figure 4.9: Results of GMPP tracking under 4 shading patterns using BA-MPPT.

The behaviour of the PSO based MPPT controller during the first partial shading pattern is shown in Fig. 4.10(a). As can be seen in this figure, the generated PV power is around 35 W, which is close to the maximum achievable power.

To show the severity of partial shading conditions, two different shading patterns having three peaks in *P-V* curve are considered. For pattern 2 having three peaks, the global peak is located at 33.81 W, where the other two local peaks are at 13.18 W and 21.03 W. Having the unique ability to differentiate local and global peak, the PSO method converges to global peak and the generated voltage is maintained around

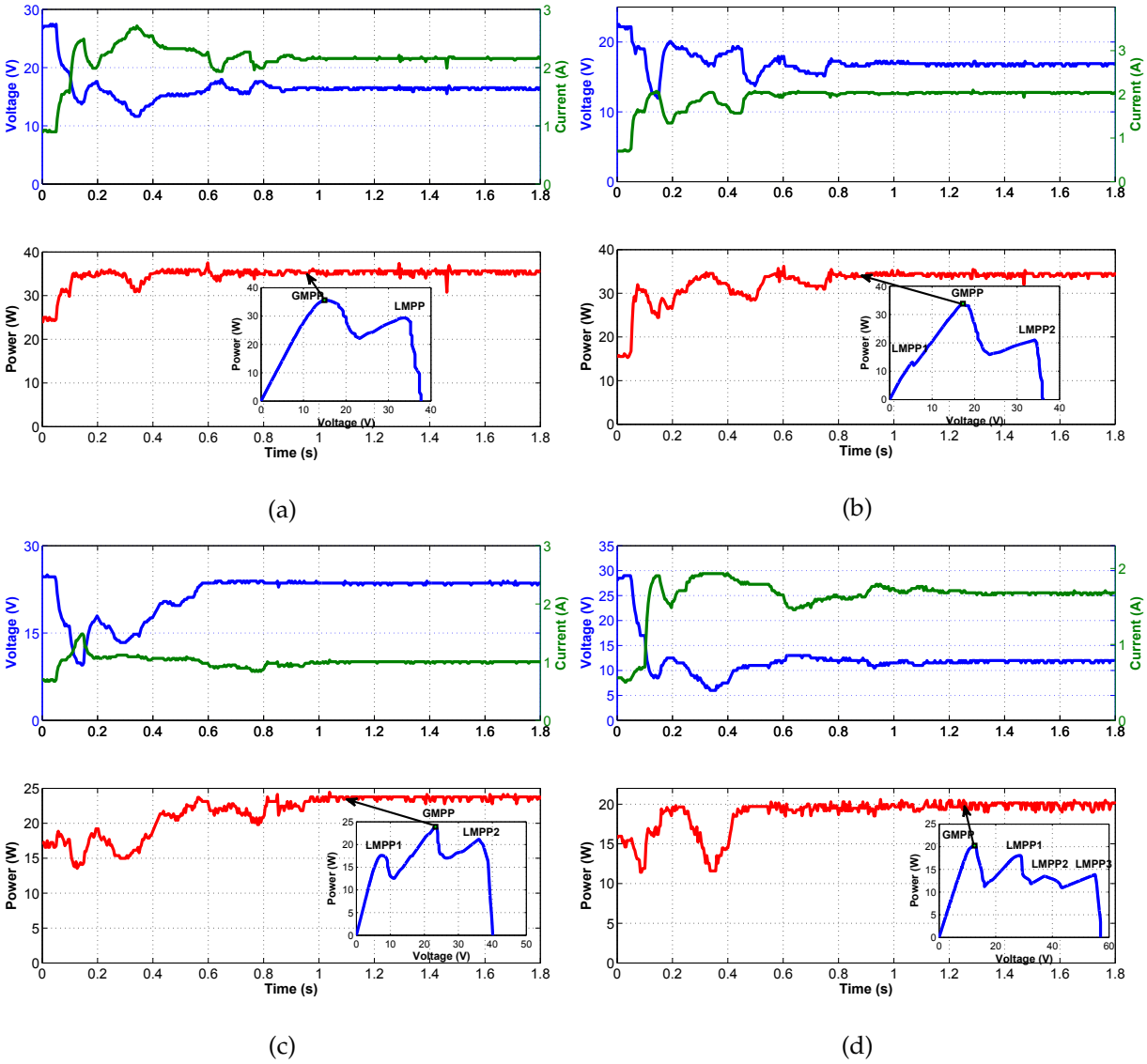

Figure 4.10: Results of GMPP tracking under 4 shading patterns using PSO-MPPT.

16.9 V. In pattern 3, the *P-V* characteristic curve for given shade introduces 3 peaks where GMPP is located at 23.91 W and LMPPs are located at 17.59 W and 21.15 W , respectively. Though multiple peaks are present, the PSO technique has founded GMPP within 1 s.

Strong shade with four peaks is introduced in pattern 4 to test the robustness of the algorithm. Very close local peaks with a similar resemblance of global peak is created to experiment PSO's suitability. The PSO method reaches the global peak of 20.16 W in this case and the voltage of the photovoltaic panel is maintained around

$V = 12$ V.

4.6.3 Tracking results with DE based MPPT

The tracking performance of proposed algorithm is tested experimentally with four shading patterns. The detailed results of such case under study are shown in Fig. 4.11. These figures shows the *P-V* curve, the PV voltage, PV current and the PV power for the DE based tracker.

The obtained experimental results for the first partial shading pattern are illustrated in Fig. 4.11(a). Under this case, there are two peaks and at the global MPP, $P = 40.57$ W, is at $V = 17.25$ V. From this figure, it can be seen that DE optimization technique caught the MPP with high tracking efficiency and the operating point is maintained around $V = 16.9$ V.

To assess the robustness of the proposed algorithm in seeking the global MPP, the PV panel has been subjected to another non-uniform irradiance pattern. As shown from Fig. 4.11(b), the global MPP of 21.15 W is located at the second point on *P-V* curve from three points of peaks. It is clearly observed, that the DE based MPPT is not trapped in the local maximum power points of the *P-V* characteristic and has converged accurately to the global MPP. From Fig. 4.11(b), one can derive that DE optimization technique can ignore the local MPPs and have an excellent capability to achieve global MPP with very high tracking efficiency.

In the third experiment, the PV array was subject to partial irradiance conditions where the corresponding *P-V* curve is shown in Fig. 4.11(c). According to this figure, the corresponding voltage and power of the GMPP are 22.51 V and 23.34 W. The corresponding dynamic responses of the voltage and the current of the PV array are given in Fig. 4.11(c). It can be seen that the generated power is around 23.22 W, which confirms the correct operation of the proposed MPPT in this case of test.

Another case of study has been taken in order to validate the DE-MPPT controller. The recorded tracking results for the fourth shading scenario are shown in Fig. 4.11(d). In this case, the system is tested with a *P-V* characteristic curve exhibiting four peaks. As shown from Fig. 4.11(d), the global MPP of 23.54 W is located at the first peak

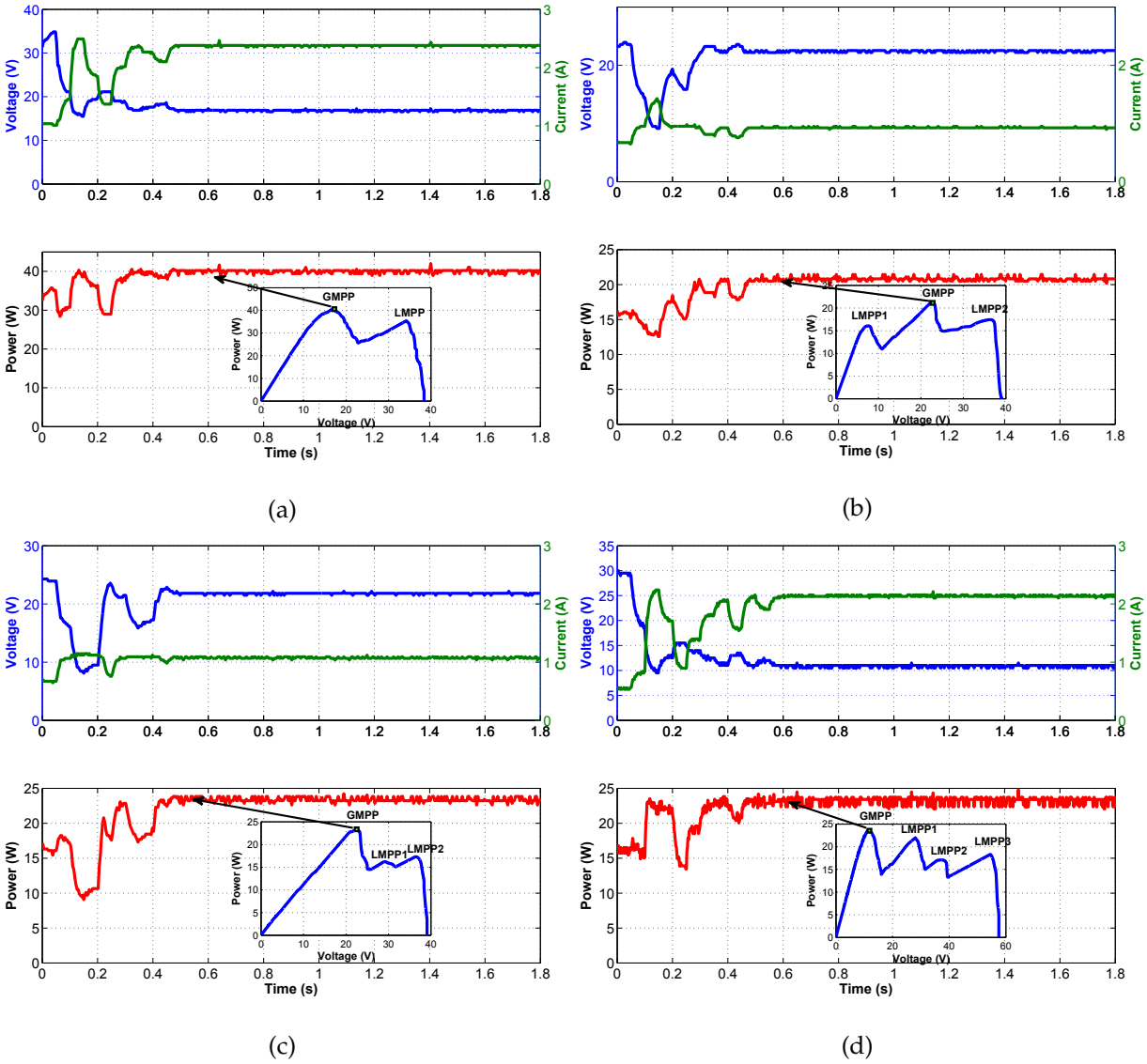

Figure 4.11: Results of GMPP tracking under 4 shading patterns using DE-MPPT.

on *P-V* curve. The tracking results show that the DE based trackers can ignore the local MPPs and have an excellent capability to achieve global MPP. The generated PV power is around 23.41 W which is close to the maximum achievable power.

4.7 Conclusion

This chapter has described the hardware implementation of BA, PSO and DE based maximum power point tracking controllers and presented the experimental results.

For the implementation, FPGA chip is used for flexible and reusable prototyping design structure. The experimental validation confirms the effectiveness of the proposed algorithms to deal with the multimodal characteristic curve of PV systems under partial shading conditions and the results are consistent and well in agreement with the simulation results. The discussion clearly demonstrates that the power extracting features of the proposed controllers in partial shading conditions are able to provide a feasible alternative solution to real-time PV systems.

GENERAL CONCLUSION

The main objective of this research is to make a contribution to the optimization of photovoltaic systems under partial shaded conditions. This objective is achieved thanks to the three proposed MPPT techniques, based respectively on the BA, PSO and DE algorithms, which allow the global point of the maximum power of the PV generator to be tracked with great efficiency. The objective of the maximum power point tracking (MPPT) algorithm is to optimize the operating point of the PV system at the particular point on the *I-V* curve at which the module or array yields the greatest power. However, achieving this goal is a demanding task because the MPP on the *P-V* characteristic curve is inconsistent due to continuous variation of solar irradiance and its temperature. The situation is worsened under partial shading (PS) conditions where the *P-V* curve becomes multi-modal.

Thanks to the ability of methaheuristcs to handle multi-modal functions, MPPT controllers based on a Bat, PSO and DE algorithms are proposed to deal with the multi-modal characteristic of photovoltaic panel under partial shading conditions. Simulations are carried out under extreme shading patterns to confirm their global search ability and their good dynamic performance. Furthermore, their performances are evaluated based on the tracking efficiency, speed and steady-state oscillation and ability to handle the partial shading. The simulations results show that the proposed methods track the GMPP with a high accuracy and yield a static efficiency above 99%. In addition, the proposed schemes outperform the P&O methods in terms of

global peak tracking. FPGA implementation is presented to validate the proposed controllers on real time application. The implemented architectures are designed using hand written VHDL codes for better optimization of hardware resource and a more flexible and reusable structures. Being reconfigurable, FPGAs can offer a high degree of flexibility and robustness. Since the PWM signal is generated with a high resolution, the performance of the tracking process is largely improved. Experimental results confirm the efficiency of the proposed methods in the global peak tracking and their accuracy under partial shading conditions.

In conclusion, this work authenticates the viability of the proposed Bat, PSO and DE algorithms for MPPT of PV system. The tests and results demonstrate that the proposed controllers are capable of effectively and accurately locating MPP even under challenging and extreme conditions where many basic algorithms fail.

In this thesis, several contributions are presented. However, there remain potentially new findings in the area of MPPT control that can still be explored. These can be summarized as follows:

- Study the influence of the different parameters on the convergence of each algorithm and propose a simple method for selecting the control parameters.
- Combination of the proposed techniques with GMPP region estimator: It is foreseen that the performance of the proposed techniques in terms of convergence speed can be further improved if an estimation technique is applied to identify the GMPP region.
- Combination of the proposed techniques with an effective strategy of detection of partial shading, which can differentiate this latter from large irradiance change.
- Extend the study to other meta-heuristic : it would be interesting to investigate the possibility of tracking during partially shaded conditions with other meta-heuristic such as such as Ant Colony Optimization (ACO) , Cuckoo search (CS) and Firfly algorithm (FA). The implementation of these algorithms in FPGA could also be envisaged.

BIBLIOGRAPHY

[1] A. Mellit, S. Kalogirou, L. Hontoria, S. Shaari, Artificial intelligence techniques for sizing photovoltaic systems: A review, Renewable and Sustainable Energy Reviews 13 (2) (2009) 406–419.

[2] F. Belhachat, C. Larbes, Modeling, analysis and comparison of solar photovoltaic array configurations under partial shading conditions, Solar Energy 120 (2015) 399–418.

[3] A. Woyte, J. Nijs, R. Belmans, Partial shadowing of photovoltaic arrays with different system configurations: literature review and field test results, Solar Energy 74 (3) (2003) 217–233.

[4] E. Karatepe, M. Boztepe, M. Colak, Development of a suitable model for characterizing photovoltaic arrays with shaded solar cells, Solar Energy 81 (8) (2007) 977–992.

[5] P. Bhatnagar, R. Nema, Maximum power point tracking control techniques: State-of-the-art in photovoltaic applications, Renewable and Sustainable Energy Reviews 23 (2013) 224–241.

[6] A. Dolara, G. C. Lazaroiu, S. Leva, G. Manzolini, Experimental investigation of partial shading scenarios on pv (photovoltaic) modules, Energy 55 (2013) 466–475.

[7] R. Eke, C. Demircan, Shading effect on the energy rating of two identical pv systems on a building façade, Solar Energy 122 (2015) 48–57.

[8] J. Ahmed, Z. Salam, A critical evaluation on maximum power point tracking methods for partial shading in pv systems, Renewable and Sustainable Energy Reviews 47 (2015) 933–953.

[9] A. Bidram, A. Davoudi, R. S. Balog, Control and circuit techniques to mitigate partial shading effects in photovoltaic arrays, IEEE Journal of Photovoltaics 2 (4) (2012) 532–546.

[10] L. L. Jiang, R. Srivatsan, D. L. Maskell, Computational intelligence techniques for maximum power point tracking in pv systems: A review, Renewable and Sustainable Energy Reviews 85 (2018) 14–45.

[11] F. Belhachat, C. Larbes, A review of global maximum power point tracking techniques of photovoltaic system under partial shading conditions, Renewable and Sustainable Energy Reviews 92 (2018) 513–553.

[12] G. N. Tiwari, S. Dubey, Fundamentals of Photovoltaic Modules and Their Applications, no. 2, Royal Society of Chemistry, 2010.

[13] S. Bhatia, 4 - solar thermal energy, in: S. Bhatia (Ed.), Advanced Renewable Energy Systems, Woodhead Publishing India, 2014, pp. 94 – 143.

[14] A. Mellit, S. A. Kalogirou, Artificial intelligence techniques for photovoltaic applications: A review, Progress in energy and combustion science 34 (5) (2008) 574–632.

[15] K. Ishaque, Z. Salam, et al., A comprehensive matlab simulink pv system simulator with partial shading capability based on two-diode model, Solar energy 85 (9) (2011) 2217–2227.

[16] G. Velasco-Quesada, F. Guinjoan-Gispert, R. Piqué-López, M. Román-Lumbreras, A. Conesa-Roca, Electrical pv array reconfiguration strategy for energy extraction improvement in grid-connected pv systems, IEEE Transactions on Industrial Electronics 56 (11) (2009) 4319–4331.

[17] D. Nguyen, B. Lehman, A reconfigurable solar photovoltaic array under shadow conditions, in: Applied Power Electronics Conference and Exposition, 2008. APEC 2008. Twenty-Third Annual IEEE, IEEE, 2008, pp. 980–986.

[18] L. Gao, R. A. Dougal, S. Liu, A. P. Iotova, Parallel-connected solar pv system to address partial and rapidly fluctuating shadow conditions, IEEE Transactions on industrial Electronics 56 (5) (2009) 1548–1556.

[19] D. Nguyen, B. Lehman, An adaptive solar photovoltaic array using model-based reconfiguration algorithm, IEEE Transactions on Industrial Electronics 55 (7) (2008) 2644–2654.

[20] E. Roman, R. Alonso, P. Ibañez, S. Elorduizapatarietxe, D. Goitia, Intelligent pv module for grid-connected pv systems, IEEE Transactions on Industrial electronics 53 (4) (2006) 1066–1073.

[21] S. V. Dhople, J. L. Ehlmann, A. Davoudi, P. L. Chapman, Multiple-input boost converter to minimize power losses due to partial shading in photovoltaic modules, in: Energy Conversion Congress and Exposition (ECCE), 2010 IEEE, IEEE, 2010, pp. 2633–2636.

[22] E. Ozdemir, S. Ozdemir, L. M. Tolbert, Fundamental-frequency-modulated six-level diode-clamped multilevel inverter for three-phase stand-alone photovoltaic system, IEEE Transactions on Industrial Electronics 56 (11) (2009) 4407–4415.

[23] E. Romero-Cadaval, G. Spagnuolo, L. G. Franquelo, C. A. Ramos-Paja, T. Suntio, W. M. Xiao, Grid-connected photovoltaic generation plants: Components and operation, IEEE Industrial Electronics Magazine 7 (3) (2013) 6–20.

[24] Y.-H. Liao, C.-M. Lai, Newly-constructed simplified single-phase multistring multilevel inverter topology for distributed energy resources, IEEE Transactions on Power Electronics 26 (9) (2011) 2386–2392.

[25] J. Rodriguez, J.-S. Lai, F. Z. Peng, Multilevel inverters: a survey of topologies, controls, and applications, IEEE Transactions on industrial electronics 49 (4) (2002) 724–738.

[26] S. Busquets-Monge, J. Rocabert, P. Rodríguez, S. Alepuz, J. Bordonau, Multilevel diode-clamped converter for photovoltaic generators with independent voltage control of each solar array, IEEE Transactions on Industrial electronics 55 (7) (2008) 2713–2723.

[27] E. Karatepe, T. Hiyama, M. Boztepe, M. Çolak, Voltage based power compensation system for photovoltaic generation system under partially shaded insolation conditions, Energy Conversion and Management 49 (8) (2008) 2307–2316.

[28] T. Shimizu, M. Hirakata, T. Kamezawa, H. Watanabe, Generation control circuit for photovoltaic modules, IEEE Transactions on Power Electronics 16 (3) (2001) 293–300.

[29] M. Z. Ramli, Z. Salam, A simple energy recovery scheme to harvest the energy from shaded photovoltaic modules during partial shading, IEEE Transactions on Power Electronics 29 (12) (2014) 6458–6471.

[30] Q. Li, P. Wolfs, A review of the single phase photovoltaic module integrated converter topologies with three different dc link configurations, IEEE Transactions on Power Electronics 23 (3) (2008) 1320–1333.

[31] A. Kouchaki, H. Iman-Eini, B. Asaei, A new maximum power point tracking strategy for pv arrays under uniform and non-uniform insolation conditions, Solar Energy 91 (2013) 221–232.

[32] Y.-H. Liu, J.-H. Chen, J.-W. Huang, Global maximum power point tracking algorithm for pv systems operating under partially shaded conditions using the segmentation search method, Solar Energy 103 (2014) 350–363.

[33] T. L. Nguyen, K.-S. Low, A global maximum power point tracking scheme employing direct search algorithm for photovoltaic systems, IEEE transactions on Industrial Electronics 57 (10) (2010) 3456–3467.

[34] K. Lian, J. Jhang, I. Tian, A maximum power point tracking method based on perturb-and-observe combined with particle swarm optimization, IEEE journal of photovoltaics 4 (2) (2014) 626–633.

[35] R.-Y. Kim, J.-H. Kim, An improved global maximum power point tracking scheme under partial shading conditions, in: Journal of International Conference on Electrical Machines and Systems, Vol. 2, Journal of International Conference on Electrical Machines and Systems, 2013, pp. 65–68.

[36] B. N. Alajmi, K. H. Ahmed, S. J. Finney, B. W. Williams, A maximum power point tracking technique for partially shaded photovoltaic systems in microgrids, IEEE Transactions on Industrial Electronics 60 (4) (2013) 1596–1606.

[37] R. Boukenoui, H. Salhi, R. Bradai, A. Mellit, A new intelligent mppt method for stand-alone photovoltaic systems operating under fast transient variations of shading patterns, Solar Energy 124 (2016) 124–142.

[38] R. Balasankar, G. T. Arasu, J. C. M. Raj, A global mppt technique invoking partitioned estimation and strategic deployment of p&o to tackle partial shading conditions, Solar Energy 143 (2017) 73–85.

[39] M. Miyatake, M. Veerachary, F. Toriumi, N. Fujii, H. Ko, Maximum power point tracking of multiple photovoltaic arrays: a pso approach, IEEE Transactions on Aerospace and Electronic Systems 47 (1) (2011) 367–380.

[40] J. Shi, W. Zhang, Y. Zhang, F. Xue, T. Yang, Mppt for pv systems based on a dormant pso algorithm, Electric Power Systems Research 123 (2015) 100–107.

[41] K. Ishaque, Z. Salam, M. Amjad, S. Mekhilef, An improved particle swarm optimization (pso)–based mppt for pv with reduced steady-state oscillation, IEEE transactions on Power Electronics 27 (8) (2012) 3627–3638.

[42] K. Ishaque, Z. Salam, A. Shamsudin, M. Amjad, A direct control based maximum power point tracking method for photovoltaic system under partial shading conditions using particle swarm optimization algorithm, Applied Energy 99 (2012) 414–422.

[43] K. Ishaque, Z. Salam, A deterministic particle swarm optimization maximum power point tracker for photovoltaic system under partial shading condition, IEEE transactions on industrial electronics 60 (8) (2013) 3195–3206.

[44] K. Kaced, C. Larbes, S. M. Ait-Chikh, M. Bounabi, Z. E. Dahmane, Fpga implementation of pso based mppt for pv systems under partial shading conditions, in: Systems and Control (ICSC), 2017 6th International Conference on, IEEE, 2017, pp. 150–155.

[45] S. M. Mirhassani, S. Z. M. Golroodbari, S. M. M. Golroodbari, S. Mekhilef, An improved particle swarm optimization based maximum power point tracking strategy with variable sampling time, International Journal of Electrical Power & Energy Systems 64 (2015) 761–770.

[46] K. Sundareswaran, S. Palani, et al., Application of a combined particle swarm optimization and perturb and observe method for mppt in pv systems under partial shading conditions, Renewable Energy 75 (2015) 308–317.

[47] Y.-H. Liu, S.-C. Huang, J.-W. Huang, W.-C. Liang, A particle swarm optimization-based maximum power point tracking algorithm for pv systems operating under partially shaded conditions, IEEE Transactions on Energy Conversion 27 (4) (2012) 1027–1035.

[48] K.-H. Chao, Y.-S. Lin, U.-D. Lai, Improved particle swarm optimization for maximum power point tracking in photovoltaic module arrays, Applied Energy 158 (2015) 609–618.

[49] M. Bounabi, K. Kaced, M. S. Ait-Cheikh, C. Larbes, Z. e. Dahmane, N. Ramzan, Modelling and performance analysis of different multilevel inverter topologies using pso-mppt technique for grid connected photovoltaic systems, Journal of Renewable and Sustainable Energy 10 (4) (2018) 043507.

[50] M. F. N. Tajuddin, S. M. Ayob, Z. Salam, M. S. Saad, Evolutionary based maximum power point tracking technique using differential evolution algorithm, Energy and Buildings 67 (2013) 245–252.

[51] K. S. Tey, S. Mekhilef, H.-T. Yang, M.-K. Chuang, A differential evolution based mppt method for photovoltaic modules under partial shading conditions, International Journal of Photoenergy 2014, (2014), Article ID 945906, 10 pages.

[52] M. A. Ramli, K. Ishaque, F. Jawaid, Y. A. Al-Turki, Z. Salam, A modified differential evolution based maximum power point tracker for photovoltaic system under partial shading condition, Energy and Buildings 103 (2015) 175–184.

[53] K. S. Tey, S. Mekhilef, M. Seyedmahmoudian, B. Horan, A. M. T. Oo, A. Stojcevski, Improved differential evolution-based mppt algorithm using sepic for pv systems under partial shading conditions and load variation, IEEE Transactions on Industrial Informatics 14 (10) (2018) 4322–4333.

[54] M. Seyedmahmoudian, R. Rahmani, S. Mekhilef, A. M. T. Oo, A. Stojcevski, T. K. Soon, A. S. Ghandhari, Simulation and hardware implementation of new maximum power point tracking technique for partially shaded pv system using hybrid depso method, IEEE Transactions on Sustainable Energy 6 (3) (2015) 850–862.

[55] J. Ahmed, Z. Salam, A maximum power point tracking (mppt) for pv system using cuckoo search with partial shading capability, Applied Energy 119 (2014) 118–130.

[56] B.-R. Peng, K.-C. Ho, Y.-H. Liu, A novel and fast mppt method suitable for both fast changing and partially shaded conditions, IEEE Transactions on Industrial Electronics 65 (4) (2018) 3240–3251.

[57] L. L. Jiang, D. L. Maskell, J. C. Patra, A novel ant colony optimization-based maximum power point tracking for photovoltaic systems under partially shaded conditions, Energy and Buildings 58 (2013) 227–236.

[58] S. Titri, C. Larbes, K. Y. Toumi, K. Benatchba, A new mppt controller based on the ant colony optimization algorithm for photovoltaic systems under partial shading conditions, Applied Soft Computing 58 (2017) 465–479.

[59] K. Sundareswaran, S. Peddapati, S. Palani, Mppt of pv systems under partial shaded conditions through a colony of flashing fireflies, IEEE Transactions on Energy Conversion 29 (2) (2014) 463–472.

[60] X.-S. Yang, Firefly algorithms for multimodal optimization, in: International symposium on stochastic algorithms, Springer, 2009, pp. 169–178.

[61] D. Teshome, C. Lee, Y. Lin, K. Lian, A modified firefly algorithm for photovoltaic maximum power point tracking control under partial shading, IEEE Journal of Emerging and Selected Topics in Power Electronics 5 (2) (2017) 661–671.

[62] K. Kaced, C. Larbes, N. Ramzan, M. Bounabi, Z. elabadine Dahmane, Bat algorithm based maximum power point tracking for photovoltaic system under partial shading conditions, Solar Energy 158 (2017) 490–503.

[63] J. P. Ram, N. Rajasekar, A new global maximum power point tracking technique for solar photovoltaic (pv) system under partial shading conditions (psc), Energy 118 (2017) 512–525.

[64] N. Kumar, I. Hussain, B. Singh, B. K. Panigrahi, Single sensor based mppt for partially shaded solar photovoltaic by using human psychology optimisation algorithm, IET Generation, Transmission & Distribution 11 (10) (2017) 2562–2574.

[65] L. Guo, Z. Meng, Y. Sun, L. Wang, A modified cat swarm optimization based maximum power point tracking method for photovoltaic system under partially shaded condition, Energy 144 (2018) 501–514.

[66] S.-C. Chu, P.-W. Tsai, J.-S. Pan, Cat swarm optimization, in: Pacific Rim International Conference on Artificial Intelligence, Springer, 2006, pp. 854–858.

[67] X.-S. Yang, Chapter 1 - introduction to algorithms, in: X.-S. Yang (Ed.), Nature-Inspired Optimization Algorithms, Elsevier, Oxford, 2014, pp. 1 – 21.

[68] K.-L. Du, M. Swamy, et al., Search and optimization by metaheuristics, Springer, 2016.

[69] X.-S. Yang, Chapter 2 - analysis of algorithms, in: X.-S. Yang (Ed.), Nature-Inspired Optimization Algorithms, Elsevier, Oxford, 2014, pp. 23 – 44.

[70] X.-S. Yang, A new metaheuristic bat-inspired algorithm, in: Nature inspired cooperative strategies for optimization (NICSO 2010), Springer, 2010, pp. 65–74.

[71] X.-S. Yang, M. Karamanoglu, S. Fong, Bat algorithm for topology optimization in microelectronic applications, in: The First International Conference on Future Generation Communication Technologies, IEEE, 2012, pp. 150–155.

[72] X.-S. Yang, Bat algorithm and cuckoo search: a tutorial, in: Artificial Intelligence, Evolutionary Computing and Metaheuristics, Springer, 2013, pp. 421–434.

[73] S. Yilmaz, E. U. Kucuksille, Improved bat algorithm (iba) on continuous optimization problems, Lecture Notes on Software Engineering 1 (3) (2013) 279.

[74] J. KENNEDY, Particle swarm optimization, in: Proc. of 1995 IEEE Int. Conf. Neural Networks,(Perth, Australia), Nov. 27-Dec., Vol. 4, 1995, pp. 1942–1948.

[75] R. Eberhart, J. Kennedy, A new optimizer using particle swarm theory, in: Micro Machine and Human Science, 1995. MHS'95., Proceedings of the Sixth International Symposium on, IEEE, 1995, pp. 39–43.

[76] Y. Shi, R. Eberhart, A modified particle swarm optimizer, in: Evolutionary Computation Proceedings, 1998. IEEE World Congress on Computational Intelligence., The 1998 IEEE International Conference on, IEEE, 1998, pp. 69–73.

[77] J. Kennedy, R. Mendes, Population structure and particle swarm performance, in: Evolutionary Computation, 2002. CEC'02. Proceedings of the 2002 Congress on, Vol. 2, IEEE, 2002, pp. 1671–1676.

[78] R. Mendes, J. Kennedy, J. Neves, The fully informed particle swarm: simpler, maybe better, IEEE transactions on evolutionary computation 8 (3) (2004) 204–210.

[79] K. V. Price, Differential evolution: a fast and simple numerical optimizer, in: Fuzzy Information Processing Society, 1996. NAFIPS., 1996 Biennial Conference of the North American, IEEE, 1996, pp. 524–527.

[80] R. Storn, K. Price, Differential evolution–a simple and efficient heuristic for global optimization over continuous spaces, Journal of global optimization 11 (4) (1997) 341–359.

[81] J. Lampinen, I. Zelinka, Mixed integer-discrete-continuous optimization by differential evolution, in: Proceedings of the 5th International Conference on Soft Computing, 1999, pp. 71–76.

[82] K. Price, R. M. Storn, J. A. Lampinen, Differential evolution: a practical approach to global optimization, Springer Science & Business Media, 2006.

[83] R. Bruendlinger, B. Bletterie, M. Milde, H. Oldenkamp, Maximum power point tracking performance under partially shaded pv array conditions, Proc. 21st EUPVSEC (2006) 2157–2160.

[84] V. Quaschning, R. Hanitsch, Numerical simulation of current-voltage characteristics of photovoltaic systems with shaded solar cells, Solar Energy 56 (6) (1996) 513–520.

[85] U. Farooq, Z. Marrakchi, H. Mehrez, Tree-based Heterogeneous FPGA Architectures: Application Specific Exploration and Optimization, Springer Science & Business Media, 2012.

[86] http://www.xilinx.com (Jul. 2017).

[87] J. Enrique, E. Duran, M. Sidrach-de Cardona, J. Andujar, Theoretical assessment of the maximum power point tracking efficiency of photovoltaic facilities with different converter topologies, Solar Energy 81 (1) (2007) 31–38.